Distribution Agreement

Randall P. Kirby Jr. April 28, 2021

Optimization of Rh_2(*S*-TPPTTL)$_4$ Through Ligand Diversification

By

Randall P Kirby Jr.

Dr. Huw M. L. Davies

Advisor

Department of Chemistry

Dr. Huw M. L. Davies

Advisor

Dr. Matthew Weinschenk

Committee Member

Dr. Manoj Thapa

Committee Member

2021

Optimization of Rh_2(*S*-TPPTTL)$_4$ Through Ligand Diversification

By

Randall P. Kirby Jr.

Dr. Huw M. L. Davies

Advisor

An abstract of
a thesis submitted to the Faculty of Emory College of Arts and Sciences
of Emory University in partial fulfillment
of the requirements of the degree of
Bachelor of Science with Honors

Department of Chemistry

2021

Abstract

Optimization of Rh_2(*S*-TPPTTL)$_4$ Through Ligand Diversification

By Randall P. Kirby Jr.

Discovering new ways to alter the classically inert C-H bond at different positions in a molecule has proven to be a valuable method to synthesize several complex structures. Dirhodium catalysts have been shown to perform these alterations with high yield and stereoselectivity. One of the most notable catalysts with promising reactions is the Rh_2(tetra-phenyl-phthalimido-tertbutyl-leucino)$_4$ catalyst (Rh_2(TPPTTL)$_4$). This catalyst has been shown to catalyze cyclopropanations and highly stereo-specific C-H functionalizations. A key factor in dictating this catalyst's specificity is its C_4 symmetry and large steric bulk, which was chosen as a promising area for optimization. Further optimization studies of this catalyst were conducted to broaden its scope of reactions and study the structure of the catalyst's active site. This was achieved by increasing the overall bulk of the catalyst and the steric demand close to the catalyst's active site.

Optimization of Rh_2(*S*-TPPTTL)$_4$ Through Ligand Diversification

By

Randall P. Kirby Jr.

Dr. Huw M. L. Davies

Advisor

A thesis submitted to the Faculty of Emory College of Arts and Sciences
of Emory University in partial fulfillment
of the requirements of the degree of
Bachelor of Science with Honors

Department of Chemistry

2021

Acknowledgements

I would like to primarily thank Professor Huw Davies for accepting me into his lab, and for advising me at every step of the way. Working in his lab has taught me skills that I've carried into every aspect of life, from attention to detail to the ever-important adaptations to the failure that research carries with it. Without the help of PhD student Jack Sharland at the lab, my interest in research would never have been cultivated so deeply.

Secondly, I would like to thank Dr. Matthew Weinschenk for inspiring me to pursue research in the realm of organic chemistry. The way he expertly described the intricacies of the zirconium catalyst system showed me that there was a profoundly important world lying beyond our vision waiting to be explored.

Lastly, I would like to thank Dr. Manoj Thapa for my experience at Yerkes Primate Research institute. My time there showed me the biological relevance of all research and the importance of maintaining a pragmatic approach towards how research is done.

1. Introduction

1.1) The Biological Relevance of Stereoselective Synthesis

From its first discovery in crystals, chirality has become one of the most important properties to the pharmaceutical industry. If a molecule is said to be chiral, it cannot be super-imposed on its mirror image. [7] This concept is often referred to as "handedness," as human hands, while mirror images, are not the same. While chirality has always surrounded us, its necessity in biological systems only became relevant in 1848 when Louis Pasteur discovered enantioselectivity, the ability for a system to differentiate between chiral molecules, in the metabolism of Tartaric Acid. The concept of chirality is displayed in Figure 1.1.1 where both enantiomers of the same crystal are displayed. [11]

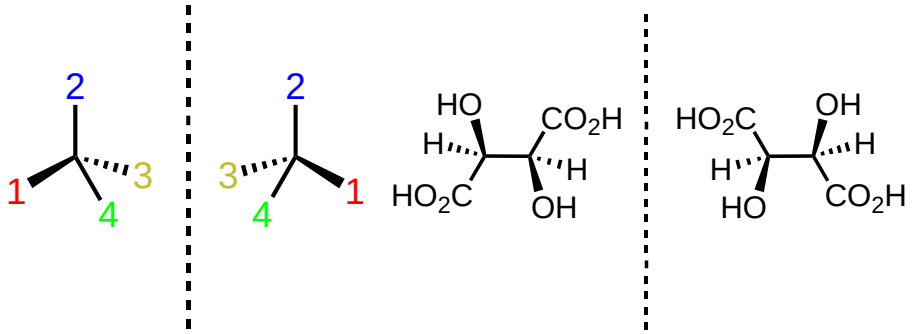

Figure 1.1.1 A representation of chiral molecules (left) and the different conformations of tartaric acid (right)

In the human body, different enantiomers of molecules can have widely different effects. Thalidomide, a drug designed to alleviate morning sickness, is a classic example. While one enantiomer exerted the desired effects, the other caused fetal defects. It was only due to the actions of FDA pharmacologist Frances Kelsey that Thalidomide was not approved in the United States.[8] The reason for these differential effects is the ubiquity of chiral molecules, like DNA and protein, that make up the human body. The human body only contains L-Amino acids and D-sugars, L and

D being delineations for one of the enantiomers of the respective molecules. While D-sugars are more stable in their cyclic form than L-sugars, the reason for humans having L-amino acids vs. D-amino acids remains unknown. Some theories suggest that polarized light creates a slight imbalance between enantiomers, but it is still the subject of significant research. Whatever the reason, the human body often responds differently to one enantiomer over the other.[13]

Pharmaceutical companies, because of the necessity for chiral medications, place a high emphasis on enantioselective synthesis. There have been several ways chemists have devised to achieve this goal: some use chiral auxiliaries that will impermanently be attached to the molecule to impart it chirality, while others use chiral catalysts. The chemistry developed in the Davies group has been used in the synthesis of pharmaceutical drugs as illustrated in Figure 1.1.2.

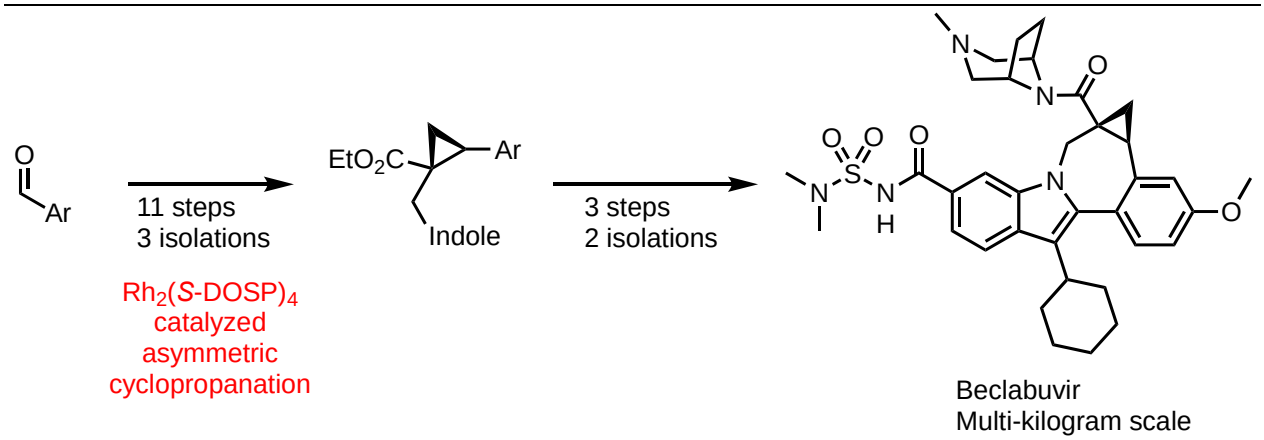

Figure 1.1.2 The total synthesis of Beclabuvir, a hepatis C polymerase inhibitor that utilized the Rh_2(*S*-DOSP)$_4$ dirhodium catalyst pioneered by the Davies group. Figure adapted from reference 15.

1.2) Dirhodium catalysts

The Davies group has developed a series of dirhodium catalysts with different selectivity profiles. Representative examples of the key catalysts are shown in Figure 1.2.1. These catalysts are very effective at catalyzing the loss of nitrogen from diazo compounds to form rhodium carbene intermediates (Figure 1.2.2).

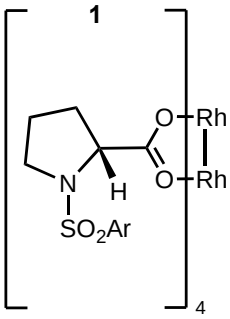

Rh_2(*R*-DOSP)$_4$

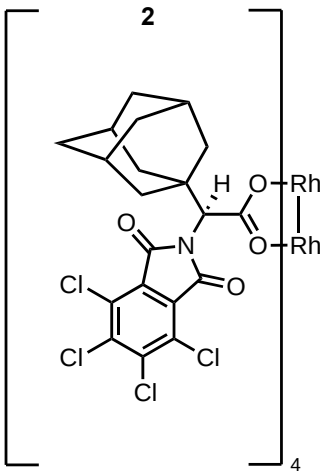

Rh_2(*S*-TCPTAD)$_4$

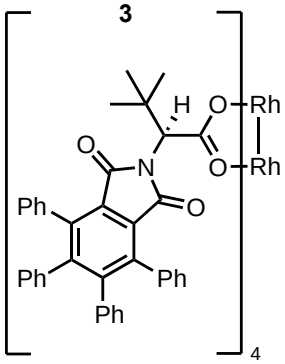

Rh_2(*S*-TPPTTL)$_4$

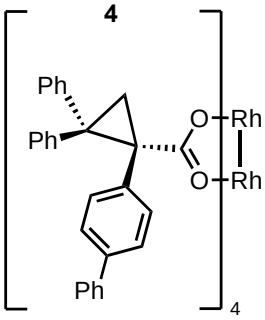

Rh_2(*S*-*p*-Ph-TPCP)$_4$

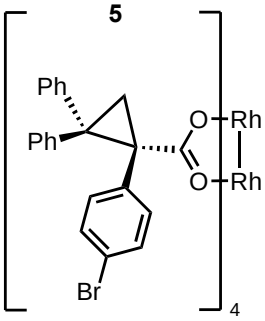

Rh_2(*S*-*p*-Br-TPCP)$_4$

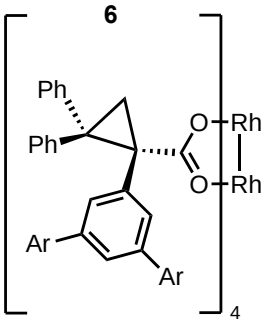

Rh_2(*R*-3,5-di(*p*-^{t}BuC$_6$H$_4$)-TPCP)$_4$

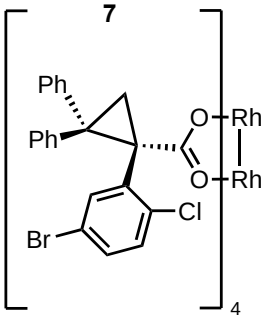

Rh_2(*S*-2-*o*-Cl-5-Br-TPCP)$_4$

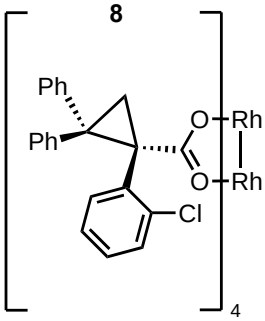

Rh_2(*S*-*o*-Cl-TPCP)$_4$

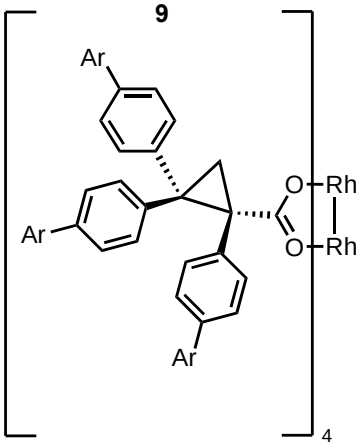

Rh_2(*R*-tris(*p*-^{t}BuC$_6$H$_4$)-TPCP)$_4$

Figure 1.2.1 The structure of several dirhodium catalysts.

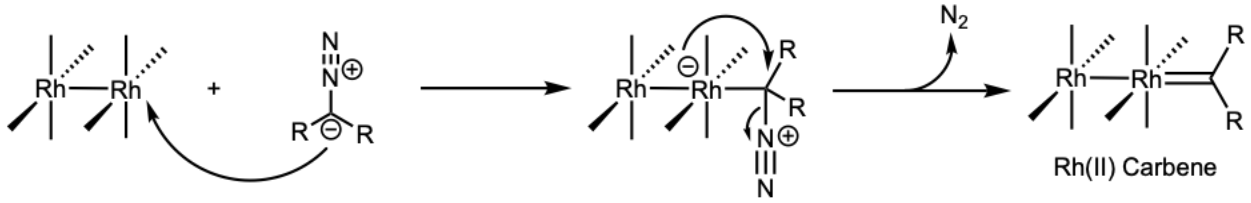

Figure 1.2.2 The formation of the rhodium carbene from a diazo group.

As dirhodium catalysts utilize the diazo group to create a reactive intermediate, a lot of work has been done to optimize the stability and reactivity of these compounds. Three major classes of diazo compounds have been developed (Figure 1.2.3.). Specifically, the Davies group utilizes "donor-acceptor" diazo compounds, which contain an electron donating group, like an aromatic system, and an electron withdrawing group, like an ester on either side of the diazo. Donor/acceptor diazo compounds are safer, easier to prepare, and are unique for giving a higher enantio- and site- selectivity amongst the various classes of diazo compounds. The development of this particular kind of diazo compound has allowed rhodium catalysts to be more widely utilized by the pharmaceutical industry. [15]

Major classes of rhodium carbenes

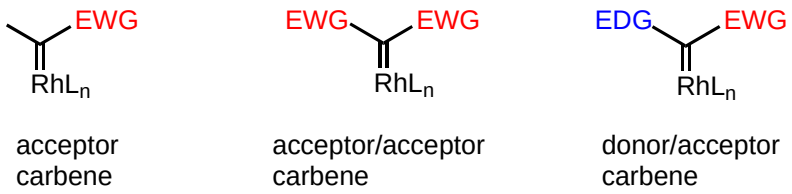

acceptor carbene | acceptor/acceptor carbene | donor/acceptor carbene

EWG= CO2R, COR, CN, PO(OR)2, SO2R, CF3
EDG= vinyl, aryl, heteroaryl, alkynyl

Figure 1.2.3: The general structure of rhodium carbenes. Figure adapted from reference 4.

Seen in Figure 1.2.3 is a key limitation of rhodium catalysis: it requires the use of a unique starting materials. Each class of carbene carries drawbacks, and rhodium catalysts rely on their properties to achieve selectivity. Acceptor carbenes are highly reactive but not very stereoselective while donor only carbenes tend to react less aggressively but are more selective. Donor/acceptor carbenes approach the goldilocks zone between reactivity and selectivity.

To manipulate how these diazo compounds react, the structure of the dirhodium catalyst needs to be able to balance the high reactivity of these compounds, and the low reactivity of the C-H bonds into which they insert. Some rhodium catalysts, like $Rh_2(TPPTTL)_4$ have a bowl-like shape (C_4 symmetry), where the reaction happens inside the bowl created by the ligands. The other side of the catalyst is blocked from reactivity by part of the ligand, in TPPTTL's case the sterically bulky ^{t}butyl amino acid. Altering the structure of the chiral ligands allows for manipulation of the diazo compound and the reactive trap as they enter the catalyst active site. The Davies group is known for using dirhodium catalysts that are able to perform a wide variety of carbene reactions with high site- and stereoselectivity. Two such reactions are cyclopropanations and C-H functionalizations. Both reactions, when performed by catalysts with chiral ligands, are performed with high stereo- and regioselectivity.

1.3) C-H Functionalization

Typically, when organic chemists attempt to synthesize a target molecule, they look at the reactive functional groups that can be easily manipulated. However, due to their higher reactivity, functional groups can interfere with future steps in a total synthesis and potentially make a molecule more difficult to work with. In the paradigm of C-H functionalization, organic chemists are able to directly activate typically inert C-H bonds. The utilization of a catalyst allows chemists to use fewer steps and forgo classically dangerous reactants.

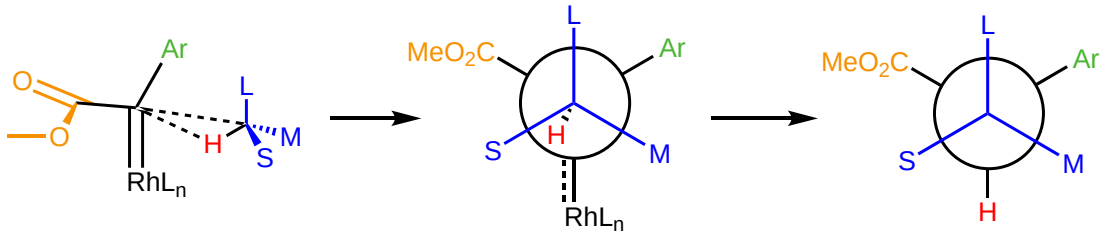

Figure 1.3.1 A visualization of the rhodium carbene as it inserts into a C-H bond. Reproduced from reference 4.

Figure 1.3.1 shows the unique way C-H bonds are forced to interact with the rhodium carbene. This conformation is forced due to the structure of the ligands attached to the ligand. This selective approach allows for the carbene to functionalize C-H bonds with high selectivity. The Newman diagram in Figure 1.3.1 shows the large group "L" avoiding the bulky rhodium catalyst, while the medium and small groups are oriented through interactions with the ligand structure.

The Davies group has pioneered several dirhodium catalysts that are each designed to target different C-H bonds in molecules. The Davies group has several collaborations with pharmaceutical companies like AbbVie and Novartis, to use this toolbox of catalysts to target different C-H bonds in different molecular environments.

Diagramed in Figure 1.3.2 are published C-H functionalization reactions that each catalyst is able to target. Through changes in structure, the Davies group is able to select different C-H

bonds on the same molecule. Catalyst **9** prioritizes the most accessible primary C-H bond, catalyst **7** can target secondary C-H bonds, and catalyst **7** targets a tertiary C-H bond. One of the more groundbreaking reactions is catalyst **3**'s functionalization of ^{t}butyl-cyclohexane; this catalyst is named $Rh_2(TPPTTL)_4$, and through optimization of its ligand structure, the Davies group could expand its reactivity into new chemical space.

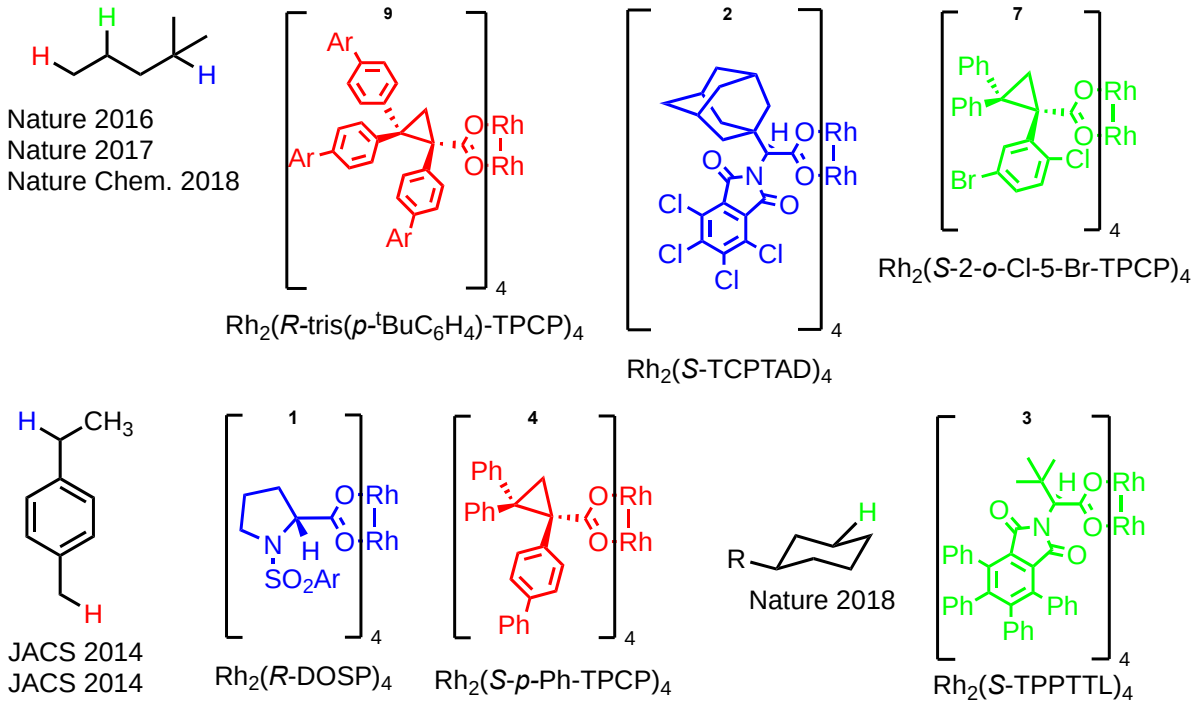

Figure 1.3.2 The different C-H bonds targeted by the Davies group dirhodium catalysts. Note the ability to differentiate between different C-H bonds on the same molecule.

1.4) The $Rh_2(TPPTTL)_4$ Catalyst

One of the more recent advancements in catalyst technology was with the $Rh_2(TPPTTL)_4$ catalyst. A PhD student in the Davies Group, Jiantao Fu, was able to use the $Rh_2(TPPTTL)_4$ to directly functionalize a specific hydrogen bond on the ^{t}butyl-cyclohexane system. His research showed that this dirhodium catalyst could distinguish, not only between the carbons in the

cyclohexane ring, but between the equatorial and axial C-H bonds. While the ligands on this catalyst are extremely large and decrease the speed at which reactions occur, they allow for greater selectivity. The extreme steric demand of the bowl enables classical Rh-carbenoid chemistry to be performed with unparalleled site- and stereo-selectivity. This selectivity is owed to the steric and electronic nature of the catalyst, forcing substrates to enter with specific orientations

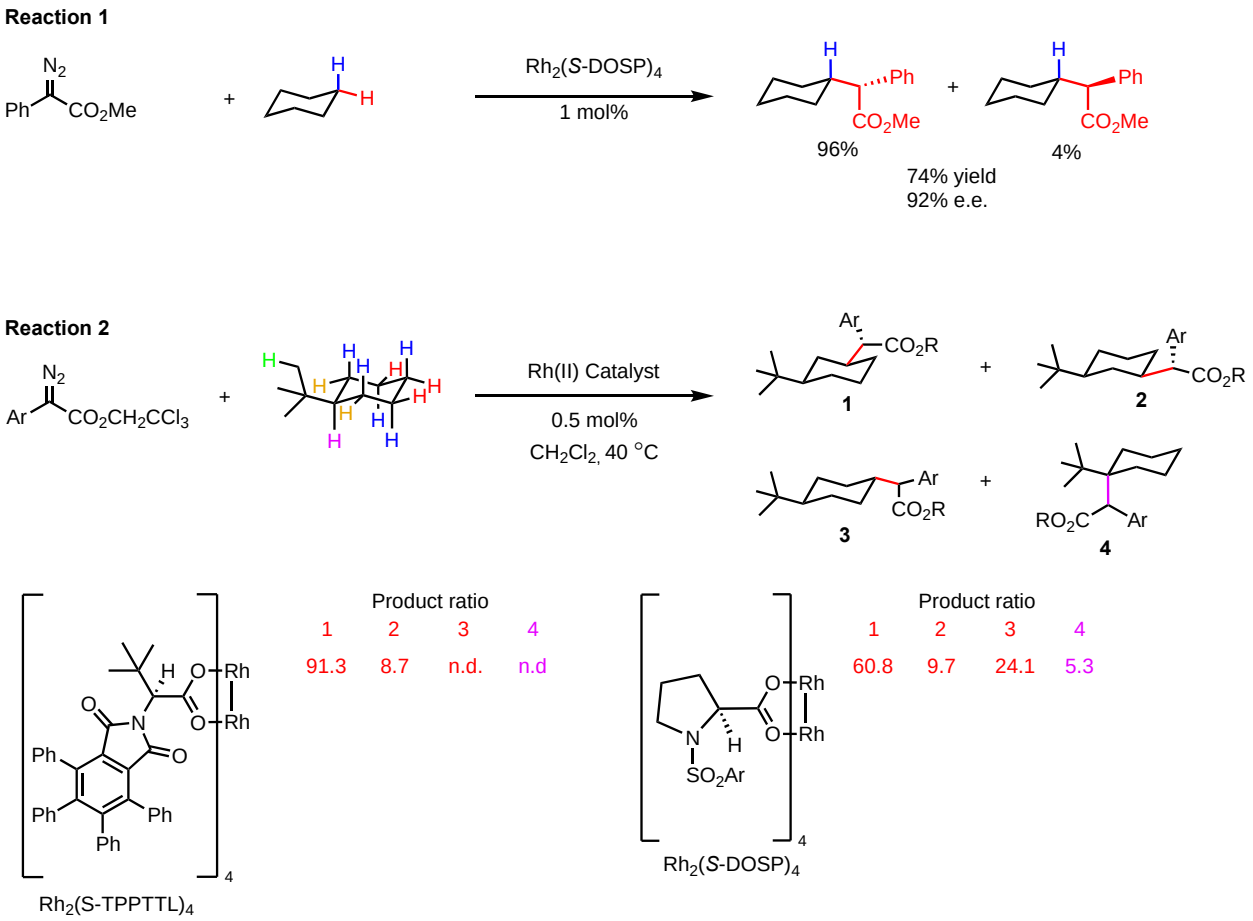

Figure 1.4.1 The structure and function of the Rh_2(*S*-TPPTTL)$_4$ catalyst compared to Rh_2(*S*-DOSP)$_4$. Adapted from reference 6.

Figure 1.4.1 demonstrates the high difference in site selectivity between Rh_2(*S*-DOSP)$_4$ and Rh_2(*S*-TPPTTL)$_4$ in their reaction with ^{t}butyl-cyclohexane. Rh_2(*S*-TPPTTL)$_4$ displayed 11:1 diastereoselectivity while Rh_2(*S*-DOSP)$_4$ showed a minor preference for diastereomer **1**.

The novel selectivity displayed by Rh_2(*S*-TPPTTL)$_4$ prompted further research into how its selectivity could be further manipulated. When studying the X-Ray crystal structure of the catalyst, it could be observed that the phenyl rings at the 5 and 6 positions of the phthalimido ligands were pointing their C3 and C5 hydrogens directly into the center of the catalysts bowl. Thus, due to the already selective nature of the Rh_2(*S*-TPPTTL)$_4$ catalyst, it would be interesting to append different groups onto those hydrogens that point towards the center of the catalyst bowl, potentially increasing the catalyst's selectivity by increasing its steric bulk. My goal was to alter those groups to study how changes to a C4-symmetric catalyst's structure can alter the way the dirhodium catalyst interacted with carbenes and C-H bonds.

2) Manipulating the TPPTTL ligand

2.1) Synthetic Scheme

The general approach for the synthesis of the desired catalyst is adapted from a synthetic scheme pioneered by Zachary Garlets, a post-doc at the Davies lab (Figure 2.1.1). The advantage of this approach is that highly functionalized derivatives can be prepared in which the desired functionality is introduced into the starting material or post modification after the catalysts is prepared.

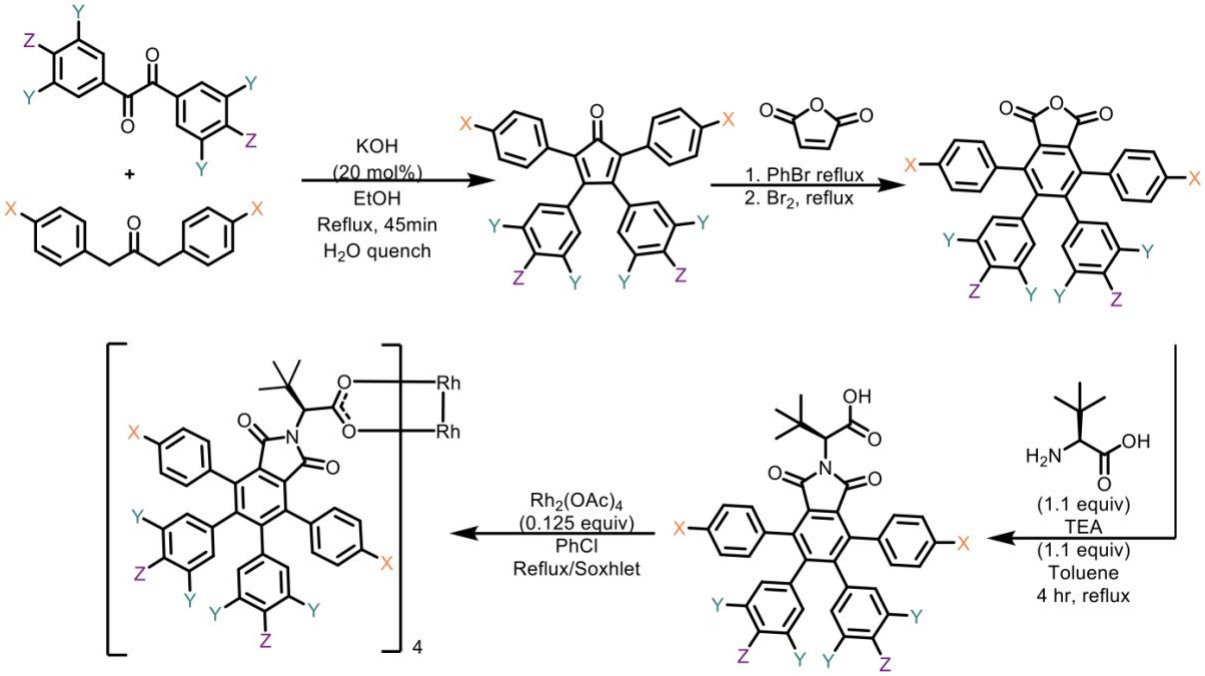

Figure 2.1.1 The synthesis of the Rh_2(*S*-TPPTTL)$_4$ catalyst. Note the X, Y, and Z groups, and the positions they correlate to on the final catalyst.

The synthesis devised by Garlets was designed to synthesize a catalyst that could be functionalized via Suzuki coupling on each phenyl ring. In Figure 2.1.1, this would involve placing a bromine at position **X** and **Z**. However, since a 16-fold-Suzuki coupling was unable to be performed on the catalyst in Figure 2.1.2, the starting materials were functionalized using a two-fold Suzuki coupling, and carried forward to the final catalyst.

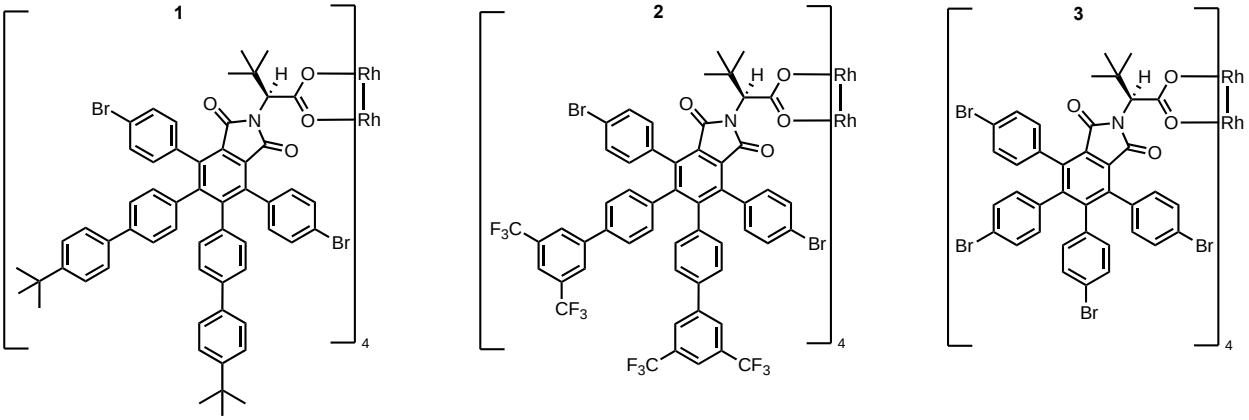

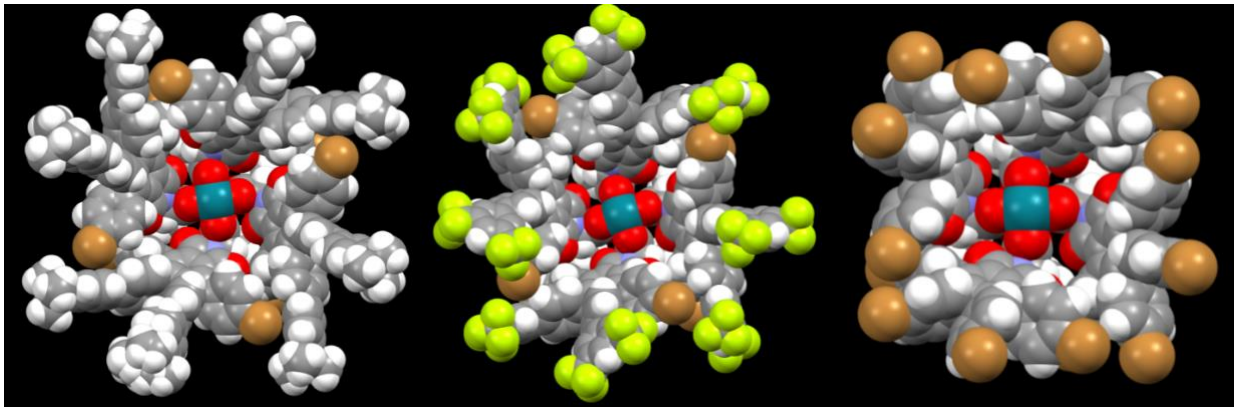

Catalyst **1** X-ray structure Catalyst **2** -ray structure. Catalyst **3** X-ray structure.

Figure 2.1.2 Catalysts synthesized by Zac Garlets.

The goal of this honors project is to make new bowl-shaped dirhodium catalysts and study their structures and their catalytic behavior. Garlets had found that a 16-fold Suzuki coupling was unable to be performed on catalyst **3** in Figure 2.1.2, and in order to make catalysts **1** and **2** it was necessary to introduce the functionality into the starting materials. The Suzuki couplings on these particular catalysts was believed to be unsuccessful, because of the inaccessible positions of the bromine atoms (brown atoms in Catalyst **1**, **2**, and **3**'s X-ray structures). To attempt to work around this synthetic challenge, my project began by preparing a catalyst with bromines only on the more exposed 5 and 6 phenyl rings, instead of all four phenyl rings (Figure 2.1.3), with the goal of achieving diversity by conducting late-stage functionalization of the preformed catalyst. With the bromines only at the 5 and 6 positions, the Suzuki coupling methodology would be easier for

palladium catalysts to access, allowing for easier access to more efficient manipulations of the Rh_2(*S*-TPPTTL)$_4$ catalyst.

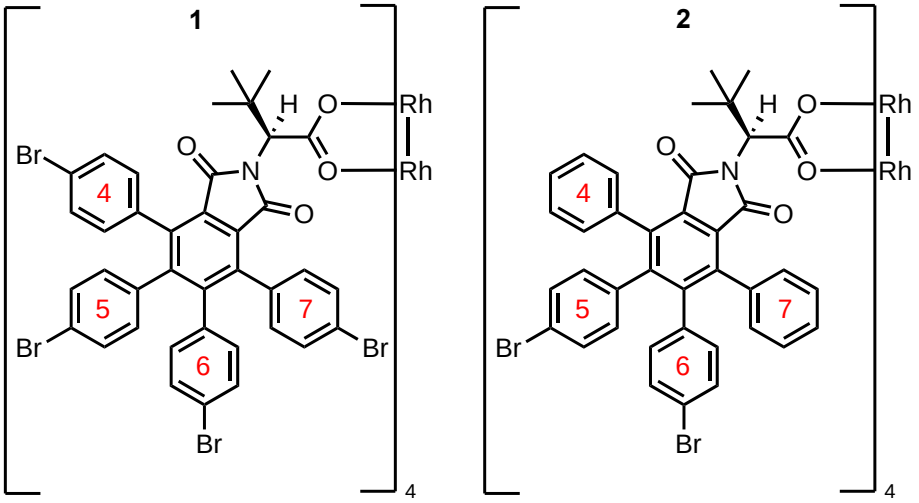

Figure 2.1.3 The difference in catalyst structure between Catalyst **1** and Catalyst **2**

2.2) Synthetic Steps

The first step in the synthesis was a direct functionalization of the benzil starting material to alter the final structure of the catalyst. This was done through a Suzuki-coupling reaction with a variety of boronic acids as illustrated in Figure 2.2.1. The starting material, di-bromo benzil is commercially available. These particular boronic acids were chosen due to their high steric bulk and competency in Suzuki cross-coupling. The yield of the *bis*-CF_3 boronic acid was particularly low, potentially due to the electron deficiency of the aryl system.

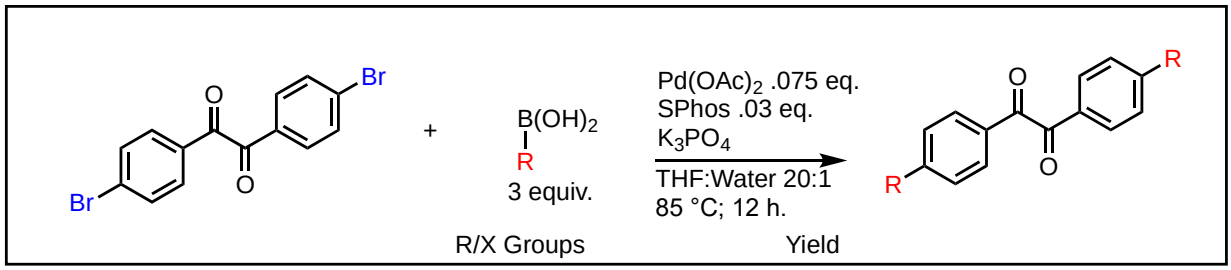

	R/X Groups	Yield
1 R=	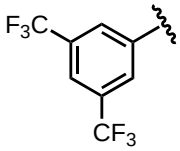	33%
2 R=	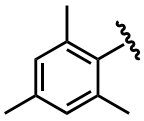	64%
3 R=	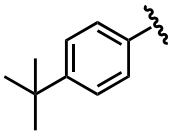	85%

Figure 2.2.1 The synthesis of the functionalized starting benzil.

The tetra-bromo benzil derivative would also be a useful starting material, but it is not commercially available. A challenging benzoin condensation from di-bromo benzaldehyde was applied to afford the desired starting material. Benzoin condensations are notoriously difficult reactions to perform, as they involve either the use of a cyanide-based catalyst, or a Vitamin B1 catalyst (**4**, **2** Figure 2.2.2). The reaction required the careful titration of the solution over the course of 30 min until the pH was exactly 9. The workup required a long aqueous workup involving ethyl

acetate, and the products were incredibly difficult to both isolate and purify. After around thirty attempts of this reaction, a careful methodology was devised to give above a 60% yield (**4,** Figure 2.2.2). A Suzuki-coupling was performed on this starting material was also attempted; however, the yield was too low to merit continuation in that direction (**1,** Figure 2.2.2).

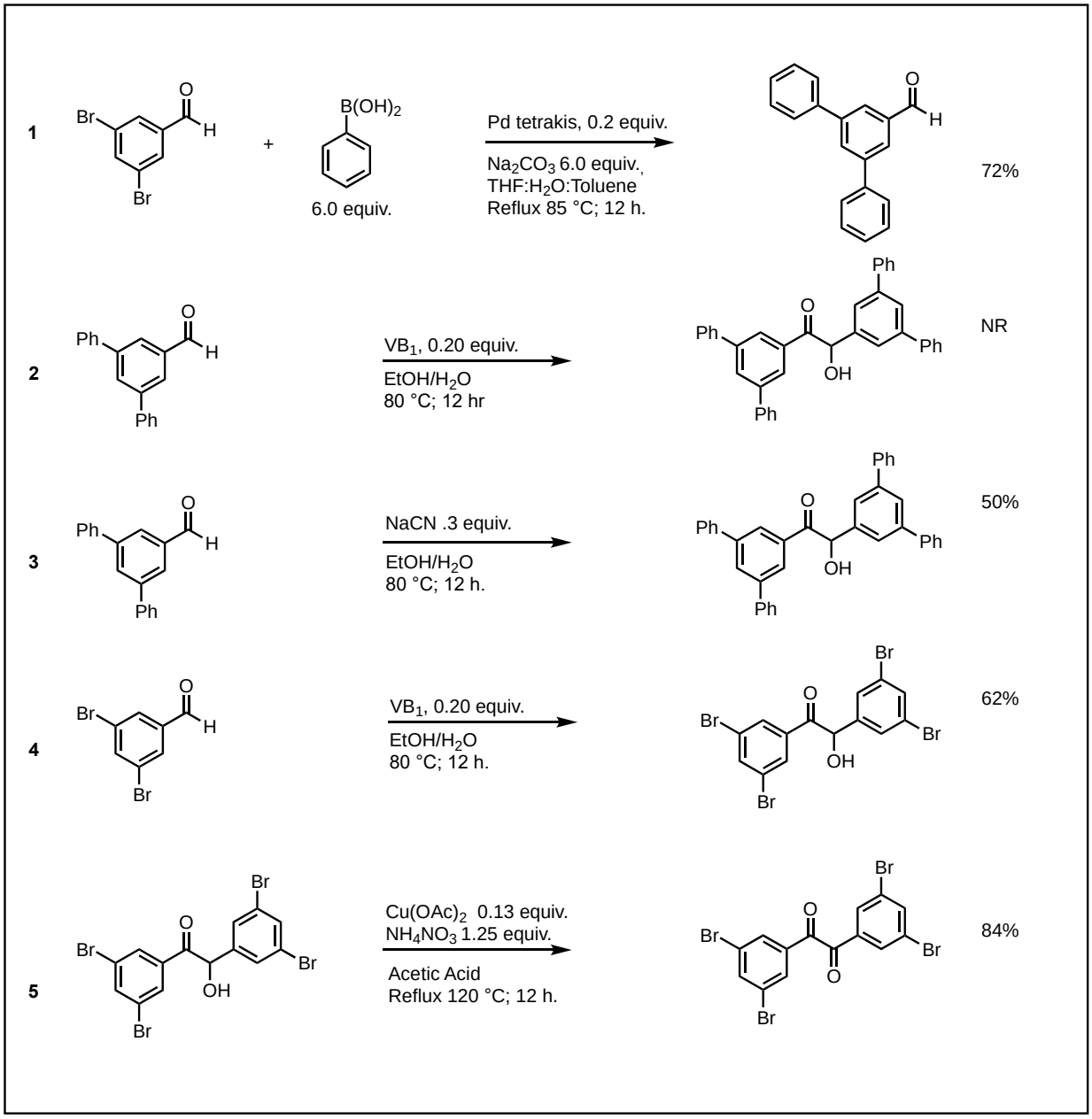

Figure 2.2.2 The attempted synthesis of a tetra-phenylated starting benzil.

Unfortunately, the only successful reaction involved the use of cyanide and was unsafe to utilize on a larger scale (**3**, Figure 2.2.2). After the unsuccessful synthesis of the tetra-phenyl benzil, the tetra-bromo benzil was carried through to the final catalyst with the potential for late-stage derivation via exhaustive Suzuki-coupling that had been previously performed on other rhodium (II) catalysts.[16]

The second step in the synthesis of the catalysts was a Knoevenagel condensation, requiring the reflux of the two starting materials in KOH and ethanol to afford a tetra-arylated cyclopentadienone (Figure 2.2.3).

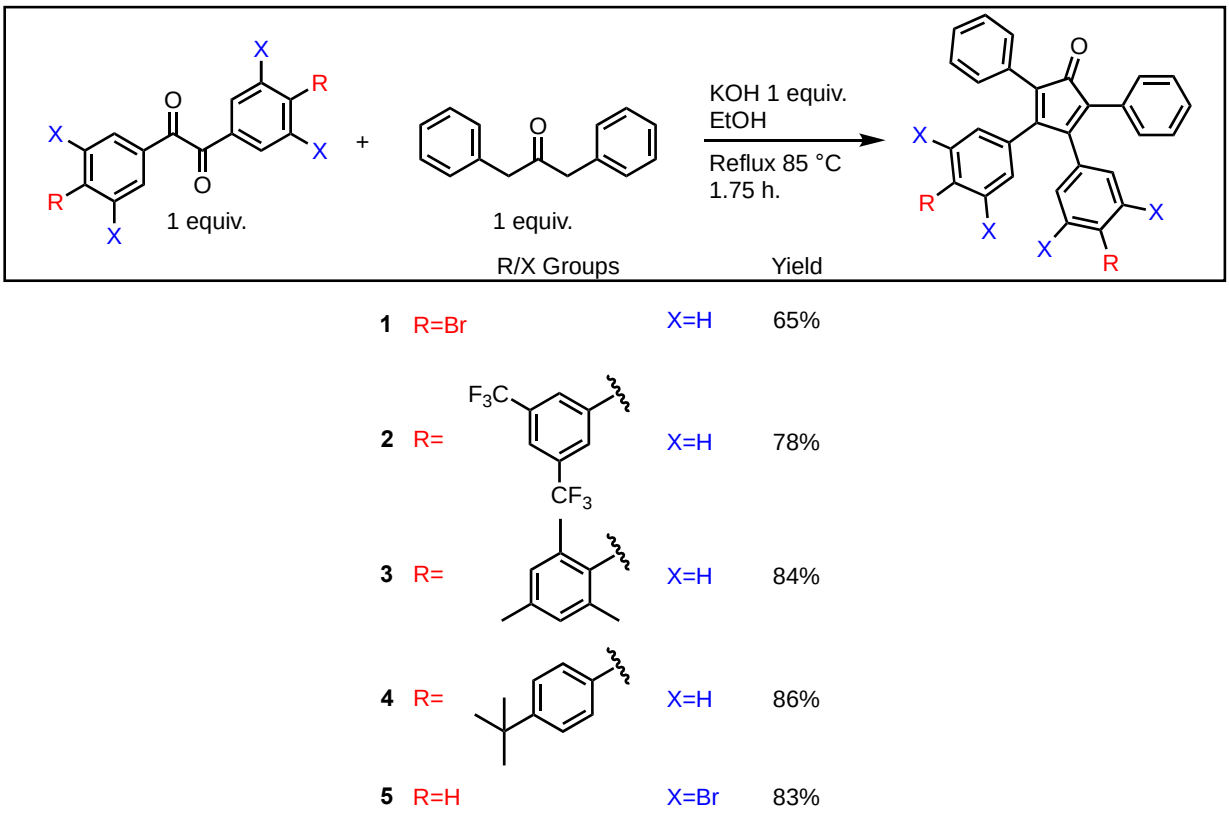

Figure 2.2.3 The Knoevenagel condensation and its yields.

The yields were consistently high across a broad array of benzoin starting materials (Figure 2.2.3). The primary methodology suggested to cool the resulting solution in an ice bath; however, a higher yield resulted from quenching the solution with water, then filtering with cold

ethanol. This gave higher yields (up to 86%) than had been previously seen. The reaction results in the production of a cyclopentadiene-one, which can then be used in a Diels-Alder reaction.

The third and fourth step of the synthesis were performed sequentially in one-pot sequence. A Diels-Alder was performed with maleic anhydride, the product of which was directly oxidized with elemental bromine to afford the desired phthalic-anhydride (Figure 2.2.4).

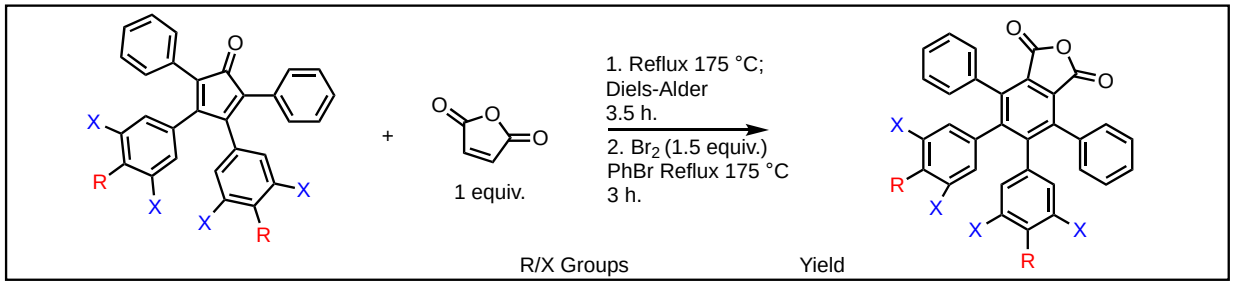

	R/X Groups		Yield
1	R=Br	X=H	72%
2	R= 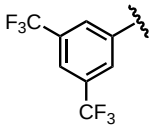	X=H	43%
3	R= 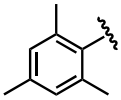	X=H	54%
4	R= 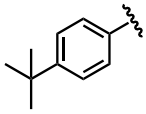	X=H	38%
5	R=H	X=Br	42%

Figure 2.2.4 The tandem Diels-Alder/oxidation and corresponding yields.

The Diels-Alder-oxidation required a significant amount of alteration due to its typically low yields. There were problems with the product's high solubility in bromobenzene and required removal of some of the solvent before filtering and washing with petroleum ether. To solve the solubility issues, the bromobenzene was partially distilled off until the solution was a brown paste, then the resulting product was washed thoroughly with petroleum ether. The bromine oxidation involved significant safety concerns involving quenching the fumes in a thiosulfate bath, but these were taken in stride and the reaction was routinely performed without incident.

The last step in the synthesis of the ligand induced the stereochemistry of the catalyst. This was achieved through condensation with of L-tert-Leucine, a chiral material to afford the carboxylate ligand (Figure 2.2.5).

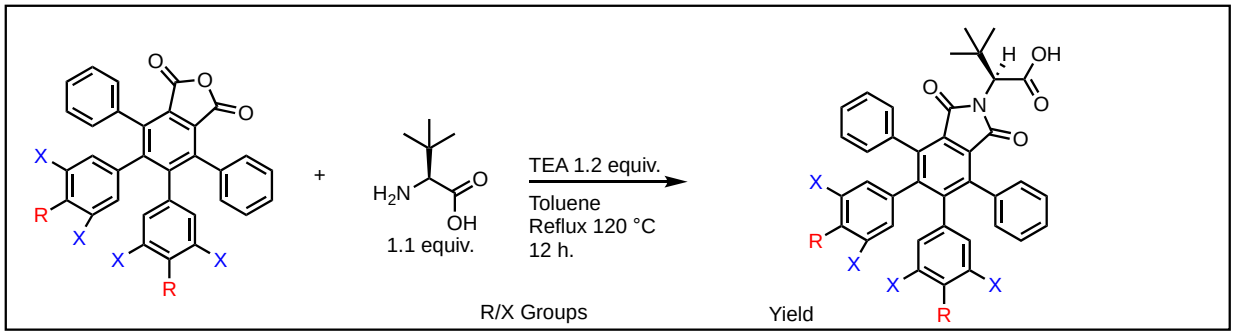

	R/X Groups		Yield
1	R=Br	X=H	84%
2	R= 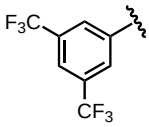	X=H	73%
3	R= 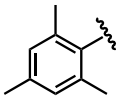	X=H	82%
4	R= 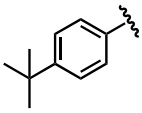	X=H	77%
5	R=H	X=Br	67%

Figure 2.2.5 The amino acid condensation and its yields.

The challenge of the amino acid condensation revolved around the solubility of both the amino acid and the phthalic anhydride in toluene. Better yields resulted from placing the solution, under argon, into the sonicator to break up the solids. The product was columned in hexanes and ethyl acetate (0-20% EtOAc/hexanes) to ensure purity before the ligand exchange.

The final step in the synthesis of the catalyst was the ligand exchange (Figure 2.2.6). The ligand transfer required a soxhlet in the presence of potassium carbonate. The carbonate acts as sponge for the acetate originally associated with the rhodium to guarantee that the novel ligand associates to the rhodium.

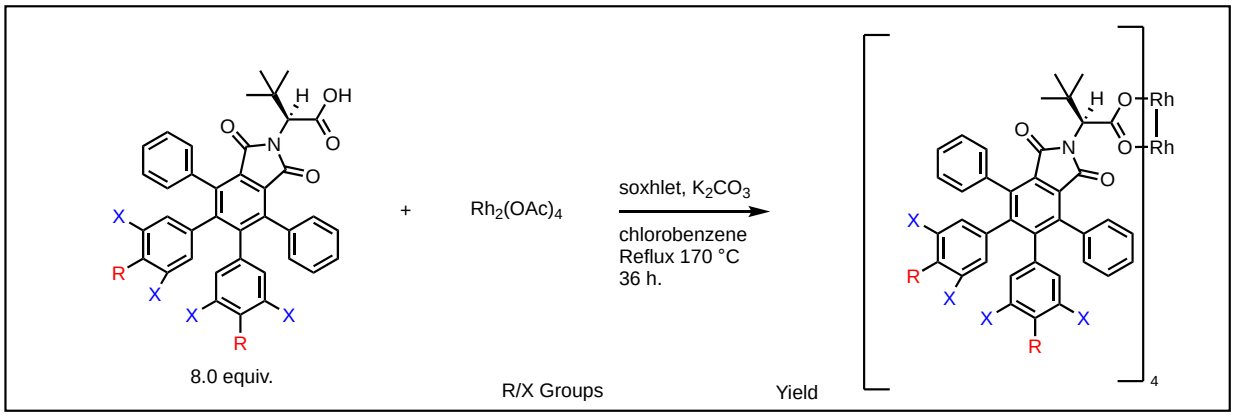

	R/X Groups		Yield
1	R=Br	X=H	89%
2	R= 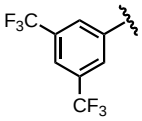	X=H	84%
3	R= 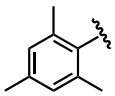	X=H	NR%
4	R= 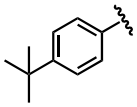	X=H	91%
5	R=H	X=Br	82%

Figure 2.2.6 The ligand transfer reaction to synthesize various TPPTTL variants

After a successful ligand transfer, the product was columned in hexanes and ethyl acetate (0-20%), without much difficulty. Of the 5 catalysts attempted, 4 were able to be synthesized through this method. Attempts to prepare the mesityl catalyst were unsuccessful, and its synthesis was not confirmed. The characterization of these catalysts was done in a combination of NMR, Mass Spec, and X-ray crystallography.

However, derivatization of the starting materials is not the most efficient way to synthesize a wide variety of catalysts. This is due both to the poor reactivity of sterically the bulky benzil and related downstream products. The most efficient method for functionalizing these catalysts would be to synthesize a brominated variant, then branch out into an entire library of functionalized catalysts through multi-fold Suzuki-coupling.

2.3) Preparation for Manipulation via Suzuki Coupling

To efficiently create a large variety of catalysts, a synthesis was done of a catalyst with bromines located at the positions delineated in Figure 2.3.1 to create a scaffold amenable to Suzuki-coupling. To this end, the first catalyst synthesized was a *para*-bromo variant of the classic $Rh_2(TPPTTL)_4$ catalyst.

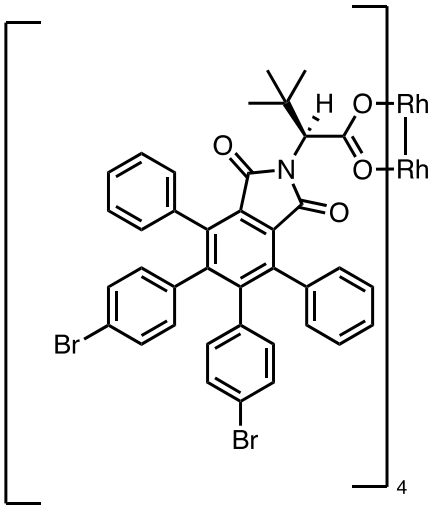

Figure 2.3.1 The first catalyst synthesized: Rh_2(*S*-*p*-Br-TPPTTL).

From this catalyst, the plan was to use Suzuki coupling to further functionalize the catalyst; the first methodology attempted was one designed by Zachary Garlets, a post doc specializing in palladium cross-coupling. After attempting the synthesis multiple times (Figure 2.3.2), utilizing microwave technology, different solvent systems, different ratios, and different ligands like tetrakis, the Suzuki-coupling on the final catalyst had little success. Since the Suzuki coupling failed, the only way to alter the final structure of $Rh_2(TPPTTL)_4$ with two internal aryl groups would be to incorporate these aryl groups into the structure of the starting materials.

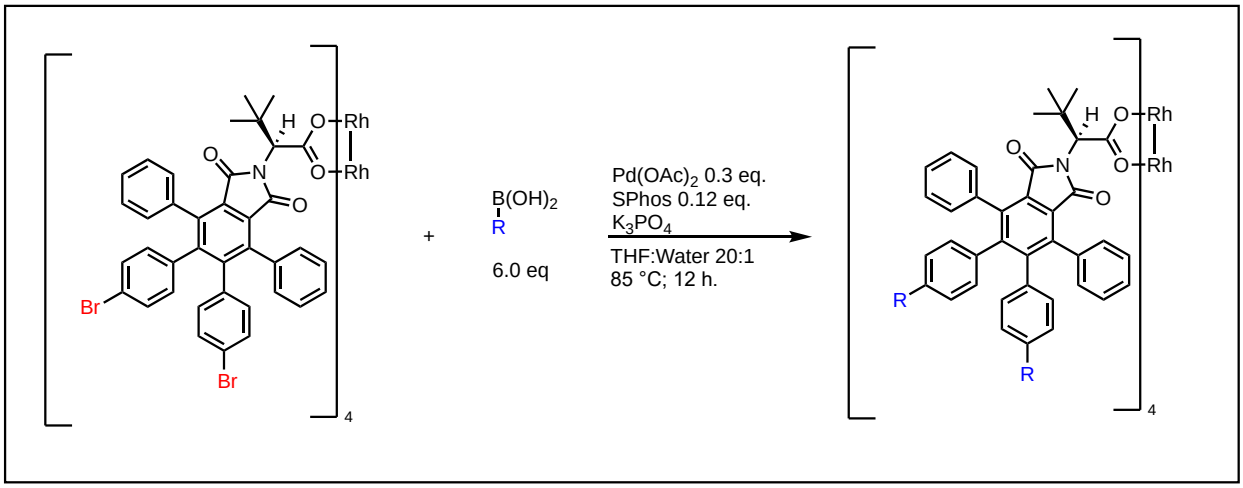

Figure 2.3.2 Using SPhos, a Buchwald ligand, no reaction was achieved with any aryl boronic acid.

2.4) Suzuki Coupling Methodology

The attempts to perform the Suzuki coupling failed until Yannick Boni, a PhD student in the lab found a palladium system that successfully completed a 16-fold Suzuki coupling on a brominated derivative of $Rh_2(NTTL)_4$, a similarly crowded catalyst.

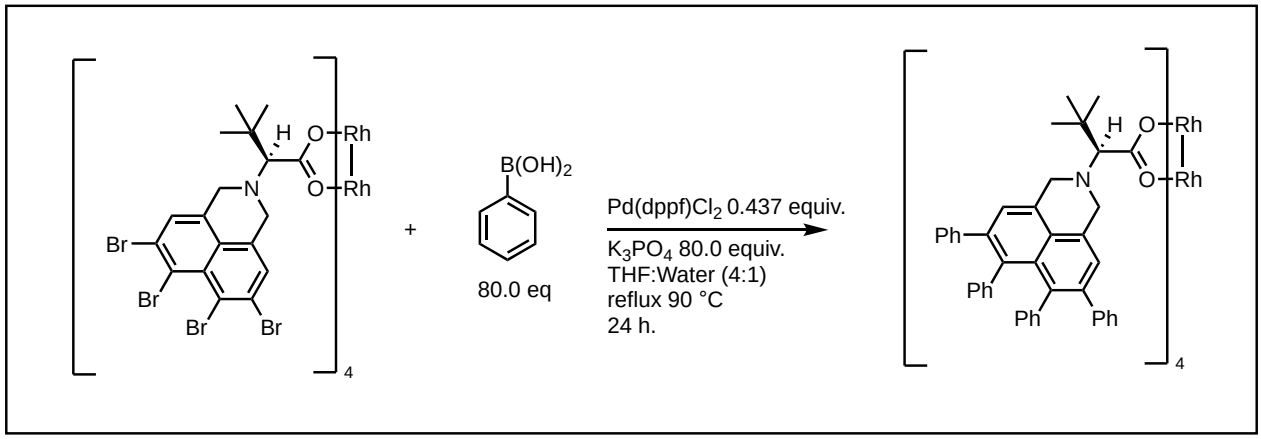

Figure 2.4.1 A successful 16-fold coupling using $Pd(dppf)Cl_2$. The reaction merited a 42 percent yield.

Following the success of a 16-fold Suzuki-coupling on a sterically hindered catalyst (Figure 2.4.1), a series of 16-fold and 8-fold Suzuki couplings were performed on the existing, brominated TPPTTL derivatives.

With catalysts previously designed, their selectivity in several reactions suggested that bromines on the catalyst had the potential to negatively affect the reactivity of the dirhodium system. Thus, the first priority was to perform a basic Suzuki coupling on the catalysts to see how that altered their reactivities. This was achieved through the use of phenylboronic acid. Phenyl boronic acid was chosen because it would have a significant steric impact on the catalyst, while it will not alter the electronics of the catalyst.

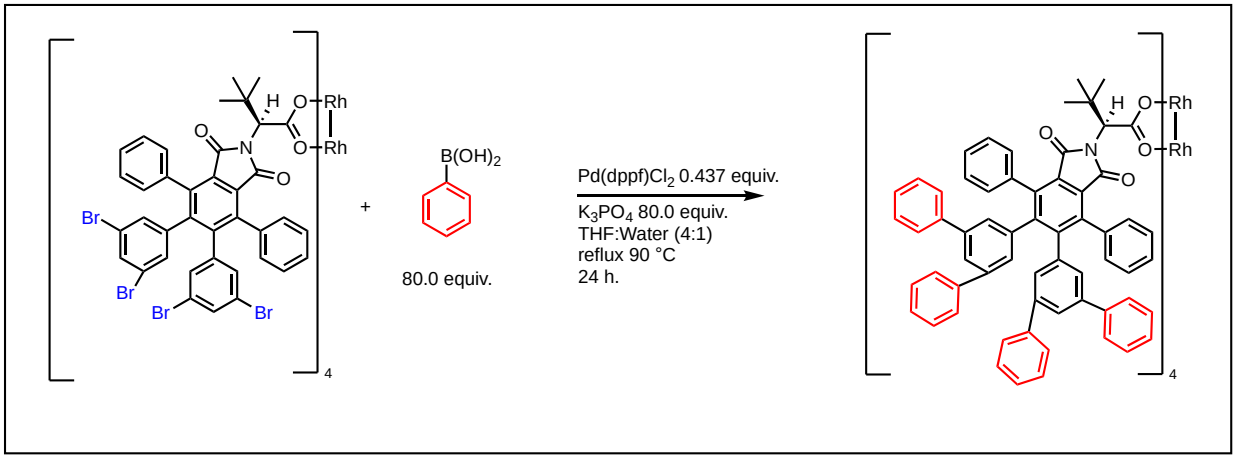

Figure 2.4.2 The successful 16-fold coupling of the tetra-brominated TPPTTL catalyst. A yield of 38% was obtained.

Following this success of the phenylated boronic acid in Figure 2.4.2, the same methodology was attempted on the di-brominated TPPTTL catalyst, except with a larger species of boronic acid was investigated in an attempt to generate more interesting derivatives. This new species of boronic acid was a bis-CF_3 a boronic acid that merited interesting results with its selectivity in the *para*-bis-CF_3 variant.

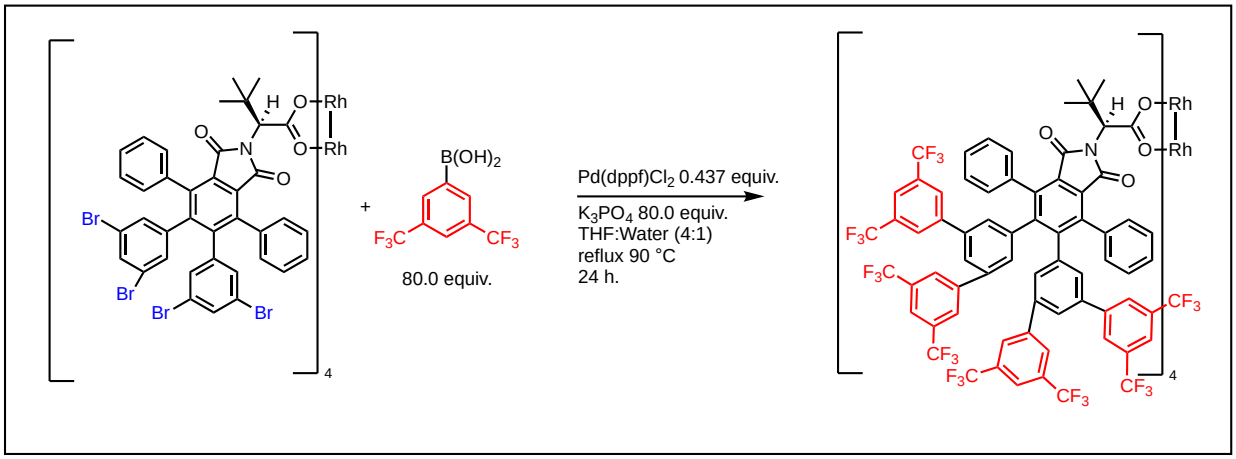

Figure 2.4.3 The successful 16-fold coupling of the tetra-brominated TPPTTL catalyst. A yield of 27% was obtained.

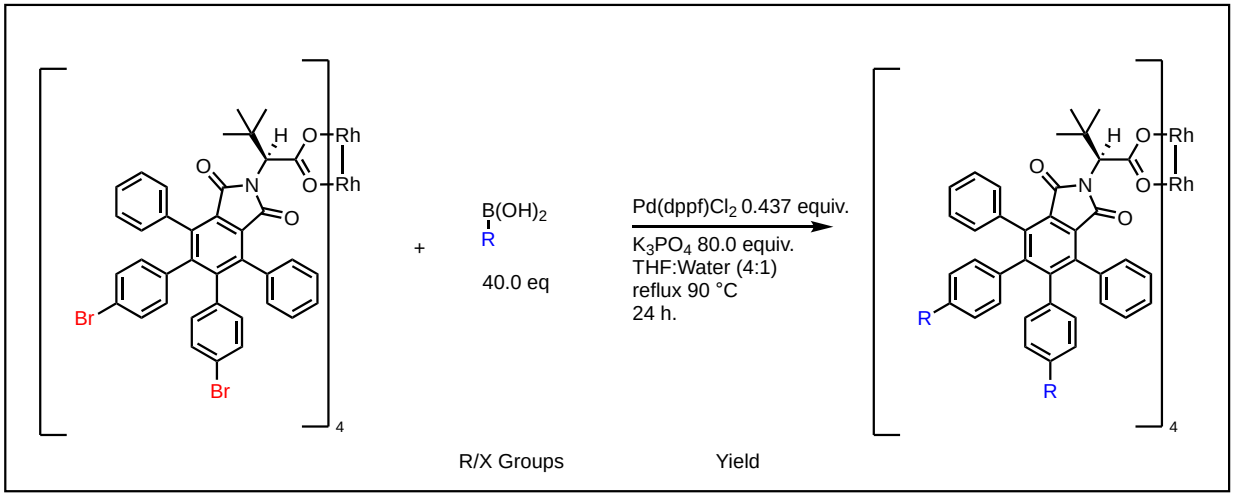

R/X Groups		Yield
R=	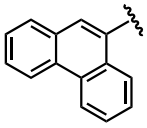	NR
R=	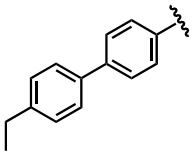	NR
R=	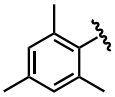	28%
R=	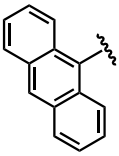	NR

Figure 2.4.4 The various boronic acids attempted to couple to the para-Br catalyst.

Based on the results seen in Figure 2.4.4, it appears that coupling bulkier boronic acids are difficult to use in the existing methodology.

3) Catalyst Characterization

An important part of this research program is to understand the structure and function of the catalysts. Valuable information about the structure of the catalysts can be obtained by proton NMR, mass spectrometry and X-ray crystallography. Below is presented some of the key structural information that has been obtained for the newly prepared catalysts.

3.1) NMR

Since the catalysts adopt C4 symmetry, meaning, if you rotate the structure 90°, it will overlap directly with itself, the catalysts have the potential to be identified through NMR spectroscopy. The more symmetrical the catalyst, the more uniform the NMR peaks will be.

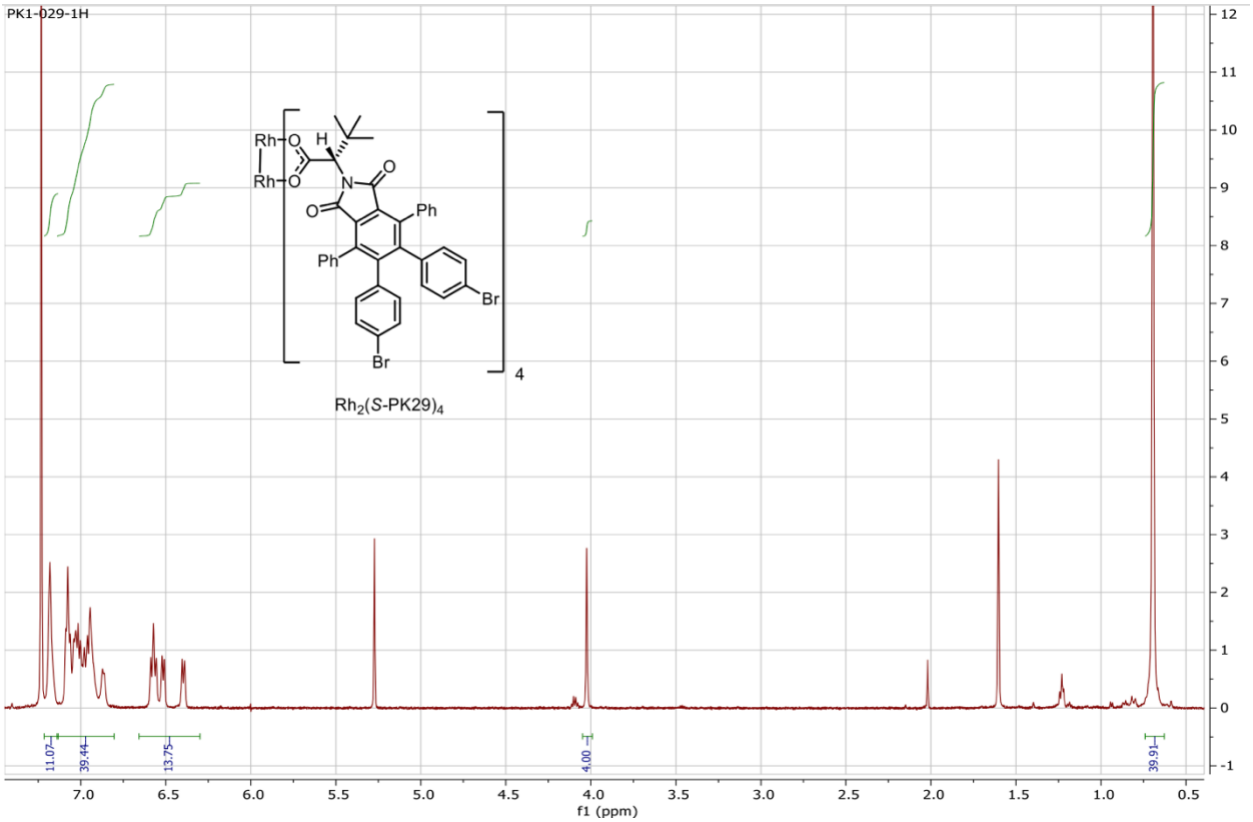

Figure 3.1.1 NMR of the Rh_2(*S*-*p*-Br-TPPTTL)$_4$ catalyst.

The Rh_2(*S*-*p*-Br-TPPTTL)$_4$ variant of the catalyst displayed very high C4 symmetry and had a splitting pattern that correctly numbered the hydrogens contained in the catalyst.

3.2) X-ray Crystallography

An X-ray structure is the best way to confirm the structure of the catalyst. Not only does it affirm the overall constitution of the catalyst, but it also identifies the degree to which the catalyst adopts C4 symmetry.

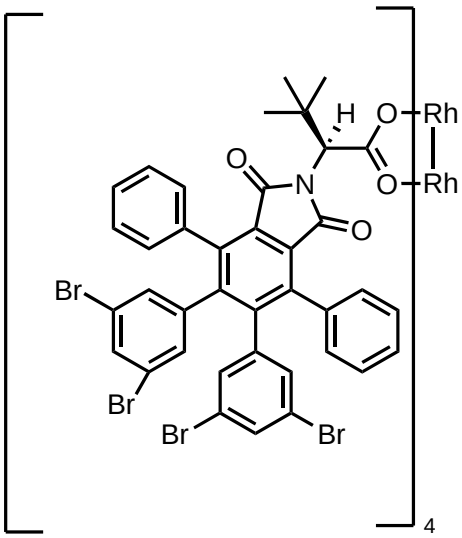

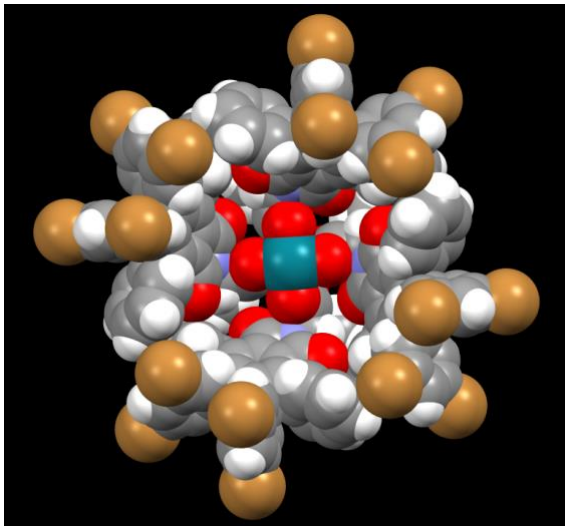

Figure 3.2.1 An X-ray structure of the Rh_2(*S-3,5-m*-Br-TPPTTL)$_4$ catalyst

While an X-ray structure is ideal, several catalysts are difficult to crystalize, leading to the use of a variety of techniques to assist in crystallization. This includes vapor diffusion crystallization, a solvent layering, and slow cooling. Solvent layering merited the highest success with benzene as the solubilizing medium, and hexanes as the crystallization phase. However, some catalysts were soluble in hexanes, making their crystallization difficult.

3.3) Mass Spectrometry

Mass Spectrometry is most reliable option for characterizing the catalysts. It only requires a nanogram amount of the material and can confirm the presence of the catalyst. However, because it will recognize even the smallest amount of catalyst, it is not a good test for the quality or the purity of the catalyst.

Peak Mass	Display Formula	RDB	Delta [ppm]	Delta [mmu]	Theo. mass	Combined Score	MS Cov. [%]
3408.34293	$C_{224}H_{201}O_{16}N_4{}^{103}Rh_2$	128.5	8.42	28.71	3408.31422	96.09	99.67

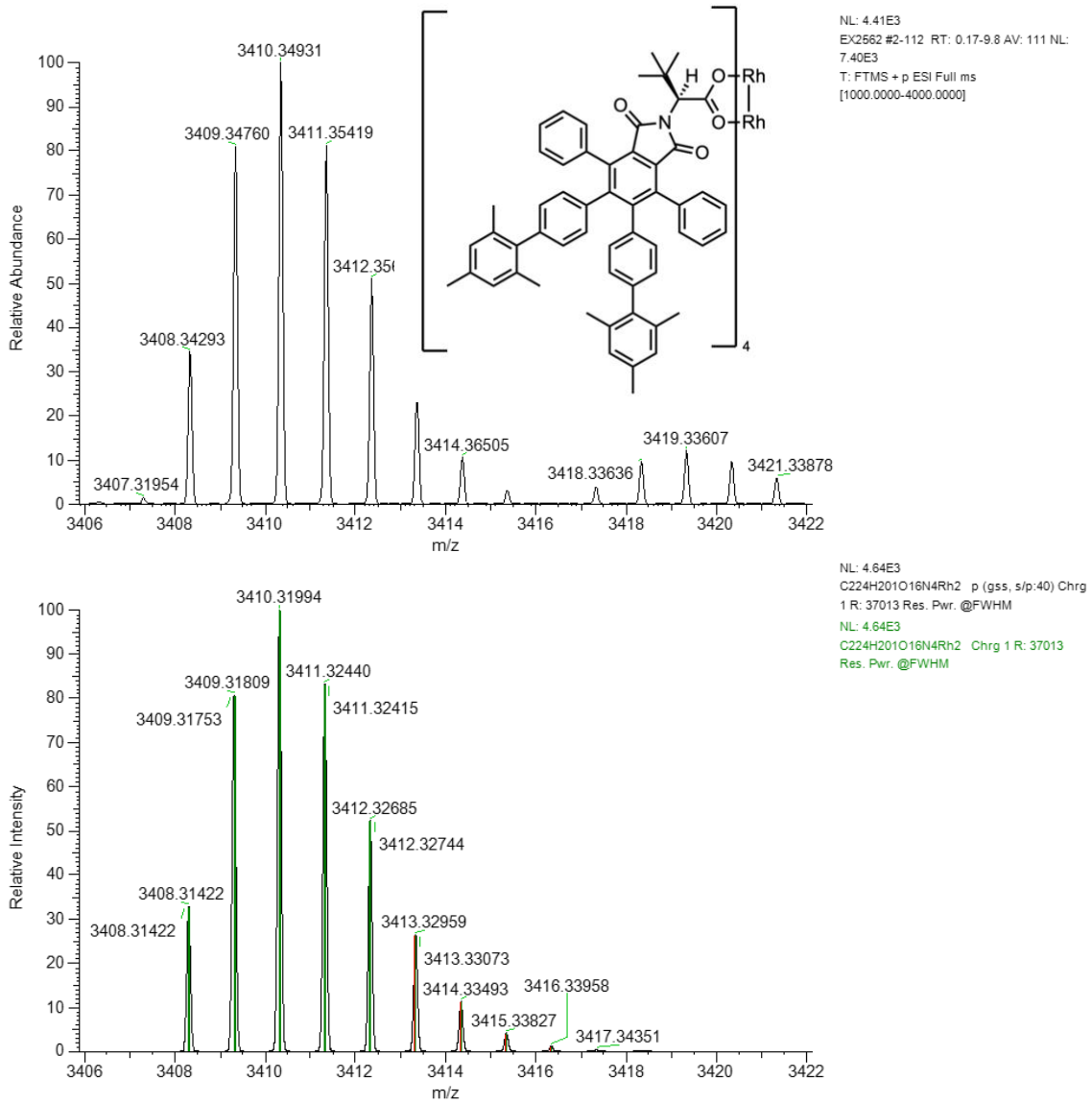

Figure 3.3.1 The mass spectrometry data for the Rh_2(*S*-*p*-mesityl-TPPTTL)$_4$ Catalyst

The Rh_2(*S*-*p*-mesityl-TPPTTL)$_4$ Catalyst has a theoretical molecular mass of 3408.31 g/mol, and adjusting for isotope effects with a peak reading of 3408.34 g/mol, there is a 99.67% likelihood of a successful synthesis. The values are not perfect due to fragmentation and isotope

effects. It is worth noting that no catalyst that was a product of Suzuki coupling had exposed, unreacted bromines in the mass spectrum.

4) Assessing the Selectivity of the TPPTTL Variants

With every manipulation of the $Rh_2(TPPTTL)_4$ catalyst, it was important to assess any changes in selectivity. To this end, a series of benchmark reactions were designed, some of them represent highly efficient transformations conducted by $Rh_2(TPPTTL)_4$ catalyst, and others have yet to be performed with any degree of selectivity. Each of these reactions are listed in Figure 4.1.1.

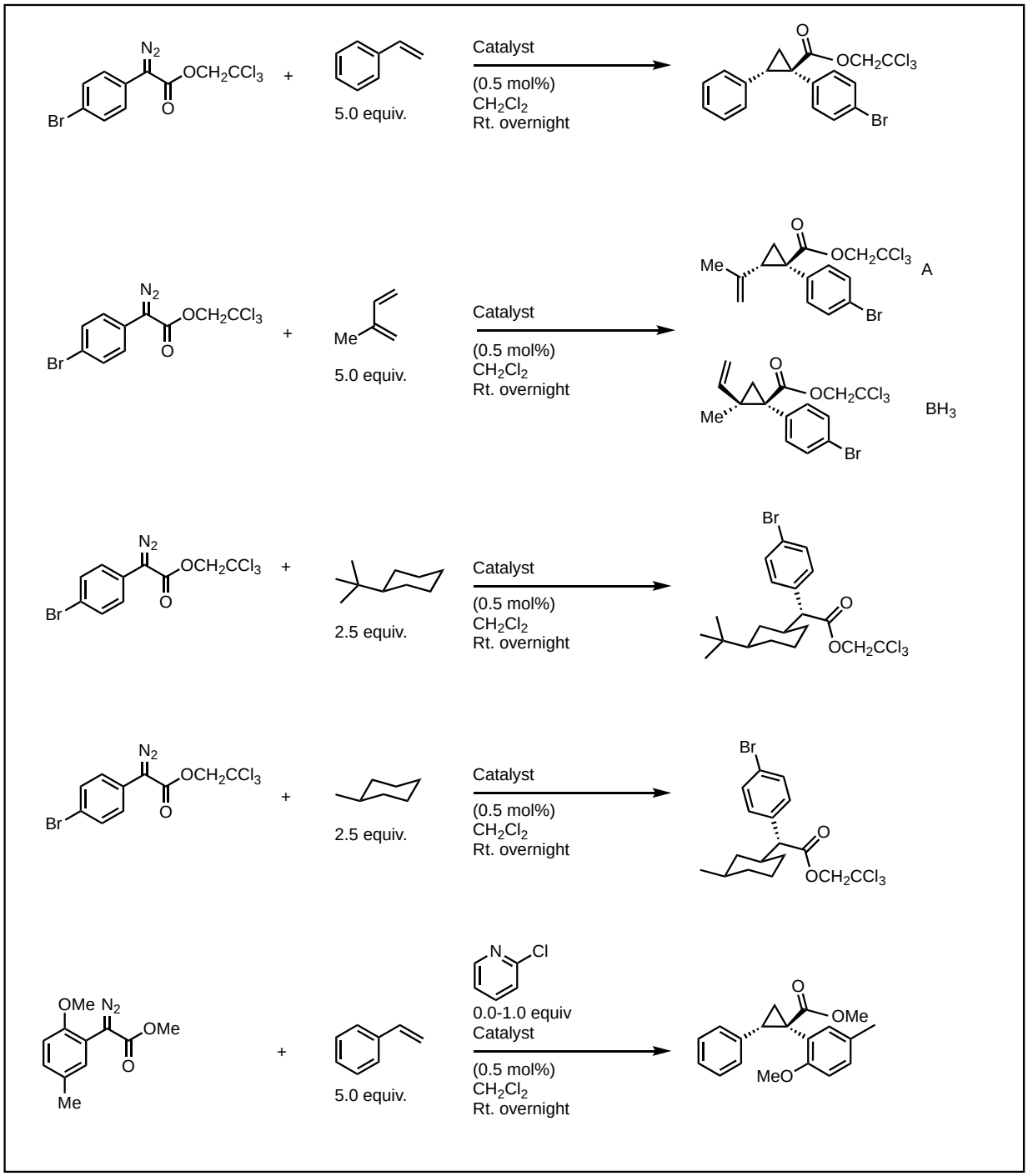

Figure 4.1.1 The reaction screen for the TPPTTL derivatives.

As a comparison for each of the newly synthesized catalysts, the un-functionalized Rh_2(*S*-TPPTTL)$_4$ catalyst is held as a benchmark.

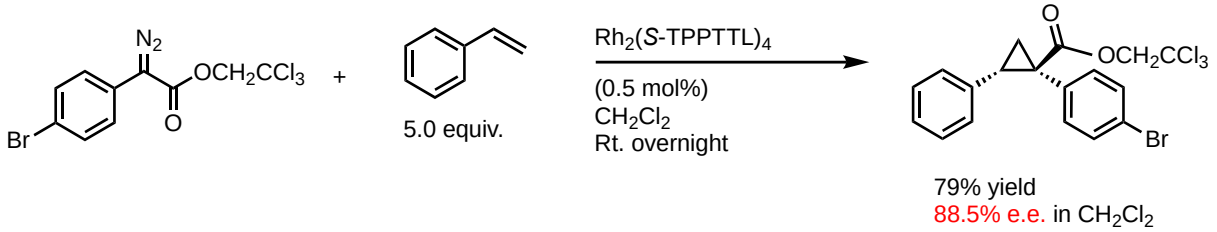

Figure 4.1.2 Performance of Rh_2(*S*-TPPTTL)$_4$ in the cyclopropanation of styrene.

This reaction (Figure 4.1.2) is a classic cyclopropanation carried out by many dirhodium catalysts. Rh_2(*S*-TPPTTL)$_4$ maintains an enantioselectivity of 88.5% with this specific reaction.

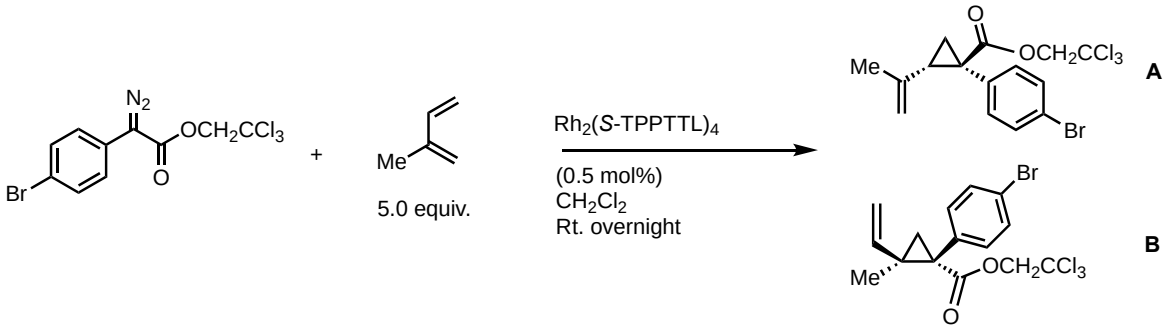

Figure 4.1.3 Selective cyclopropanation of isoprene.

The selective cyclopropanation of isoprene (Figure 4.1.3) is an exploratory reaction that Rh_2(*S*-TPPTTL)$_4$ is unable to selectively complete.

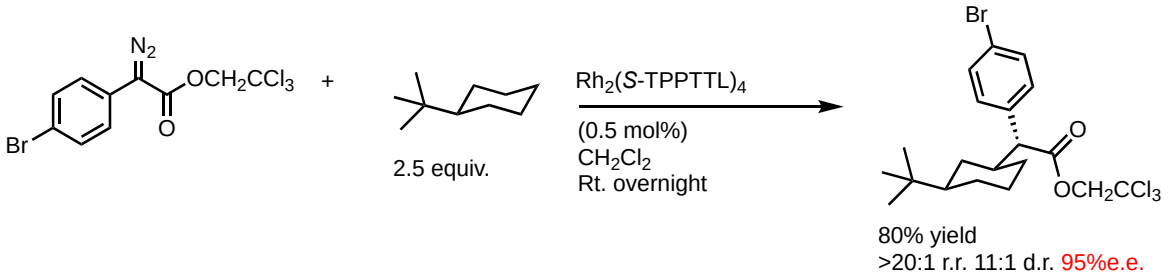

Figure 4.1.4 Selective C-H functionalization of ^{t}Butyl-cyclohexane

The selective C-H functionalization of ᵗButyl-cyclohexane is the most unique reaction that, out of every dirhodium catalyst, is performed the most selectively by Rh_2(*S*-TPPTTL)$_4$.

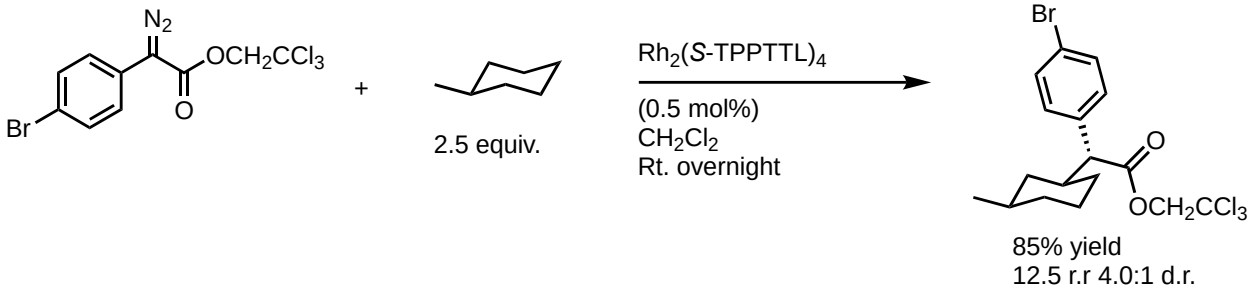

Figure 4.1.5 Selective C-H functionalization of methylcyclohexane

The selective C-H functionalization of methylcyclohexane is a reaction Rh_2(*S*-TPPTTL)$_4$ can successfully catalyze, although it does not have high selectivity.

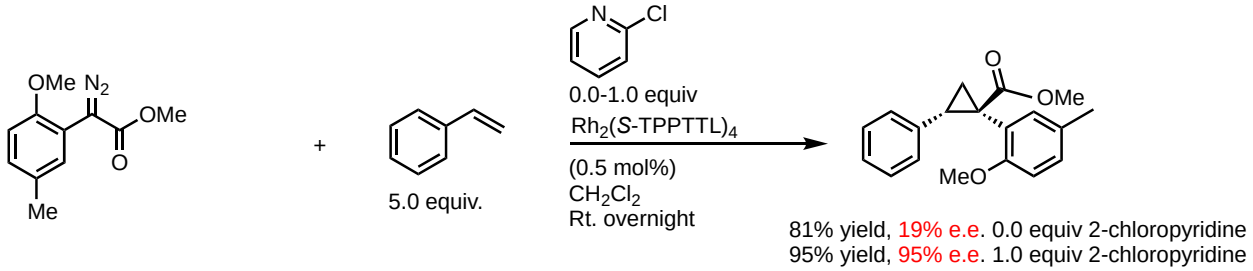

Figure 4.1.6 Performance of Rh_2(*S*-TPPTTL)$_4$ in the cyclopropanation of styrene utilizing a more reactive diazo and testing for the co-ordination ability of 2-chloropyridine.

2-chloropyridine has the ability to coordinate to the rhodium catalyst, changing its properties and increase selectivity with Rh_2(*S*-TPPTTL)$_4$. This reaction is highly sensitive to water and must be run with 4Å molecular sieves.

4.2) Rh_2(*S*-*p*-Br-TPPTTL)$_4$

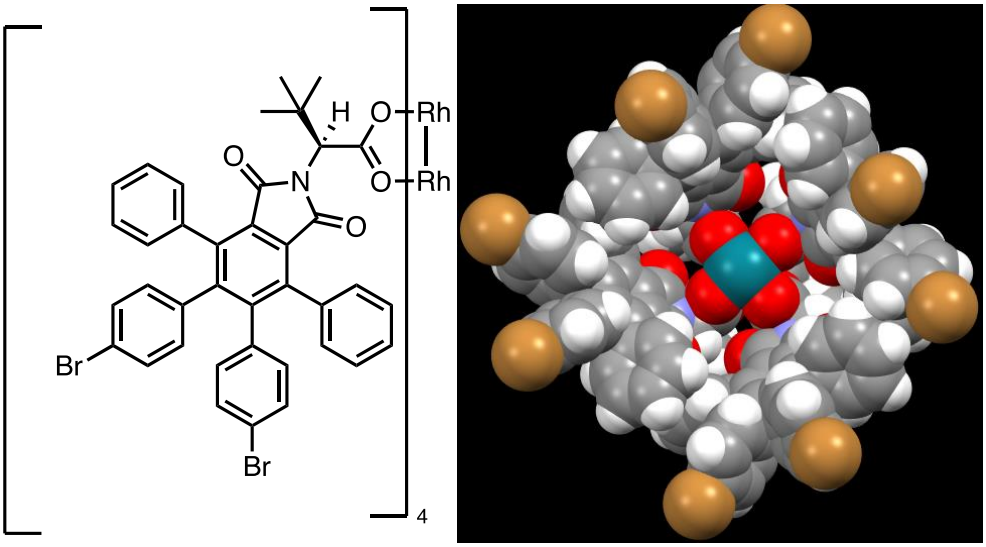

Figure 4.2.1 The molecular and X-ray structure of the Rh_2(*S*-*p*-Br-TPPTTL)$_4$ catalyst. Note the position of the bromines (brown) at the periphery of the bowl.

This variant was directly related to a previous catalyst synthesized, that contained a *p*-bromo group on each phenyl ring of the TPPTTL Ligand. However, due to the position of the bromines on that catalyst, the bromines expanded the diameter of the bowl. With the catalyst synthesized with only two *p*-bromines, it allowed the catalyst to expand upward instead of widening out the diameter of the bowl. Additionally, without bromines impinging on adjacent TPPTTL ligands this new catalyst may be much more flexible than the per-*p*-brominated analogue.

Four of the six characterization reactions were done on this catalyst to gain a preliminary understanding of how a small change in the bowl would change the catalyst stereoselectivity.

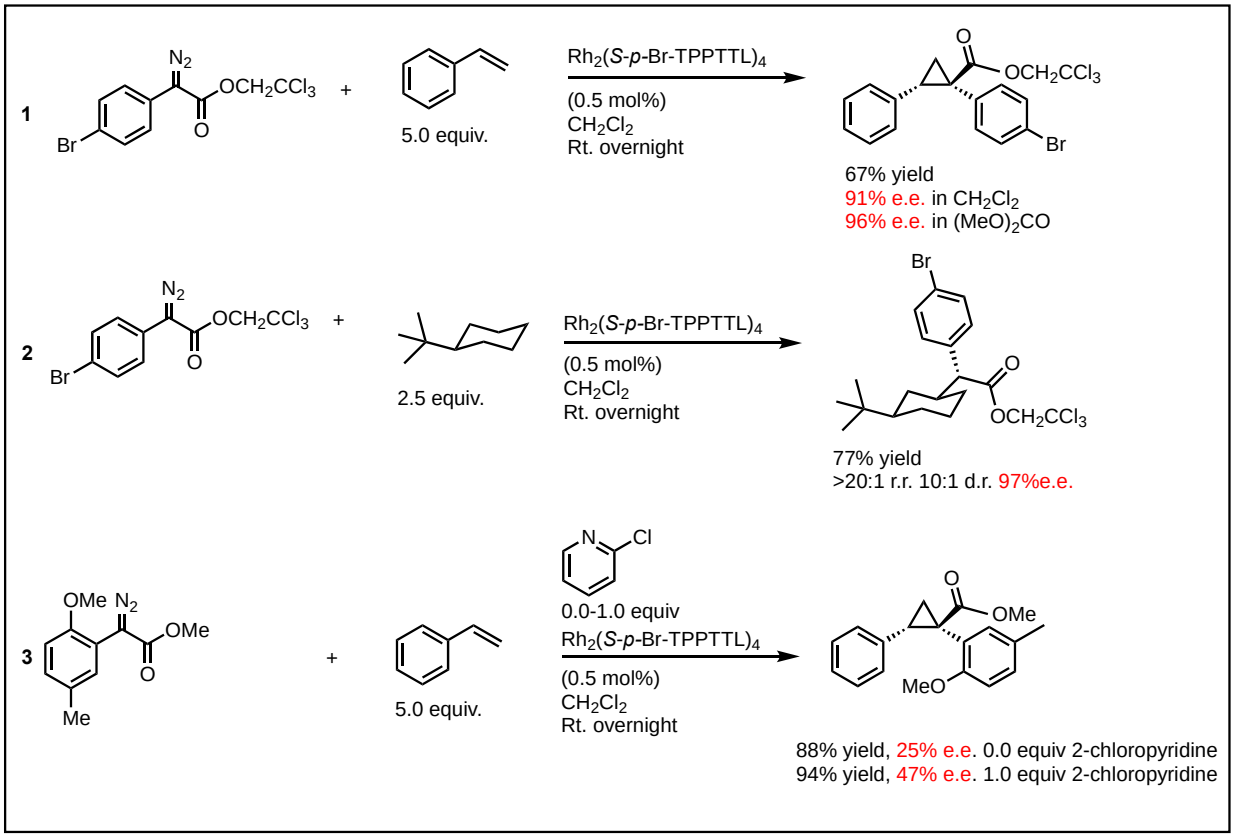

Figure 4.2.2 The activity of the Rh_2(*S*-*p*-Br-TPPTTL)$_4$ catalyst.

The first cyclopropanations yielded a high enantioselectivity of 91%, similar to Rh_2(TPPTTL)$_4$ enantioselectivity of 89% (**1**, Figure 4.2.2). With the ^{t}Butyl-cyclohexane, the same regioselectivity was observed, while a slightly less diastereoselectivity was observed compared to Rh_2(TPPTTL)$_4$ which had a diastereoselectivity of 12:1 d.r. (**2**, Figure 4.2.2) Promisingly, the high levels of similarity between the two catalysts, and the higher e.e. with Rh_2(*S*-*p*-Br-TPPTTL)$_4$, suggest reactivity is not hampered upon the addition of a group at the *para* position.

4.3) Rh_2(*S-3,5-m*-Br-TPPTTL)$_4$

The next catalyst tested was the tetrabrominated version of TPPTTL. With this catalyst, two of the bromines were pointed inward toward the bowl of the catalyst where the reaction occurs.

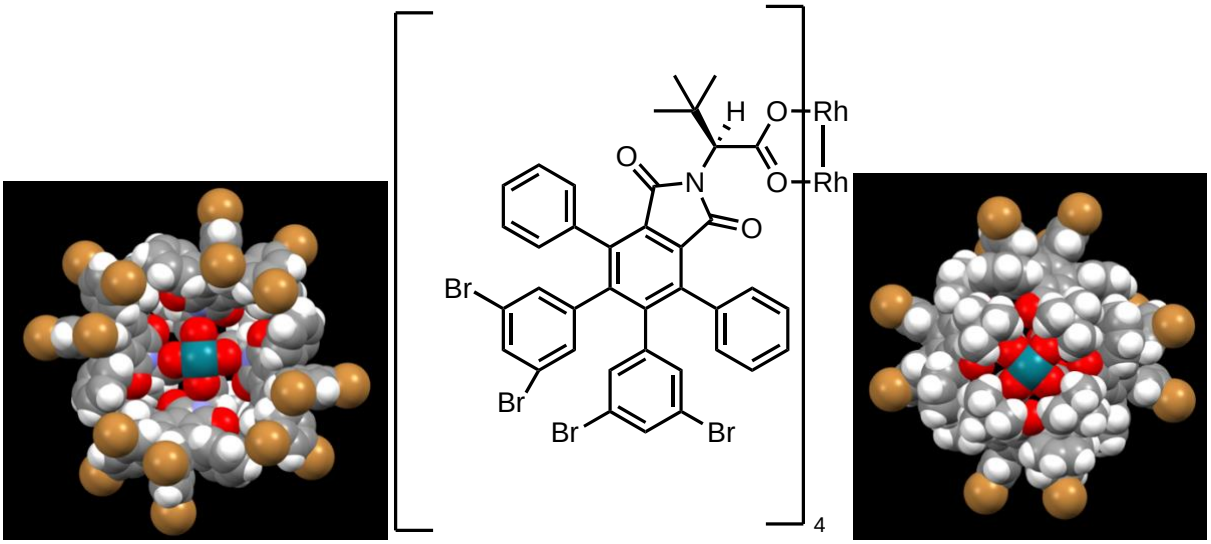

Top view Bottom view

Figure 4.3.1 The molecular structure of the Rh_2(*S-3,5-m*-Br-TPPTTL)$_4$

The x-ray structures are shown from both above the catalyst (Figure 4.3.1), where the depth of the bowl is visible, and from the bottom, where the ^{t}butyl leucine is covering the other face of the catalyst. This forces the reaction to occur in the bowl of the catalyst.

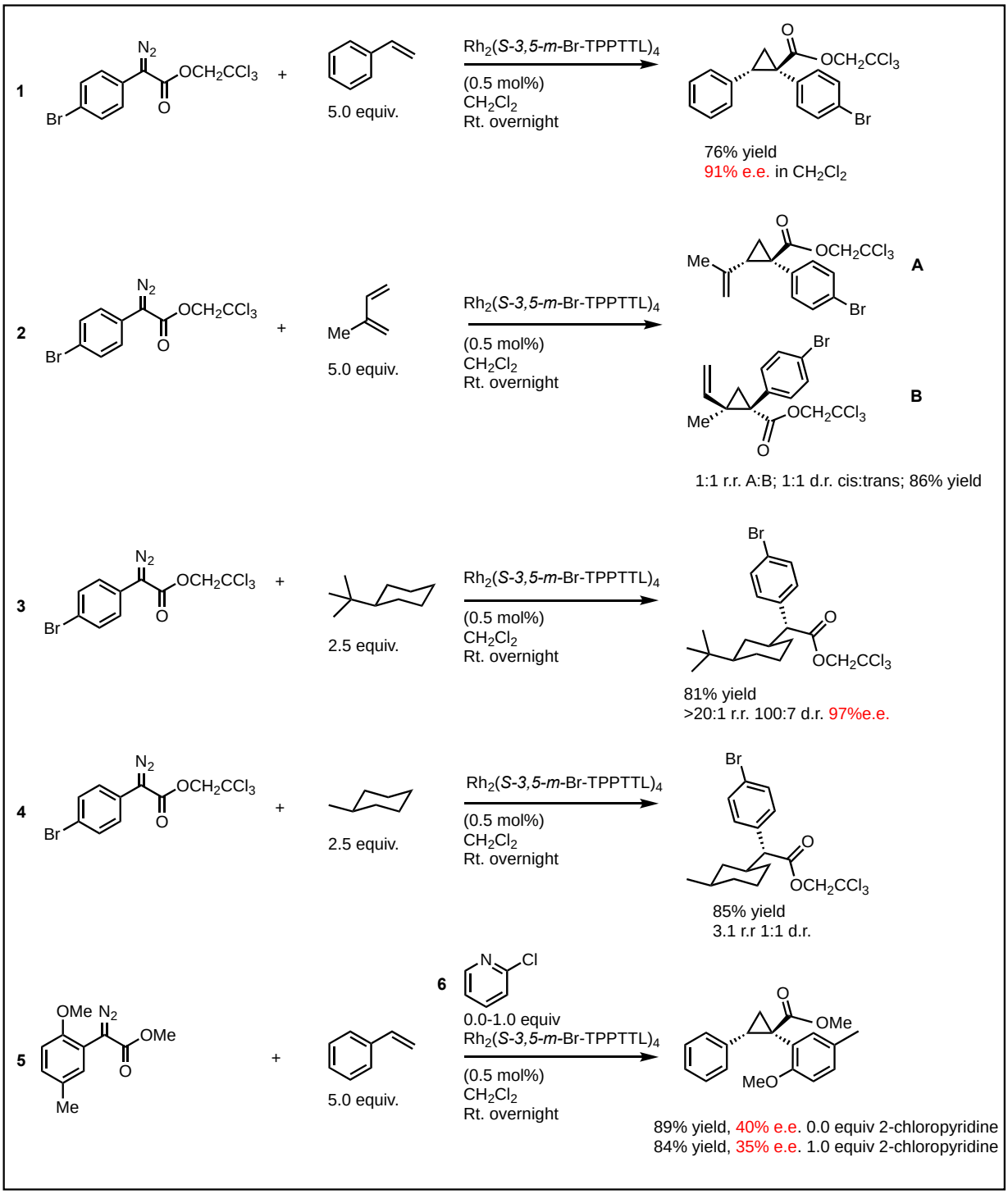

Figure 4.3.2 The activity of the Rh_2(*S-3,5-m*-Br-TPPTTL)$_4$ catalyst.

The range of reactivity for **1** was similar to Rh_2(*S*-TPPTTL)$_4$ with an enantioselectivity of 91%. In **2** there was no selectivity whatsoever, similar to Rh_2(*S*-TPPTTL)$_4$. There was a slightly

higher e.e in **3**; the only difference found between this catalyst and Rh_2(*S*-TPPTTL)$_4$ was in **5** and **6** where Rh_2(*S-3,5-m*-Br-TPPTTL)$_4$ displayed no improvement in response to 2-chloropyridine.

4.4) Rh_2(*S-p-*^{t}butyl-TPPTTL)$_4$

While phenyl rings alone are easy to add via Suzuki Coupling, they are relatively flat. Since the goal was to see how significantly the catalyst would change its activity in response to increasing steric bulk, a ^{t}butyl group was chosen in addition to the phenyl ring. ^{t}Butyl groups provide a large three-dimensional blocking group at the mouth of the catalytic pocket that could significantly influence catalyst activity.

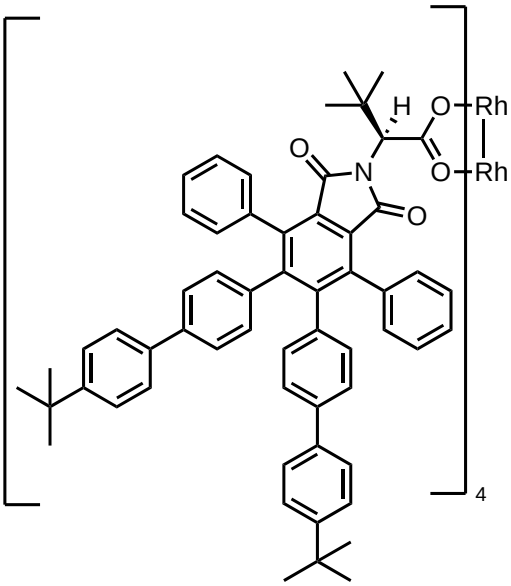

PK1-TBU

Peak Mass	Display Formula	RDB	Delta [ppm]	Delta [mmu]	Theo. mass	Combined Score	MS Cov. [%]
3184.41494	$C_{215}H_{86}O_{16}N_4{}^{103}Rh_2$	177	0.19	0.6	3184.41434	94.6	97.67
3184.41494	$C_{203}H_{215}O_{16}N_5{}^{103}Rh_2$	101	-3.74	-11.9	3184.42684	87.34	91.02
3184.41494	$C_{214}H_{84}O_{16}N_5{}^{103}Rh_2$	177.5	4.14	13.17	3184.40177	82.63	85.83

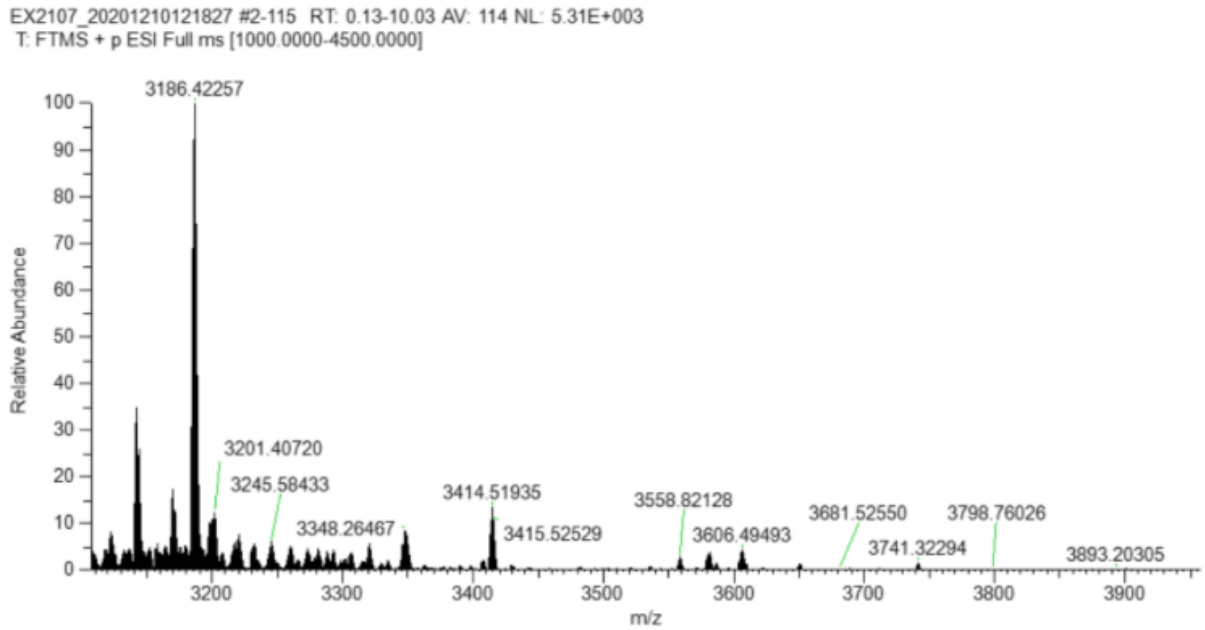

Figure 4.4.1 The molecular structure of the Rh_2(*S*-*p*-^{t}butyl-TPPTTL)$_4$. Mass spectrometry data for Rh_2(*S*-*p*-^{t}butyl-TPPTTL)$_4$.

The mass spec data confirms the identity of the catalyst to be Rh_2(*S*-*p*-^{t}butyl-TPPTTL)$_4$. The spectrum is highly scattered, potentially due to a disassociation of any number of ligands during the ionization process (Figure 4.4.1).

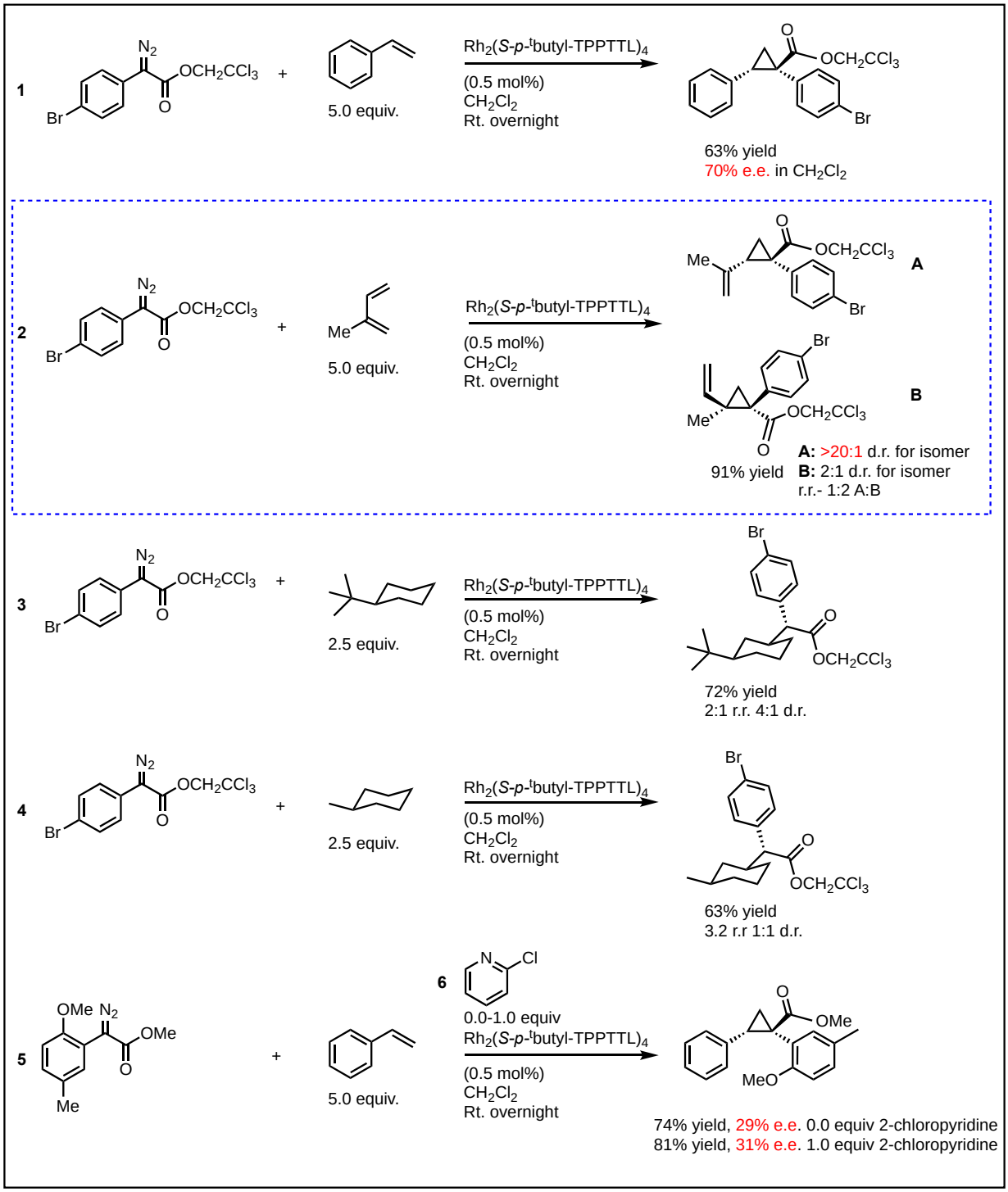

Figure 4.4.2 The activity of the Rh_2(*S*-*p*-^{t}butyl-TPPTTL)$_4$ catalyst.

With this catalyst, significant changes to catalyst selectivity can be seen, both positive and negative. With the classic cyclopropanation **1**, a lower enantioselectivity and yield are observed, however, with isoprene, although selectivity for one olefin over the other is insignificant, there is a significant preference for one diastereomer of product **A**. The addition of the ^{t}butyl group also significantly decreased the catalyst's selectivity for the C3 equatorial C-H bond in **3** (Figure 4.4.2). This catalyst was the bulkiest catalyst yet synthesized, and the results it merited suggested that further altering the steric bulk of the TPPTTL catalyst warranted additional investigation.

4.5) Rh_2(*S*-*p*-bisCF_3-TPPTTL)$_4$

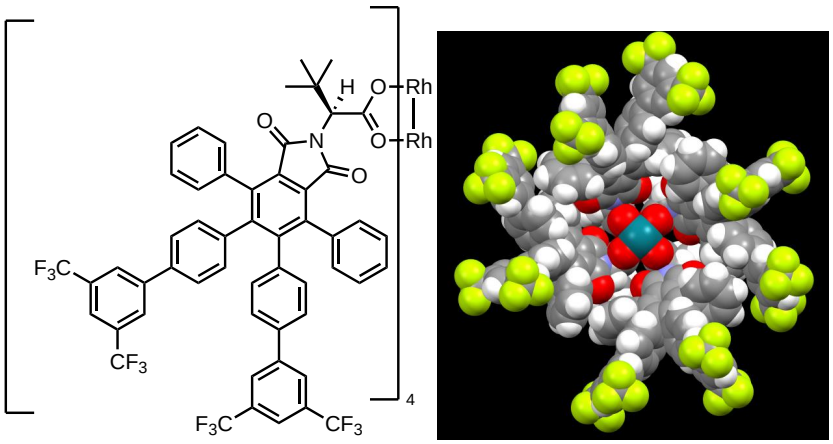

Rh_2(*S*-*p*-bisCF_3-TPPTTL)$_4$

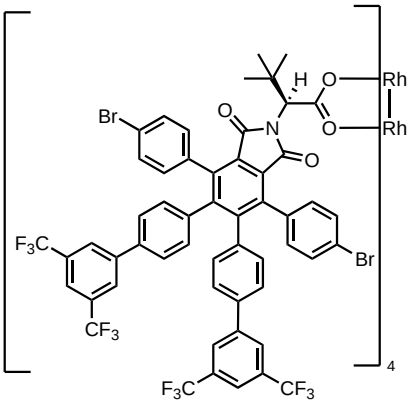

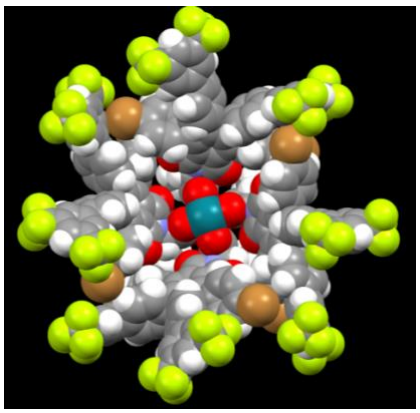

Zac Garlets's variant

Figure 4.5.1 The molecular structure of the Rh_2(*S*-*p*-bisCF_3-TPPTTL)$_4$ and Zac Garlets's variant of the *bis*-CF3 catalyst are shown. The X-ray structures are shown from the top of the bowl.

This particular adjustment to the Rh_2(*S*-*p*-Br-TPPTTL)$_4$ system resulted in a structure that displayed a much higher flexibility in comparison to Zac Garlet's catalyst: the ligands on this particular catalyst were not forced to maintain a perfect C4 symmetry (Figure 4.5.1). Interestingly, much higher selectivity was achieved with this catalyst in several of the benchmark reactions. The relative success of the bisCF_3 alteration directed research to prioritize the use of the bisCF_3 boronic acid for future catalyst alterations.

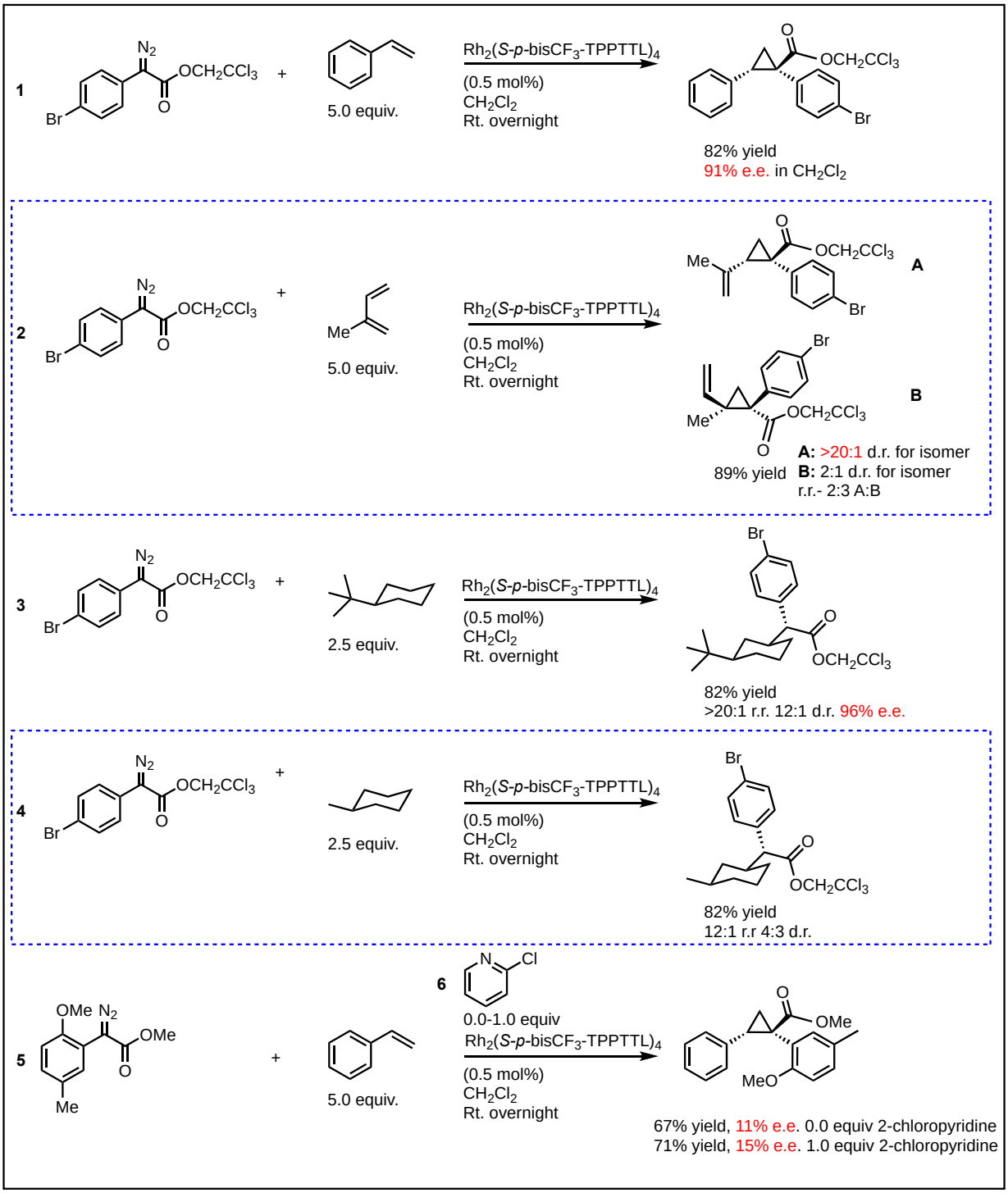

Figure 4.5.2 The activity of the Rh_2(*S*-*p*-bisCF_3-TPPTTL)$_4$ catalyst.

The most notable part of the Rh_2(*S*-*p*-bisCF_3-TPPTTL)$_4$ is its versatility. It can perform reaction **2** with selectivity, which Rh_2(*S*-TPPTTL)$_4$ is unable to accomplish, but unlike Rh_2(*S*-*p*-^{t}butyl-TPPTTL)$_4$, it can still perform reactions **1** and **3** with comparable selectivity to Rh_2(*S*-TPPTTL)$_4$ (Figure 4.5.2).

4.6) Rh_2(*S*-*p*-mesityl-TPPTTL)$_4$ Catalyst

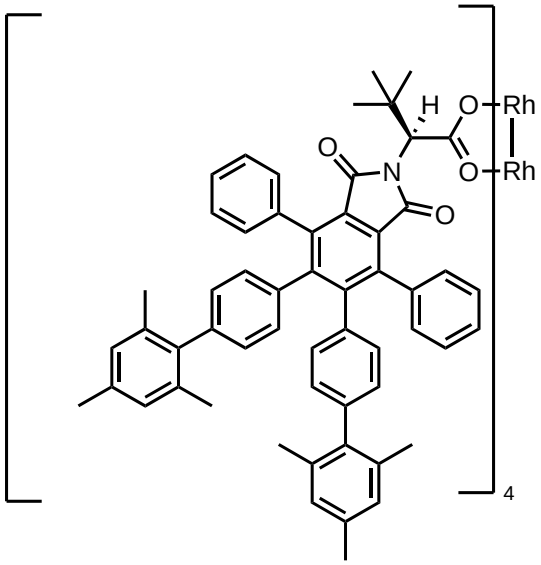

Peak Mass	Display Formula	RDB	Delta [ppm]	Delta [mmu]	Theo. mass	Combined Score	MS Cov. [%]
3408.34293	$C_{224}H_{201}O_{16}N_4{}^{103}Rh_2$	128.5	8.42	28.71	3408.31422	96.09	99.67

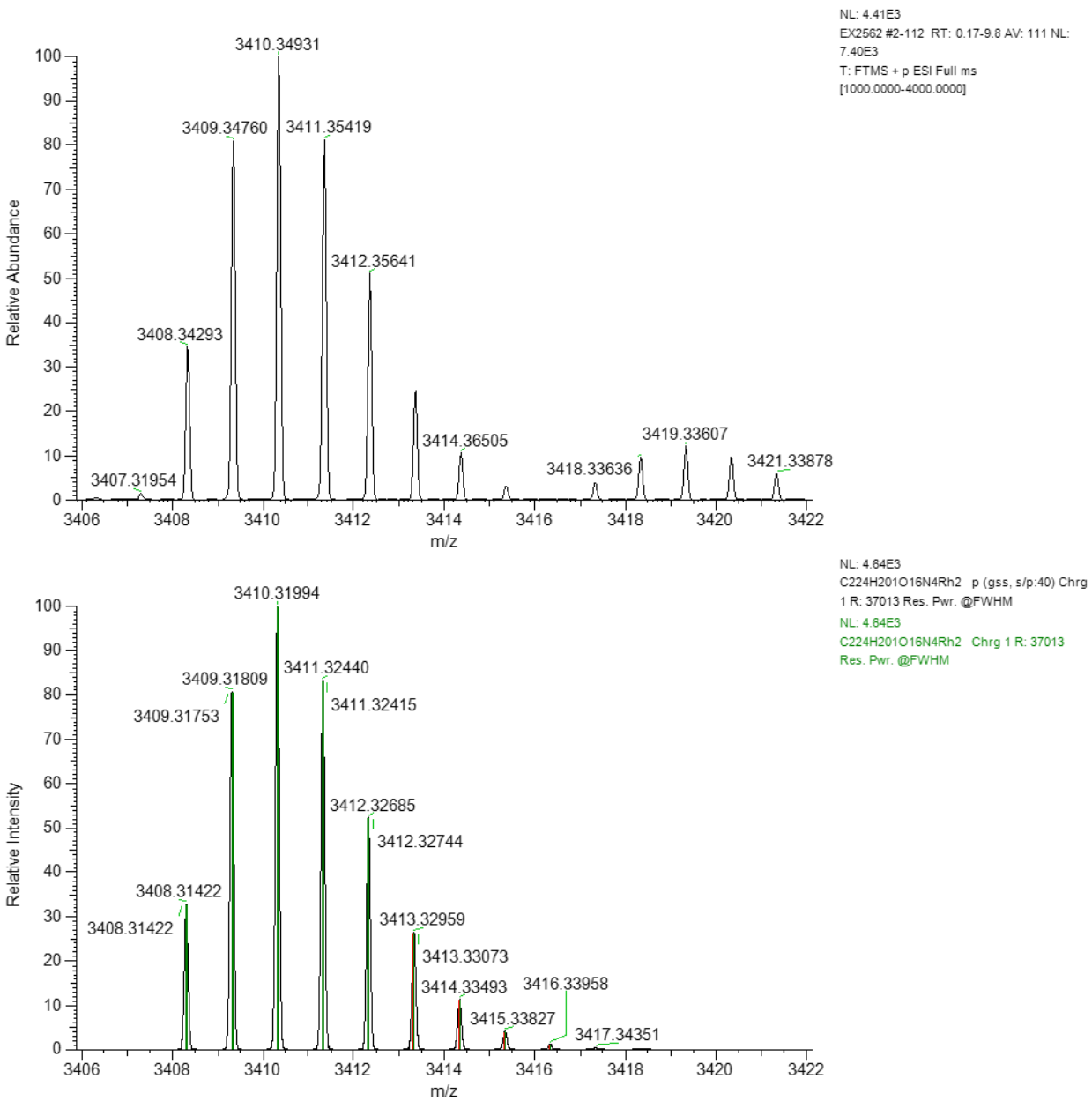

Figure 4.6.1 The molecular structure of the Rh_2(*S*-*p*-mesityl-TPPTTL)$_4$ catalyst.

While an X-ray structure was unable to be taken, the successful synthesis of Rh_2(*S*-*p*-mesityl-TPPTTL)$_4$ was confirmed by mass spectrometry (Figure 4.6.1).

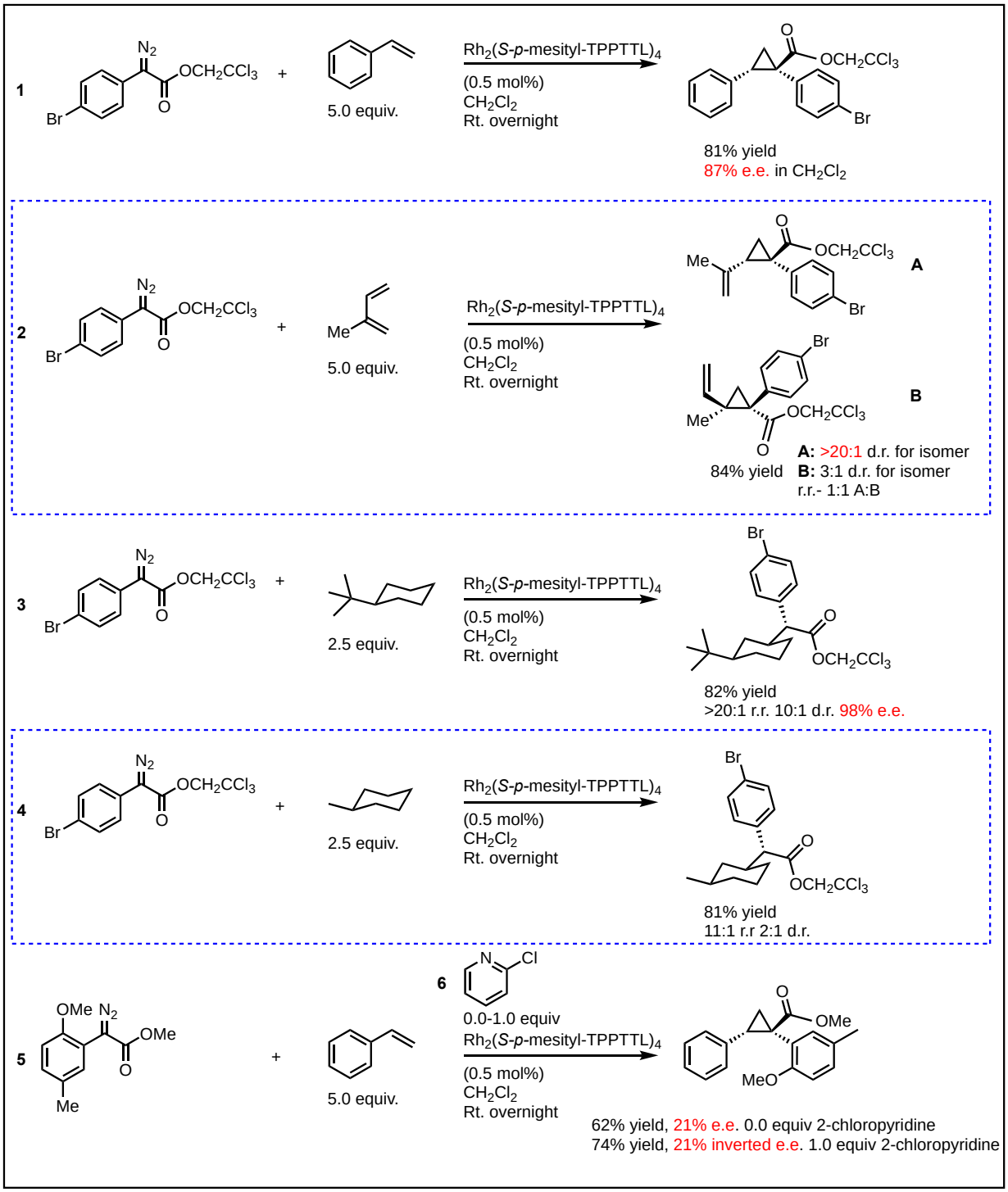

Figure 4.6.2 The activity of the Rh_2(*S*-*p*-mesityl-TPPTTL)$_4$ catalyst.

The Rh_2(*S*-*p*-mesityl-TPPTTL)$_4$ catalyst and the Rh_2(*S*-*p*-bisCF_3-TPPTTL)$_4$ catalyst were nearly identical in all of their selectivities (Figure 4.6.2). Reactions **1, 2, 3, 4, 5,** and **6** did not differ by more than 6% e.e. across the board. This effect suggests that it is not the electronics of the fluorine groups, but rather, their steric interactions that lead to the increases in selectivity, as the mesityl group has no electronic effect.

4.7) Rh_2(*S*-*3,5*-*m*-ph-TPPTTL)$_4$

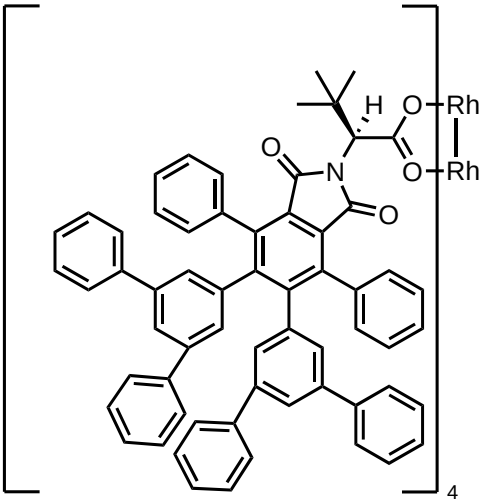

Peak Mass	Display Formula	RDB	Delta [ppm]	Delta [mmu]	Theo. mass	Combined Score	MS Cov. [%]
3679.18511	$C_{248}H_{186}O_{15}N_5{}^{103}Rh_2$	160.5	-5.41	-19.89	3679.205	35.65	37.04
3679.18511	$C_{248}H_{184}O_{16}N_4{}^{103}Rh_2$	161	1.06	3.92	3679.18119	20.06	20.95

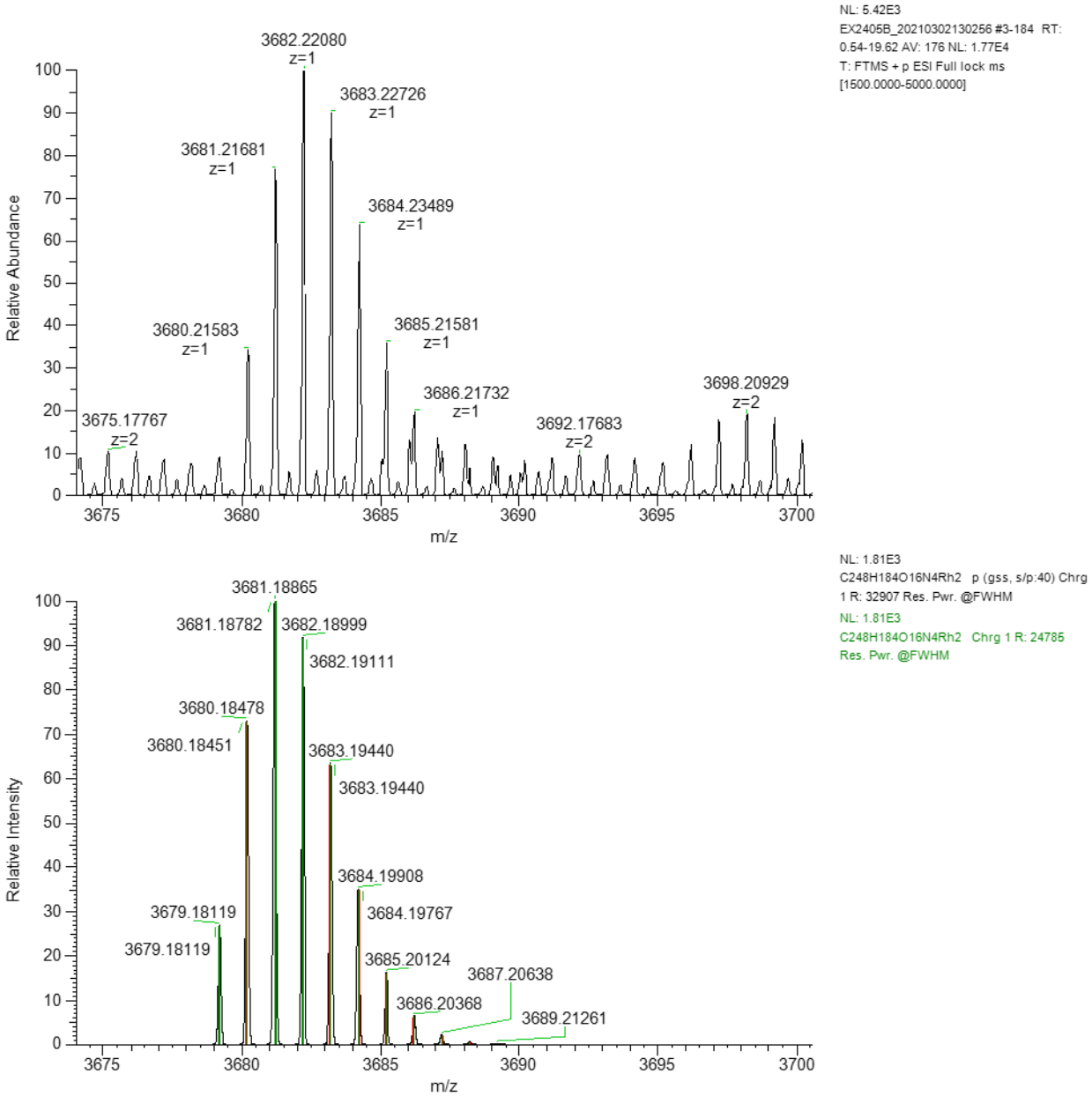

Figure 4.7.1 The molecular structure of the Rh_2(*S-3,5-m*-ph-TPPTTL)$_4$ catalyst and its mass spectrometry data.

Following the confirmation of the 16-fold Suzuki coupling through mass spectrometry (Figure 4.7.1), the Rh_2(*S-3,5-m*-ph-TPPTTL)$_4$ catalyst was tested for its selectivity.

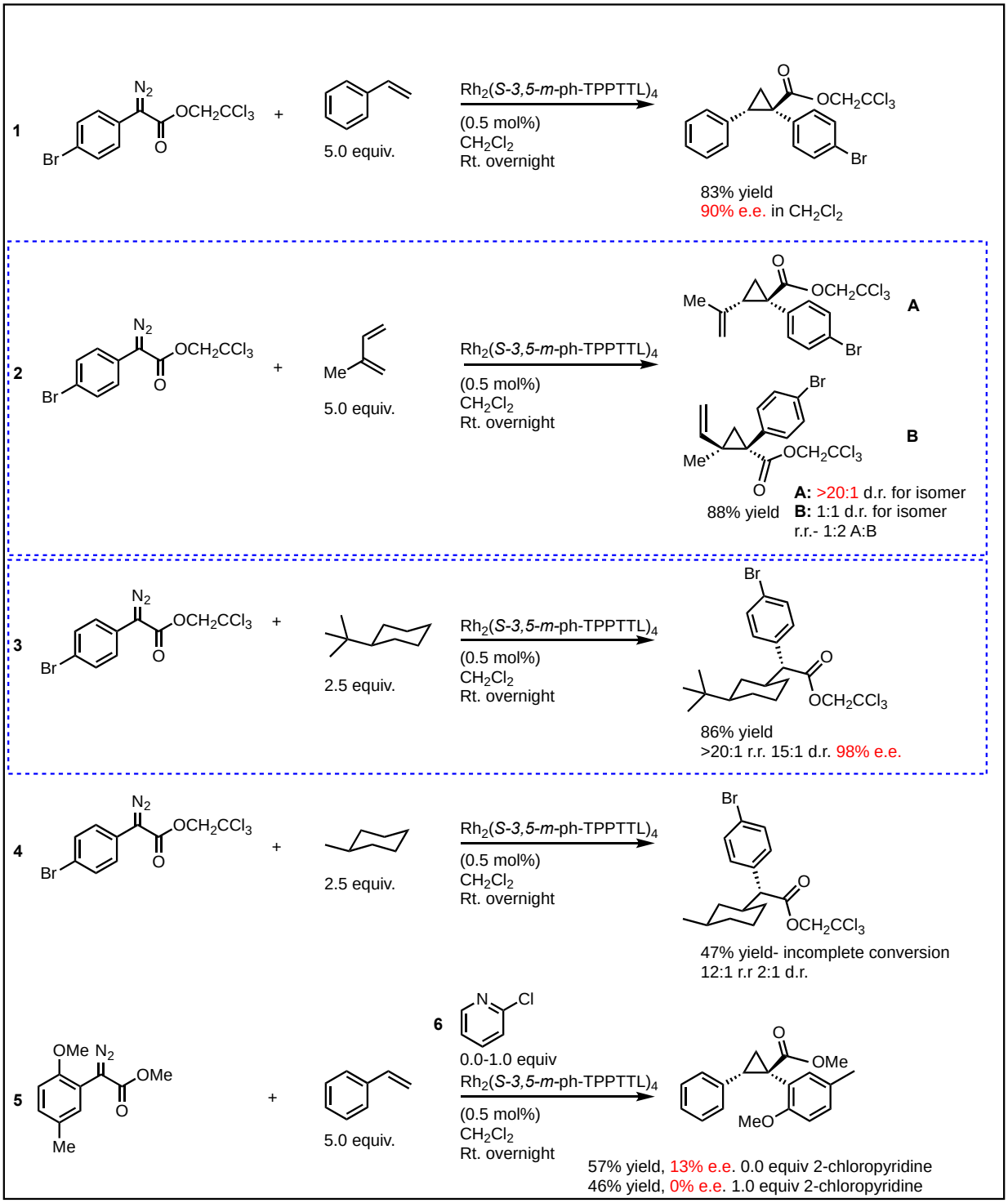

Figure 4.7.2 The activity of the Rh_2(*S-3,5-m*-ph-TPPTTL)$_4$ catalyst.

For reactions **1** and **2**, this catalyst showed similar selectivity to both the Rh_2(*S*-*p*-mesityl-TPPTTL)$_4$ and Rh_2(*S*-*p*-bisCF_3-TPPTTL)$_4$, while showing superior diastereoselectivity in reaction **3**. However, in reaction **4**, there was incomplete conversion of the 2,2,2-trichloroethyl 2-(4-bromophenyl)-2-diazoacetate, and in reaction **5** and **6**, it performed with a low yield and a low e.e. This could be due to the sensitivity of these reactions to an impure catalyst, or potentially that the methylcyclohexane is a less reactive system than the ^{t}butyl-cyclohexane. The reaction proceeded with a less vigorous liberation of nitrogen gas than the ^{t}butyl-cyclohexane, but more control over the variables is necessary to make conclusions.

4.8) Rh_2(*S*-*3,5*-*m*-bisCF_3-TPPTTL)$_4$

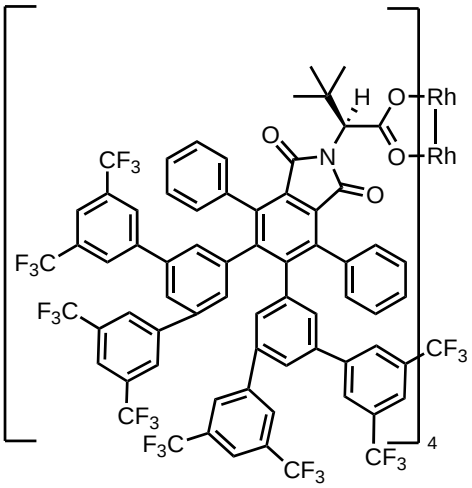

Peak Mass	Display Formula	RDB	Delta [ppm]	Delta [mmu]	Theo. mass	Combined Score	MS Cov. [%]
5854.80014	$C_{269}H_{283}O_{16}N_4F_{96}{}^{103}Rh_2$	84.5	-0.42	-2.44	5854.80258	70.51	72.81
5854.80014	$C_{280}H_{152}O_{16}N_4F_{96}{}^{103}Rh_2$	161	3.87	22.64	5854.7775	55.82	57.67

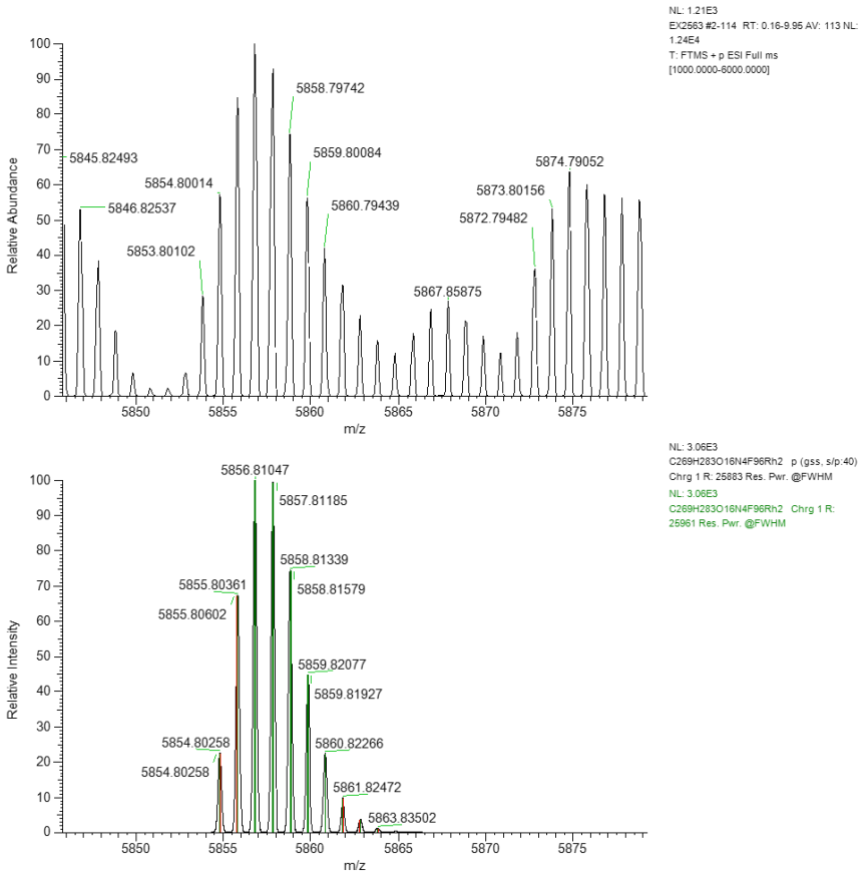

Figure 4.8.1 The molecular structure of Rh_2(*S-3,5-m*-bisCF_3-TPPTTL)$_4$ and its mass spectrometer data.

The purification of this catalyst was a challenge due to its high solubility in pure hexanes, pentane, and petroleum ether. It is impure by TLC however, but since the presence of the catalyst was confirmed with 72.81% (Figure 4.8.1), the test reactions were still performed.

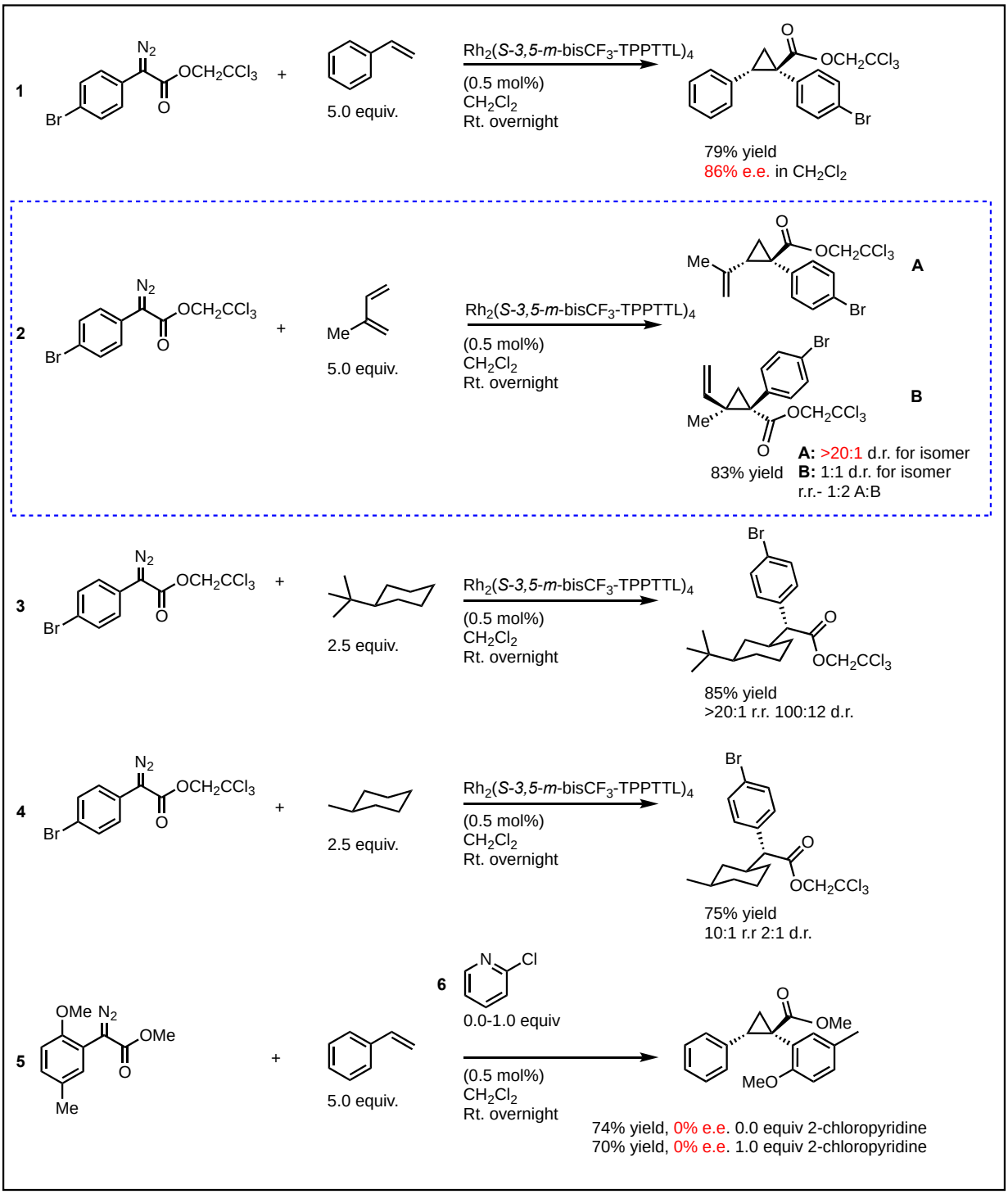

Figure 4.8.2 the activity of the Rh_2(*S-3,5-m*-bisCF_3-TPPTTL)$_4$ catalyst.

In similar trend to the Rh_2(*S-3,5-m*-ph-TPPTTL)$_4$ catalyst, a less vigorous liberation of nitrogen gas was observed in its reaction with both methylcyclohexane (**4**) and with the 2-chloropyridine (**6**). The enantioselectivity with both reactions **5** and **6** were negligible, and its enantioselectivity in **1** was also low.

5) Conclusion

When a catalyst performs a reaction as uniquely as TPPTTL's highly regio and stereoselective functionalization of the equatorial C3 C-H bond in ^{t}butyl-cyclohexane, it is important to gain a more functional understanding of how this catalyst performs its reactions to better understand how to improve its catalytic selectivity. With this project, the goal was to expand the unique reactivity seen with Rh_2(TPPTTL)$_4$ into new chemical space.

An exploration of Rh_2(TPPTTL)$_4$'s selectivity will also help us to further understand how dirhodium carbenes interact with cyclic ring systems. Exploring these systems may give us insight into how to alter the catalyst's structure to potentially alter molecules like methylcyclohexane with high site- and diastereoselectivity.

Evidence gathered from the variety of catalysts suggested that diversifying the *para*-position of the Rh_2(TPPTTL)$_4$ ligand can alter the selectivity profile as significantly as introducing a group at the meta position. This conclusion opposes the hypothesis that if a group is introduced close to the catalyst's binding site, then a more significant change in reactivity will be observed. The data gathered from the reaction data involving the C-H functionalization of methylcyclohexane and the diastereoselective cyclopropanations of isoprene suggest that more sterically bulky catalysts could impart greater selectivity in these simple systems. To complete this avenue of research, more detailed characterizations need to be performed. This will include X-ray crystallography data on each catalyst, to better understand how alterations affect the general

structure of the catalyst bowl, and variable temperature NMR to study the flexibility of the different conformations the catalyst occupies. Furthermore, the discovery of an efficient 8-16-fold Suzuki cross-coupling will allow for the use of Rh_2(*S*-*p*-Br-TPPTTL)$_4$. analogues to more efficiently access a wide variety of new catalysts.

6) Experimental

Synthesis of TPPTTL Variants General Procedure

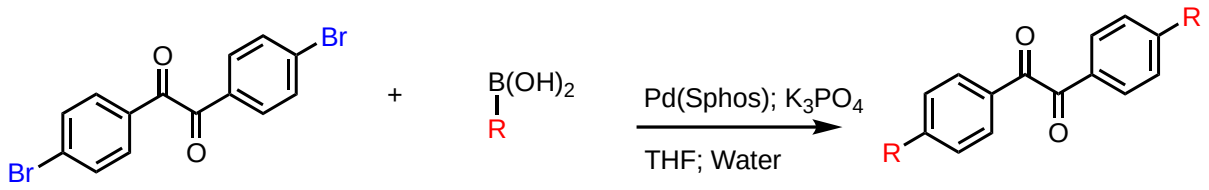

1. Functionalized Benzil. Round bottom flask was flame dried under argon, and charged with the solids Benzil (5mmol, 1 equiv, 1.84g), K_3PO_4 (20mmol, 4 equiv.), SPhos (.375mmol, .075equiv.). THF (20mL) and water (1mL) were added, and the solution was degassed under nitrogen stream for 30 minutes. Pd $(OAc)_2$ (.15 mmol, .03 equiv.) was added, followed by the boronic acid (15mmol, 3 equiv.). Solution was heated to 85°C and stirred for 12 h. Solvent was removed *in vacuo*, and the resulting yellow solid was re-dissolved in DCM. The solution as washed with water 3x, Brine, and filtered over $MgSO_4$. Solvent was removed in vacuo to yield a pale-yellow solid which was subsequently columned in Hexane: Ethyl acetate (1-10% over 18 CV). Product was isolated as a yellow solid in 33-85% yield.

1,2-bis(2',4',6'-trimethyl-[1,1'-biphenyl]-4-yl) ethane-1,2-dione - Prepared via procedure 1 with **mesitylboronic acid** 164.01 g/mol, 2.46 grams. Yields a pale-yellow solid. 65% yield, 1.4514g.

1,2-bis(4'-(*tert*-butyl)-[1,1'-biphenyl]-4-yl) ethane-1,2-dione- Prepared via general procedure 1 with **(4-(*tert*-butyl) phenyl) boronic acid**, 178.04 g/mol, 2.67 grams. Yields a pale-yellow solid. 85% yield, 2.0257g.

1,2-bis(3',5'-bis(trifluoromethyl)-[1,1'-biphenyl]-4-yl) ethane-1,2-dione - Prepared via general procedure 1 with **(3,5-bis(trifluoromethyl)phenyl) boronic acid,** 257.93 g/mol 3.87 grams. Yields a pale-yellow solid. 33% yield, .4256g.

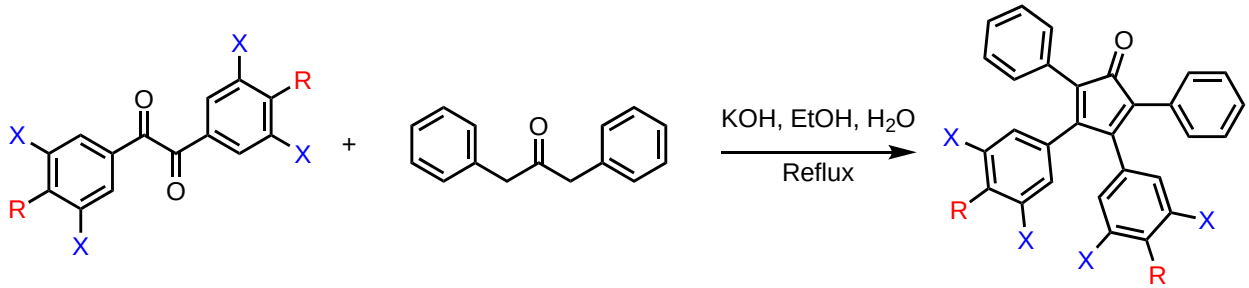

2. 2,3,4,5-tetraphenylcyclopenta-2,4-dien-1-one Round bottom flask was flame dried under argon and charged with benzil (10 mmol, 1 equiv.) and 1,2-diphenylpropan-2-one (10mmol, 1equiv.). 65 mL of dry ethanol was added the solution was then refluxed for 1 h. A solution of KOH (1 equiv., .56 in 6mL EtOH) was added dropwise, and refluxed for a further 45 minutes, or until starting material had disappeared by TLC. Solution was chilled in ice bath for 2 h., then quenched with water (50 ml) resulting in precipitation of a rusty colored solid. The solid was filtered via Büchner funnel and washed with cold EtOH to afford the product as a rusty colored powder with a 76-84% yield.

3,4-bis(4-bromophenyl)-2,5-diphenylcyclopenta-2,4-dien-1-one Prepared via general procedure 2 with **1,2-bis(4-bromophenyl) ethane-1,2-dione,** 368.02 g/mol, 3.68g scale. Yields a brown solid, 65% yield, 3.525g.

3,4-bis(3',5'-bis(trifluoromethyl)-[1,1'-biphenyl]-4-yl)-2,5-diphenylcyclopenta-2,4-dien-1-one Prepared via general procedure 2 with **1,2-bis(3',5'-bis(trifluoromethyl)-[1,1'-biphenyl]-4-yl) ethane-1,2-dione**, 634.42 g/mol, 6.34g. Yields a light brown solid, 78% yield, 6.3076g.

2,5-diphenyl-3,4-bis(2',4',6'-trimethyl-[1,1'-biphenyl]-4-yl)cyclopenta-2,4-dien-1-one Prepared via general procedure 2 with **1,2-bis(2',4',6'-trimethyl-[1,1'-biphenyl]-4-yl) ethane-1,2-dione,** 446.59 g/mol. 4.45g scale. Yields a brown solid, 84% yield, 5.215g.

3,4-bis(4'-(*tert*-butyl)-[1,1'-biphenyl]-4-yl)-2,5-diphenylcyclopenta-2,4-dien-1-one Prepared via general procedure 2 with **1,2-bis(4'-(*tert*-butyl)-[1,1'-biphenyl]-4-yl) ethane-1,2-dione**, 474.64 g/mol, 4.75g scale. Yields a brown solid, 86% yield, 5.58g.

3,4-bis(3,5-dibromophenyl)-2,5-diphenylcyclopenta-2,4-dien-1-one Prepared via general procedure 2 with **1,2-bis(3,5-dibromophenyl) ethane-1,2-dione**, 525.82 g/mol, 5.25g. Yields a Brown solid, 83% yield, 5.810g.

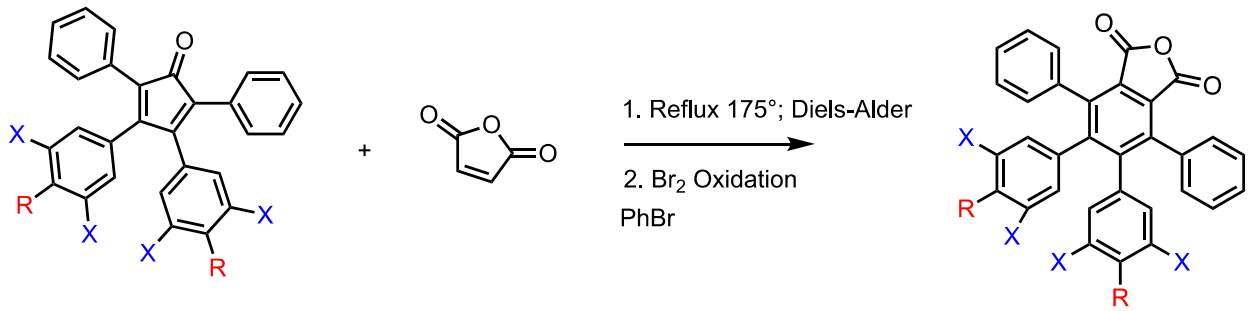

3. 4,5,6,7-tetraphenylisobenzofuran-1,3-dione Round bottom flask was flame dried under argon and charged with 2,3,4,5-tetraphenylcyclopenta-2,4-dien-1-one (7.7 mmol, 1 equiv.) and maleic anhydride (7.7 mmol, 1 equiv.). PhBr (10mL) was added, and the solution was refluxed for 3.5 h.

at 175° C, or until starting materials disappeared via TLC. Solution was then cooled to rt. under air stream. Br_2 was added as a solution in PhBr (1.85g or .6mL in 2mL PhBr, 1.5 equiv.) dropwise. Solution was then heated to 175° C and refluxed for a further 3 h. A solution of sodium thiosulfate was prepared to quench the bromine liberated from the reaction via reverse-funnel trap. The solution was cooled in an ice bath for 3 h. then filtered via Büchner funnel and washed with petroleum ether to afford the product as a dark red/brown solid in 38-67% yield.

5,6-bis(4-bromophenyl)-4,7-diphenylisobenzofuran-1,3-dione Prepared via general procedure 3. **3,4-bis(4-bromophenyl)-2,5-diphenylcyclopenta-2,4-dien-1-one**, with 542.27g/mol, 4.18g scale. Yields a dark red powder, 72% yield, 3.38g.

5,6-bis(3',5'-bis(trifluoromethyl)-[1,1'-biphenyl]-4-yl)-4,7-diphenylisobenzofuran-1,3-dione Prepared via general procedure 3. **3,4-bis(3',5'-bis(trifluoromethyl)-[1,1'-biphenyl]-4-yl)-2,5-diphenylcyclopenta-2,4-dien-1-one**, 808.67 g/mol, 6.23g scale. Yields a dark red powder, 43% yield, 2.90g.

4,7-diphenyl-5,6-bis(2',4',6'-trimethyl-[1,1'-biphenyl]-4-yl) isobenzofuran-1,3-dione Prepared via general procedure 3. **2,5-diphenyl-3,4-bis(2',4',6'-trimethyl-[1,1'-biphenyl]-4-yl)cyclopenta-2,4-dien-1-one**, 620.84 g/mol, 4.78g scale. Yields a dark brown powder, 54% yield, 2.86g.

5,6-bis(4'-(*tert*-butyl)-[1,1'-biphenyl]-4-yl)-4,7-diphenylisobenzofuran-1,3-dione Prepared via general procedure 3. **3,4-bis(4'-(*tert*-butyl)-[1,1'-biphenyl]-4-yl)-2,5-diphenylcyclopenta-2,4-dien-1-one**, 648.89 g/mol, 5.00g scale. Yields a dark red powder, 38% yield, 2.098g.

5,6-bis(3,5-dibromophenyl)-4,7-diphenylisobenzofuran-1,3-dione Prepared via general procedure 3. **3,4-bis(3,5-dibromophenyl)-2,5-diphenylcyclopenta-2,4-dien-1-one**, 700.06 g/mol, 5.39g scale. Yields a black powder, 42% yield, 2.484g.

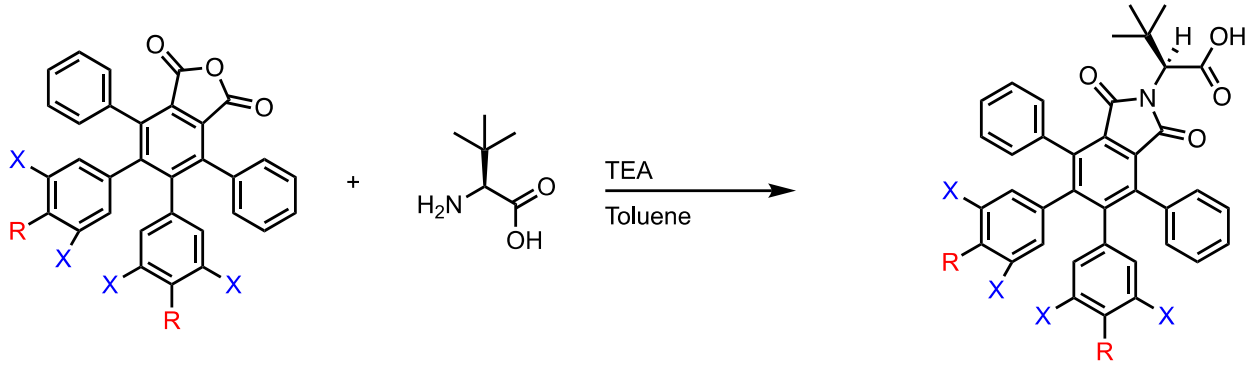

4. (S)-2-(1,3-dioxo-4,5,6,7-tetraphenylisoindolin-2-yl)-3,3-dimethylbutanoic acid. Round bottom flask was dried under argon and charged with 4,5,6,7-tetraphenylisobenzofuran-1,3-dione (5mmol, 1 equiv.) and L-*tert*-Leucine (5.5 mmol, 1.1. equiv.). Toluene (50mL) was added, followed by triethylamine (6mmol, 1.2 equiv.). The solution was refluxed at 120° C overnight or until starting materials have disappeared via TLC. The reaction mixture was then cooled, and diluted with ethyl acetate, washed with 1M HCl, and dried with brine. The solution was then dried, filtered over magnesium sulfate and solvent was removed in vacuo to afford a light tan powder. Crude material was columned (0-20% ethyl acetate: hexanes 20 CV) and the product was obtained as a white or light brown solid in 82-96% yield.

(*S*)-2-(5,6-bis(4-bromophenyl)-1,3-dioxo-4,7-diphenylisoindolin-2-yl)-3,3-dimethylbutanoic acid Prepared via general procedure 4. **5,6-bis(4-bromophenyl)-4,7-diphenylisobenzofuran-1,3-dione** 610.30 g/mol, 4.699g scale. White powder, 84% yield, 3.039g.

(*S*)-2-(5,6-bis(3',5'-bis(trifluoromethyl)-[1,1'-biphenyl]-4-yl)-1,3-dioxo-4,7-diphenylisoindolin-2-yl)-3,3-dimethylbutanoic acid Prepared via general procedure 4. **5,6-bis(3',5'-bis(trifluoromethyl)-[1,1'-biphenyl]-4-yl)-4,7-diphenylisobenzofuran-1,3-dione** 876.70 g/mol, 6.75g scale. Light brown powder, 73% yield, 3.613g.

(*S*)-2-(1,3-dioxo-4,7-diphenyl-5,6-bis(2',4',6'-trimethyl-[1,1'-biphenyl]-4-yl)isoindolin-2-yl)-3,3-dimethylbutanoic acid Prepared via general procedure 4. **4,7-diphenyl-5,6-bis(2',4',6'-trimethyl-[1,1'-biphenyl]-4-yl) isobenzofuran-1,3-dione** 688.87 g/mol, 5.30g scale. Light brown powder, 82% yield, 3.29g.

(*S*)-2-(5,6-bis(4'-(*tert*-butyl)-[1,1'-biphenyl]-4-yl)-1,3-dioxo-4,7-diphenylisoindolin-2-yl)-3,3-dimethylbutanoic acid Prepared via general procedure 4. **5,6-bis(4'-(*tert*-butyl)-[1,1'-biphenyl]-4-yl)-4,7-diphenylisobenzofuran-1,3-dione** 716.92 g/mol, 5.52g scale. Light brown powder, 77% yield, 3.196g.

(*S*)-2-(5,6-bis(3,5-dibromophenyl)-1,3-dioxo-4,7-diphenylisoindolin-2-yl)-3,3-dimethylbutanoic acid Prepared via general procedure 4. **5,6-bis(3,5-dibromophenyl)-4,7-diphenylisobenzofuran-1,3-dione** 768.09 g/mol, 5.91g scale. Light brown powder, 67% yield, 2.95g.

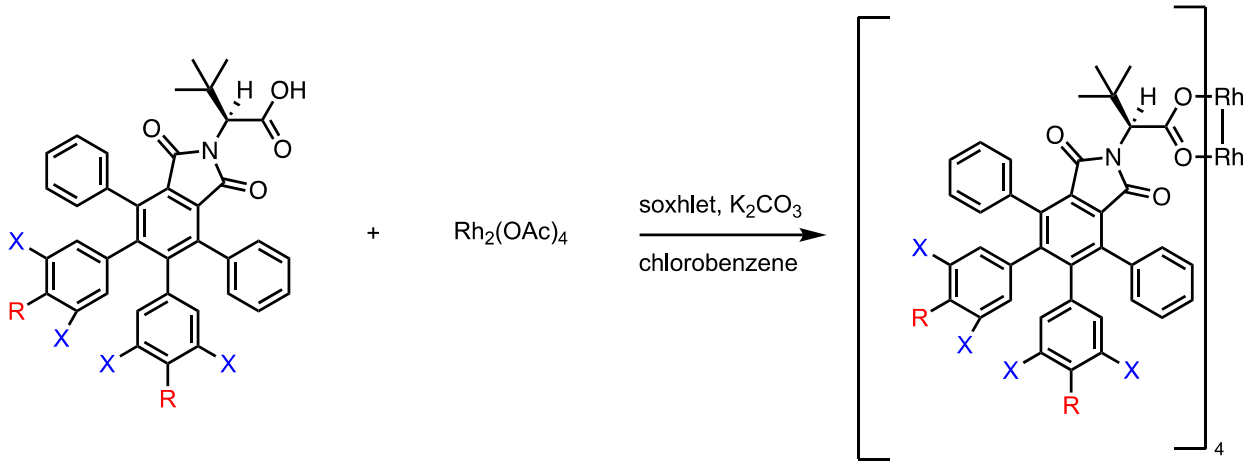

5. Rh_2(*S*-TPPTTL)$_4$ Variants Round bottom flask was dried under argon, then charged with (S)-2-(1,3-dioxo-4,5,6,7-tetraphenylisoindolin-2-yl)-3,3-dimethylbutanoic acid (2.27mmol, 8equiv.) and $Rh_2(OAc)_4$ (.28mmol, 1equiv.). Solids were dissolved in anhydrous chlorobenzene (42mL). A Soxhlet was attached with a thimble of K_2CO_3, and a water condenser was added. Solution was refluxed at 170°C for 36 h. Chlorobenzene was removed by distillation, then the resulting dark green glass was columned (0-20% ethyl acetate: hexanes). Green fractions were isolated to give the product as a green powder with an 83-92% yield.

Rh_2(*S*-*p*-Br-TPPTTL)$_4$ Prepared via general procedure 5. **(*S*)-2-(5,6-bis(4-bromophenyl)-1,3-dioxo-4,7-diphenylisoindolin-2-yl)-3,3-dimethylbutanoic acid**, 723.46 g/mol, 1.64g scale. Green powder, 89% yield, 0.7724g.

Rh_2(*S*-*p*-bisCF_3-TPPTTL)$_4$ Prepared via general procedure 5. **(*S*)-2-(5,6-bis(3',5'-bis(trifluoromethyl)-[1,1'-biphenyl]-4-yl)-1,3-dioxo-4,7-diphenylisoindolin-2-yl)-3,3-dimethylbutanoic acid** 989.86 g/mol, 2.25g scale. Green powder, 84% yield, .9788g.

Rh_2(*S*-*p*-mesityl-TPPTTL)$_4$ Prepared via general procedure 5. **(*S*)-2-(1,3-dioxo-4,7-diphenyl-5,6-bis(2',4',6'-trimethyl-[1,1'-biphenyl]-4-yl)isoindolin-2-yl)-3,3-dimethylbutanoic acid** 802.3 g/mol, 1.82g scale. N/R

Rh_2(*S*-*p*-^{t}butyl-TPPTTL)$_4$ Prepared via general procedure 5. **(*S*)-2-(5,6-bis(4'-(*tert*-butyl)-[1,1'-biphenyl]-4-yl)-1,3-dioxo-4,7-diphenylisoindolin-2-yl)-3,3-dimethylbutanoic acid** 830.08 g/mol, 1.88g scale. Green powder, 91% yield, .8974g.

Rh_2(*S*-*3,5*-*m*-Br-TPPTTL)$_4$ Prepared via general procedure 5. **(*S*)-2-(5,6-bis(3,5-dibromophenyl)-1,3-dioxo-4,7-diphenylisoindolin-2-yl)-3,3-dimethylbutanoic acid** 881.25 g/mol, 2.00g scale. Green powder, 82% yield, .8566g.

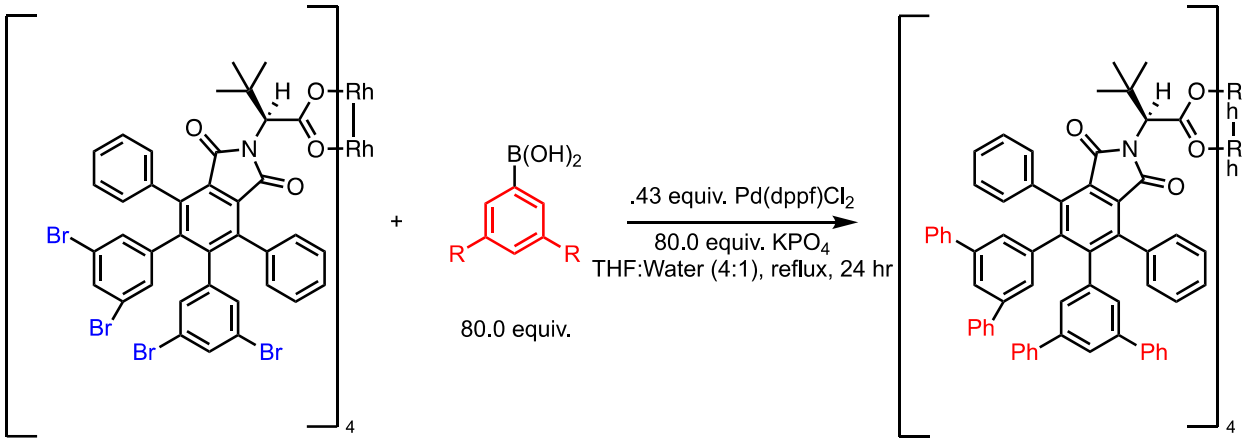

6. Tetraphenylated Rh_2(*S*-TPPTTL)$_4$ Round bottom flask was flame dried under argon, then charged with Rh_2(*S-3,5-m*-Br-TPPTTL)$_4$ (1.0 equiv., 53.67µmol), phenylboronic acid (80.0 equiv., 4.253 mmol), and potassium phosphate (80.0 equiv., 4.253 mmol). THF (20mL) and water (5mL) were added to the reaction mixture and the solution was degassed under a nitrogen stream for 1 h. Pd(dppf)Cl_2 (.437 equiv., 23.45 µmol) was added, and reaction mixture was refluxed for 24 h. or until Rh_2(*S-3,5-m*-Br-TPPTTL)$_4$ disappeared via TLC. Reaction mixture was concentrated *in vacuo* and diluted with DCM. Solution was washed with water (3x10mL), brine (3x10mL), and the organic layer was dried over $MgSO_4$. Solution was concentrated to afford a black oil, and columned in hexanes: ethyl acetate. (0-20%) to give the product as a green powder with a 37% yield.

Rh_2(*S-3,5-m*-ph-TPPTTL)$_4$ Prepared via general procedure 6. **Phenylboronic acid** 121.93 g/mol, .519g scale. 38% yield, green powder, .198g.

Rh_2(*S-3,5-m*-bisCF_3-TPPTTL)$_4$ Prepared via general procedure 6. **(3,5-bis(trifluoromethyl)phenyl)boronic acid** 257.93 g/mol, 1.097g scale. 27% yield, green powder, .0849g.

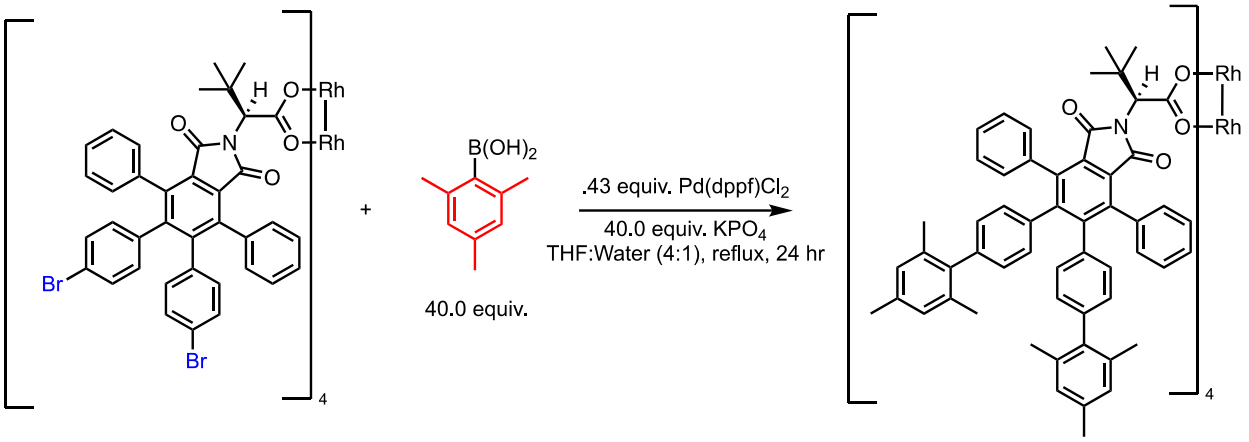

7. Rh_2(*S*-*p*-mesityl-TPPTTL)$_4$ Round bottom flask was flame dried under argon, then charged with Rh_2(*S-3,5-m*-Br-TPPTTL)$_4$ (1.0 equiv., 53.67µmol), phenylboronic acid (40.0 equiv., 2.127 mmol), and potassium phosphate (40.0 equiv., 2.127 mmol). THF (20mL) and water (5mL) were added to the reaction mixture and the solution was degassed under a nitrogen stream for 1 h. Pd(dppf)Cl_2 (.437 equiv., 23.45 µmol) was added, and reaction mixture was refluxed for 24 h. or until Rh_2(*S-3,5-m*-Br-TPPTTL)$_4$ disappeared via TLC. Reaction mixture was concentrated *in vacuo* and diluted with DCM. Solution was washed with water (3x10mL), brine (3x10mL), and the organic layer was dried over $MgSO_4$. Solution was concentrated to afford a black oil, and columned in hexanes: ethyl acetate. (0-20%) to give the product as a green powder with a 37% yield.

Rh_2(*S*-*p*-mesityl-TPPTTL)$_4$ Prepared via general procedure 7 with **mesitylboronic acid**, 164.01 g/mol, .349g scale. 28% yield, green powder, .0512g.

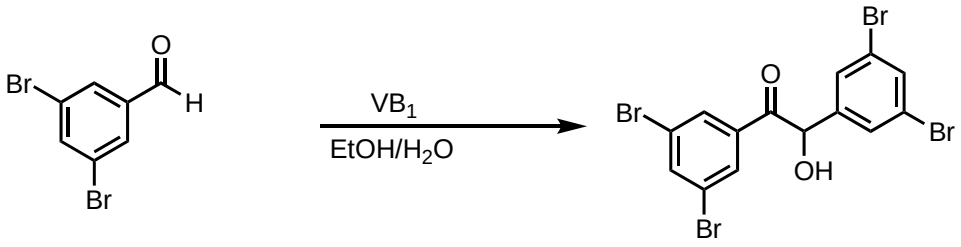

7. 1,2-bis(3,5-dibromophenyl)-2-hydroxyethan-1-one round bottom flask was dried under argon, then charged with Vitamin B1 (20 mmol, 5g, 18.5mol%) in water (5mL) and ethanol (100mL). Cooled in an ice-salt bath, then NaOH was added as a solution in EtOH until the pH was equal to 9. 3,5-dibromobenzaldehyde (108mmol, 1 equiv.) was added and the solution was heated to 65°C for 12hr. The solvent was removed, and the resulting solid was redissolved with ethyl acetate. The product was washed with water (3x100mL) and Brine (3x100mL), and the product was dried over $MgSO_4$ and concentrated *in vacuo* to afford a yellow solid. Product was a mixture of benzil and benzoin and was carried forward to the next step without further characterization.

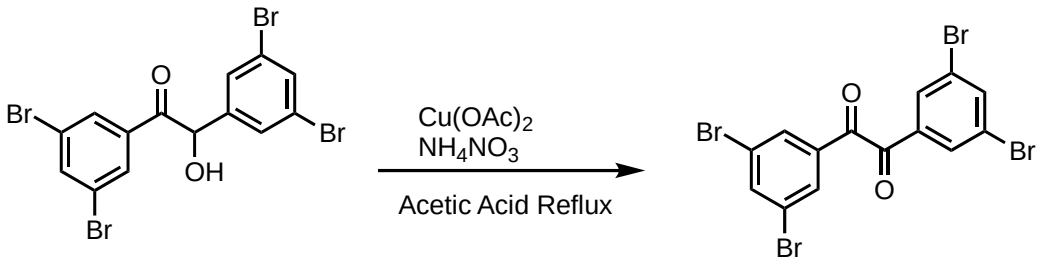

8. 1,2-bis(3,5-dibromophenyl) ethane-1,2-dione round bottom flask flame dried under argon. 1,2-bis(3,5-dibromophenyl)-2-hydroxyethan-1-onen (1.35 mmol, 1 equiv.), NH_4NO_3 (1.69 mmol, 1.25), and $Cu(OAc)_2$-H_2O (.17 mmol, .126 equiv.) were added to acetic acid(5.5mL) and refluxed at 120°C for 2 h. Precipitate was filtered with water and cold ethanol until the solution runs clear and colorless to yield the product as bright yellow powder. Yield: 82% over 2 steps

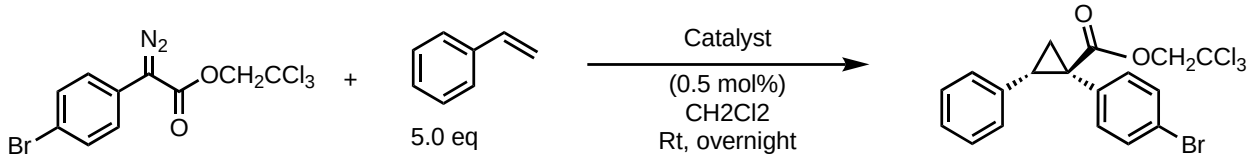

9. 1-((1*R*,2*S*)-1-(4-bromophenyl)-2-phenylcyclopropyl)ethan-1-one--(2,2,2-trichloroethyl)-λ^{1}-oxidane (1/1). After filtration over a silica plug, Styrene (5.0 equiv., .00134mol) and dirhodium catalyst (.005 equiv., 1.3416µmol) were added to flame dried vial under argon in dry DCM (3mL). 2,2,2-trichloroethyl 2-(4-bromophenyl)-2-diazoacetate (1 equiv., 2.683mmol) was added over a minute in dry DCM (1mL) to the reaction mixture. After 1 h., the reaction mixture was vacuum dried, and the mixture was columned in hexanes: ethyl acetate. (0-20% ethyl acetate). The product was vacuum dried and tested for enantiomeric purity via HPLC (ADH 1mL 1% 30min).

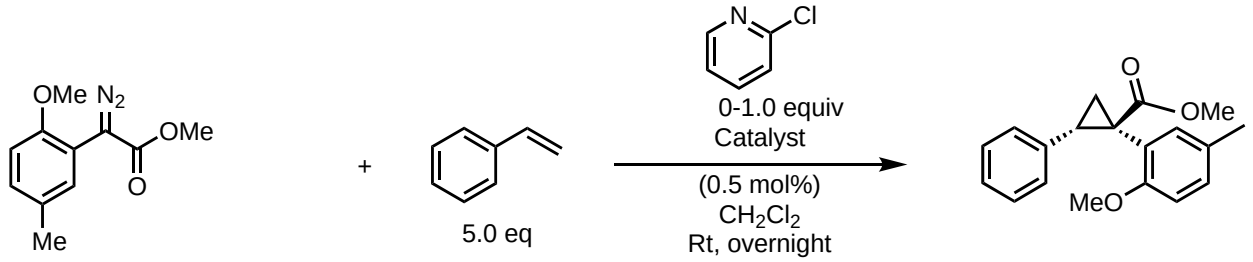

10. 1-((1*R*,2*S*)-1-(2-methoxy-5-methylphenyl)-2-phenylcyclopropyl)ethan-1-one--methyl- λ^{1}-oxidane (1/1) After filtration over a silica plug, Styrene (5.0 equiv., .00134mol) and dirhodium catalyst (.005 equiv., 1.3416µmol) were added to flame dried vial under argon in dry DCM (3mL). methyl 2-diazo-2-(2-methoxy-5-methylphenyl) acetate (1 equiv., 2.683mmol) was added over a minute in dry DCM (1mL) to the reaction mixture. To a separate reaction vessel, the reaction was tested with the coordinating group 2-chloropyridine (1 equiv., 2.683 mmol), After 1 h., the reaction

mixture was vacuum dried, and the mixture was columned in hexanes:ethyl acetate. (0-20% ethyl acetate). The product was isolated *in vacuo* and tested for enantiomeric purity via HPLC (ADH 1mL 1% 30min).

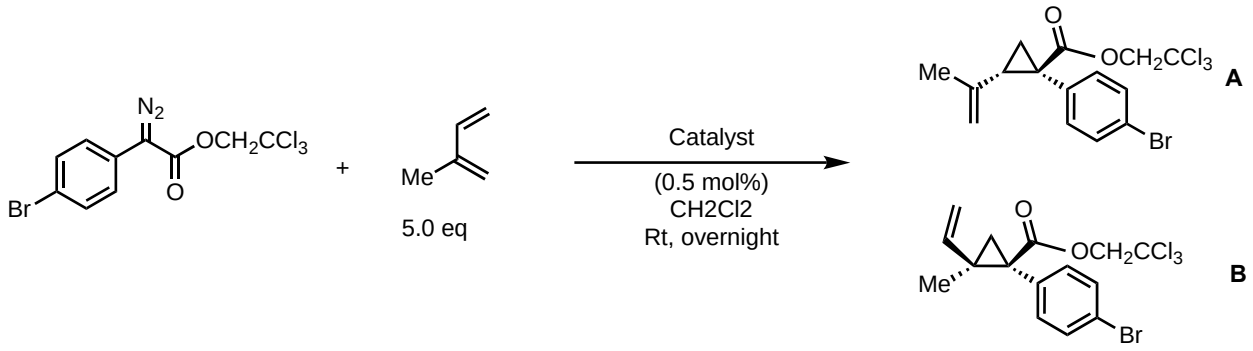

11. 1-((1*R*,2*S*/*R*)-1-(4-bromophenyl)-2-(prop-1-en-2-yl)cyclopropyl)ethan-1-one—trichloro(λ^{1}-methoxy)- λ^{6}-methane (1/1) After filtration over a silica plug, isoprene (5.0 equiv., .00134mol) and dirhodium catalyst (.005 equiv., 1.3416µmol) were added to flame dried vial under argon in dry DCM (3mL). 2,2,2-trichloroethyl 2-(4-bromophenyl)-2-diazoacetate (1 equiv., 2.683mmol) was added over a minute in dry DCM (1mL) to the reaction mixture. After 1 h., the reaction mixture was vacuum dried, and the mixture was columned in hexanes:ethyl acetate. (0-20% ethyl acetate).

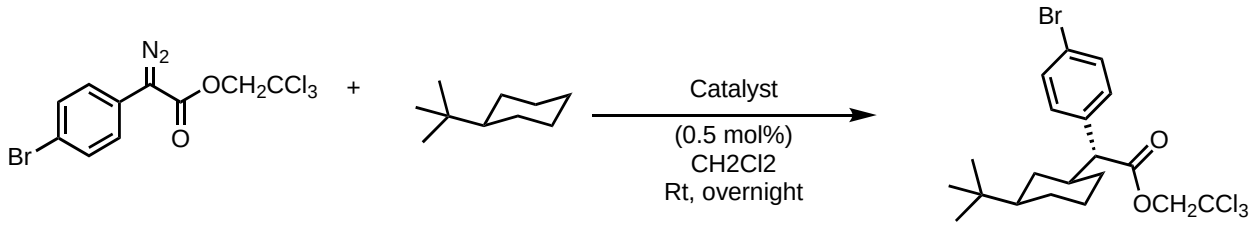

12. 2,2,2-trichloroethyl(*R*)-2-(4-bromophenyl)-2-((1*S*,3*R*)-3-(*tert*-butyl)cyclohexyl)acetate *tert*-butylcyclohexane (2.5 equiv., .00067mol) and dirhodium catalyst (.005 equiv., 1.3416µmol) were added to flame dried vial under argon in dry DCM (3mL). 2,2,2-trichloroethyl 2-(4-bromophenyl)-2-diazoacetate (1 equiv., 2.683mmol) was added over a minute in dry DCM (1mL)

to the reaction mixture. After 1 h., the reaction mixture was vacuum dried, and the crude mixture was assessed via NMR to test for selectivity.

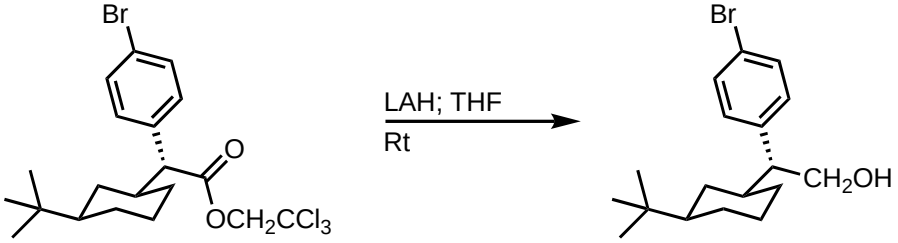

13. (*R*)-2-(4-bromophenyl)-2-((1*S*,3*R*)-3-(*tert*-butyl)cyclohexyl)ethan-1-ol to assess the enantioselectivity of the reaction, a reduction by lithium aluminum hydride was required to increase separation via HPLC. The reaction mixture was treated with a LAH solution in THF (1.2 equiv., 1M). Left open to air for 40 minutes, then quenched with hydrated sodium sulfate ($Na_2SO_4 \cdot 10H_2O$). The resulting mixture was filtered over celite and eluted with DCM. Mixture purified via column chromatography (hexanes: ethyl acetate; 4:1) and tested for enantioselectivity on the HPLC (ADH 1mL 1% 30min).

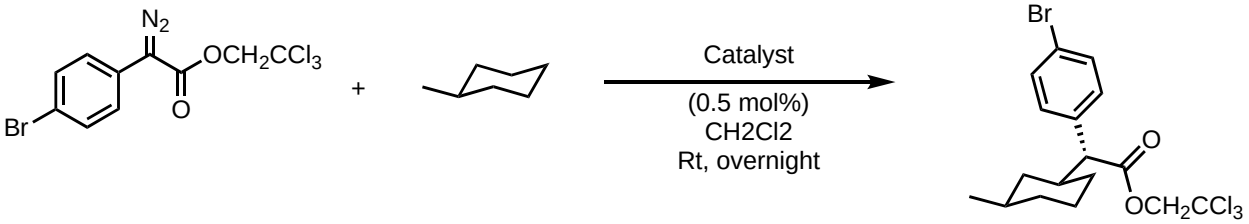

14. 2,2,2-trichloroethyl(*R*)-2-(4-bromophenyl)-2-((1*S*,3*R*)-3-methylcyclohexyl)acetate

Methylcyclohexane (2.5 equiv., .00067mol) and dirhodium catalyst (.005 equiv., 1.3416µmol) were added to flame dried vial under argon in dry DCM (3mL). 2,2,2-trichloroethyl 2-(4-bromophenyl)-2-diazoacetate (1 equiv., 2.683mmol) was added over a minute in dry DCM (1mL) to the reaction mixture. After 1 h., the reaction mixture was vacuum dried, and the crude mixture was assessed via NMR to test for site and diastereoselectivity.

7) HPLC and NMR Data

Rh_2(*S*-*p*-Br-TPPTTL)$_4$ Catalyst Data

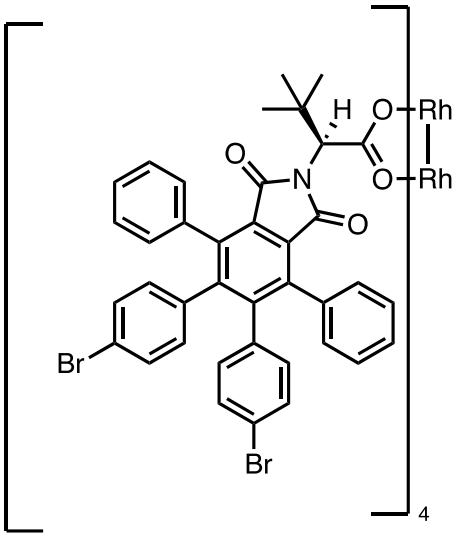

NMR Data for **Rh_2(*S*-*p*-Br-TPPTTL)$_4$** catalyst

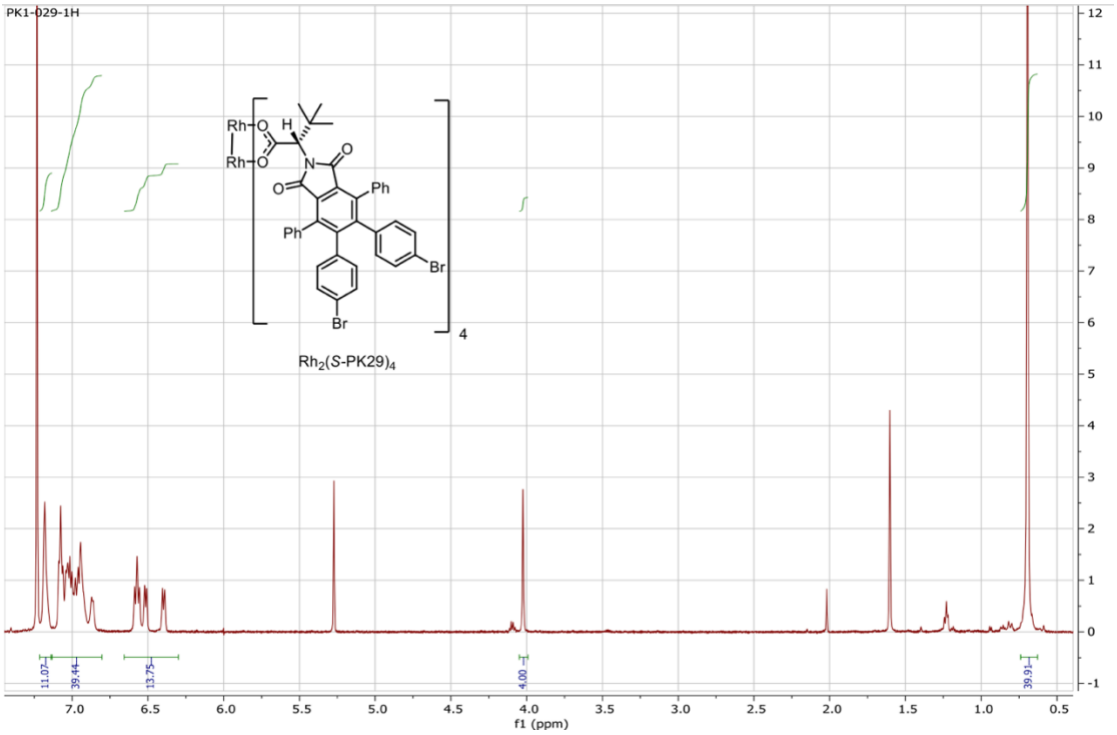

Rh_2(*S*-*p*-Br-TPPTTL)$_4$ C-H Functionalization of ^{t}butyl-cyclohexane **Reaction 12**

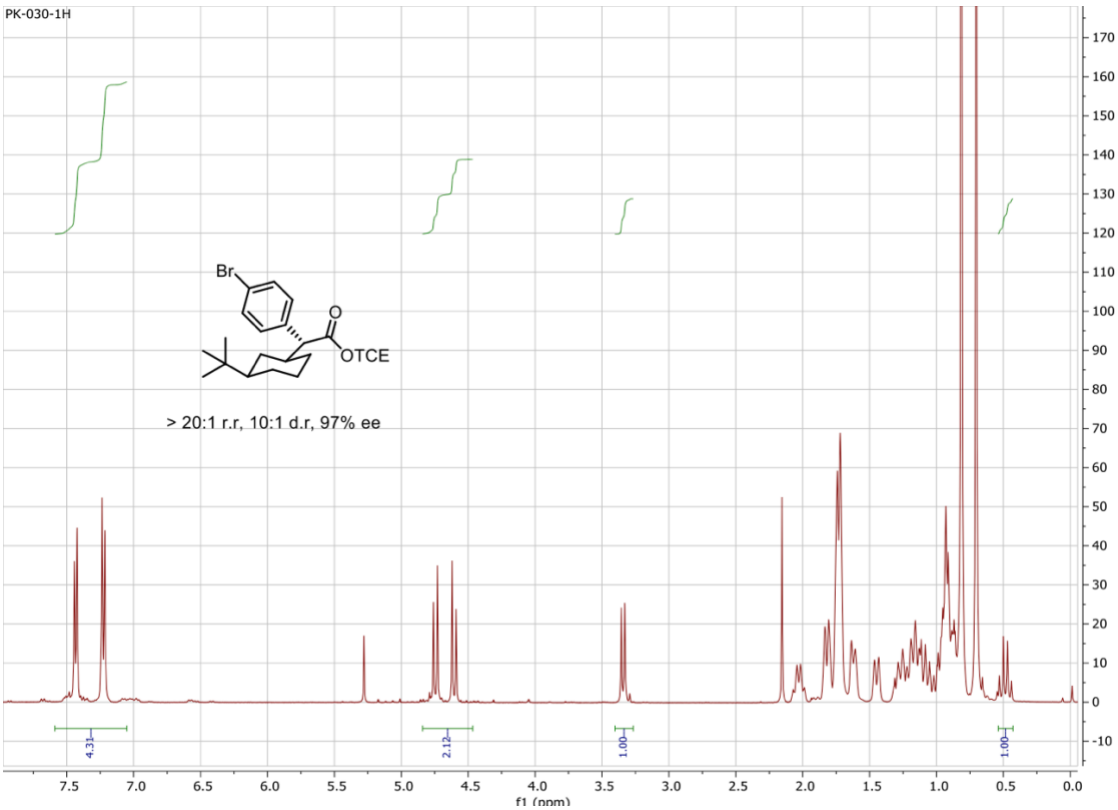

Rh_2(*S-3,5-m*-Br-TPPTTL)$_4$ Catalyst Data

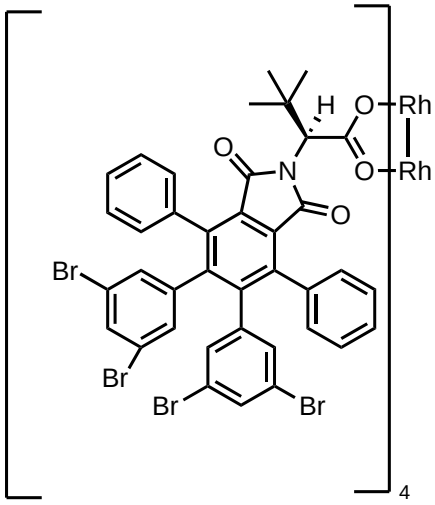

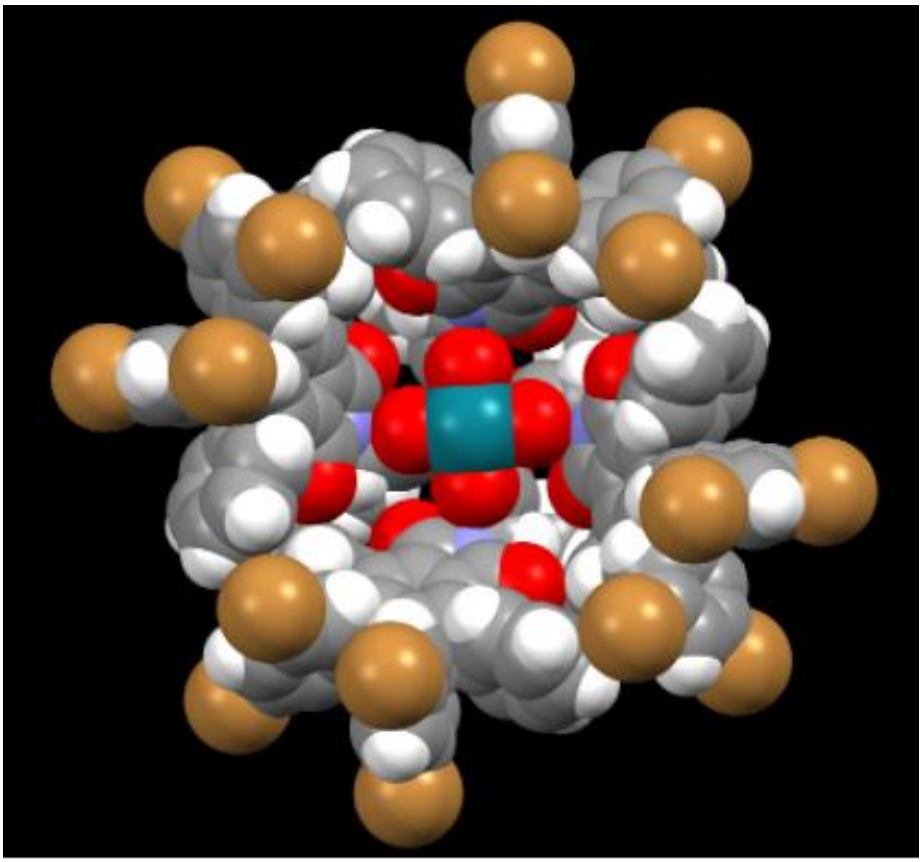

Rh_2(*S-3,5-m*-Br-TPPTTL)$_4$ - cyclopropanation of styrene and 2,2,2-trichloroethyl 2-(4-bromophenyl)-2-diazoacetate **Reaction 9**

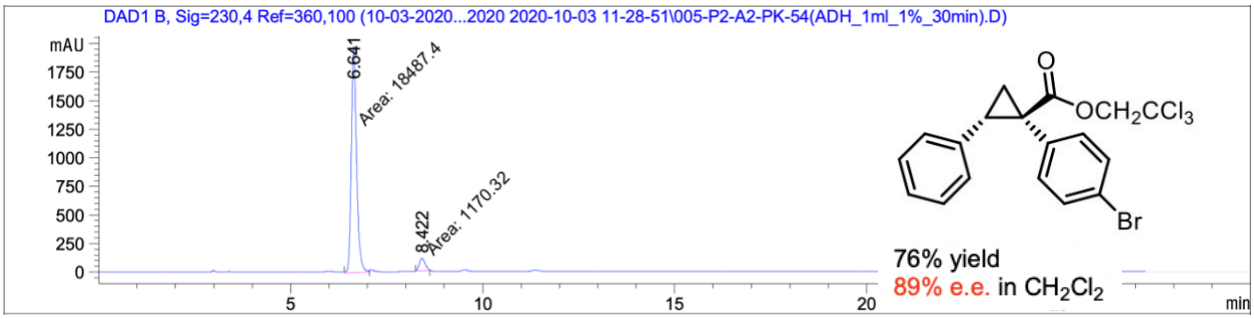

Signal 2: DAD1 B, Sig=230,4 Ref=360,100

Peak #	RetTime [min]	Type	Width [min]	Area [mAU*s]	Height [mAU]	Area %
1	6.641	MM	0.1560	1.84874e4	1975.19458	94.0465
2	8.422	MM	0.1748	1170.31726	111.57094	5.9535

Rh_2(*S-3,5-m*-Br-TPPTTL)$_4$ cyclopropanation of styrene and methyl 2-diazo-2-(2-methoxy-5-methylphenyl) acetate with 0-1.0 equiv. 2-chloropyridine. **Reaction 10**

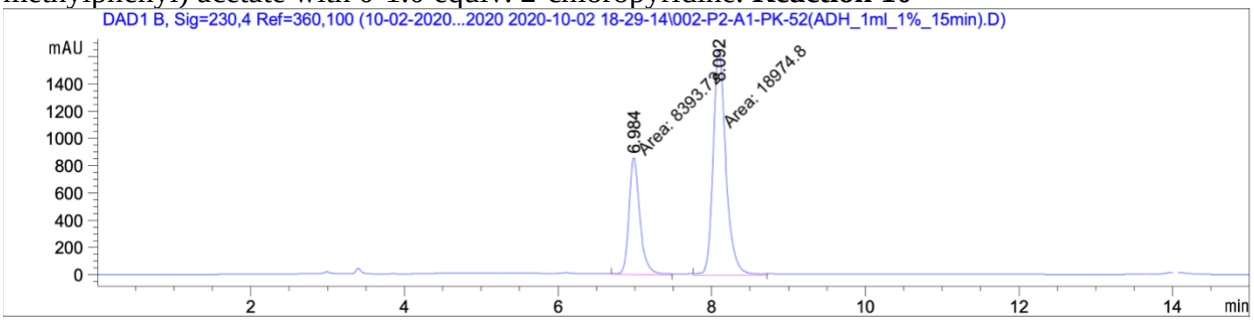

Peak #	RetTime [min]	Type	Width [min]	Area [mAU*s]	Height [mAU]	Area %
1	6.984	MM	0.1634	8393.72266	856.19513	30.6692
2	8.092	MM	0.1914	1.89748e4	1652.46179	69.3308

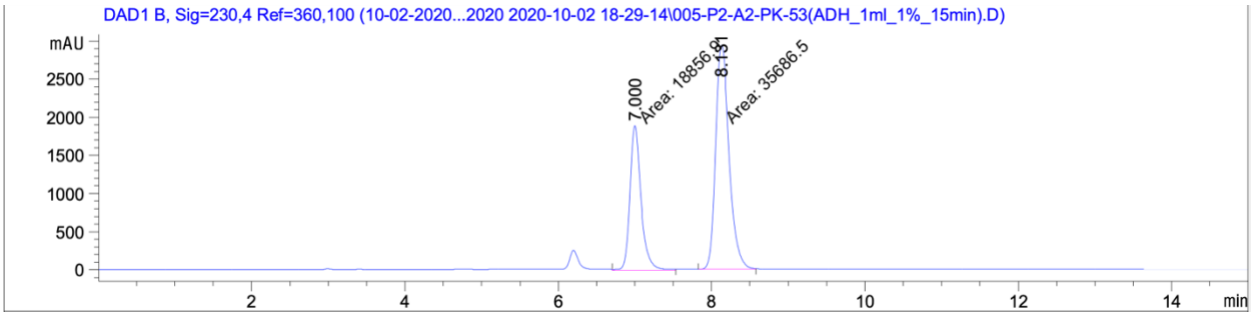

Peak #	RetTime [min]	Type	Width [min]	Area [mAU*s]	Height [mAU]	Area %
1	7.000	MM	0.1658	1.88569e4	1895.53394	34.5723
2	8.131	MM	0.2027	3.56865e4	2934.85083	65.4277
Totals :				5.45434e4	4830.38477	

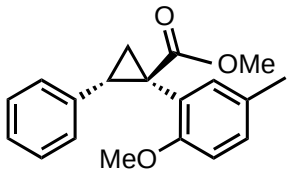

89% yield, 40% e.e. 0.0 equiv 2-chloropyridine
84% yield, 35% e.e. 1.0 equiv 2-chloropyridine

Rh_2(*S-3,5-m*-Br-TPPTTL)$_4$ Selective Cyclopropanations of Isoprene **Reaction 11**

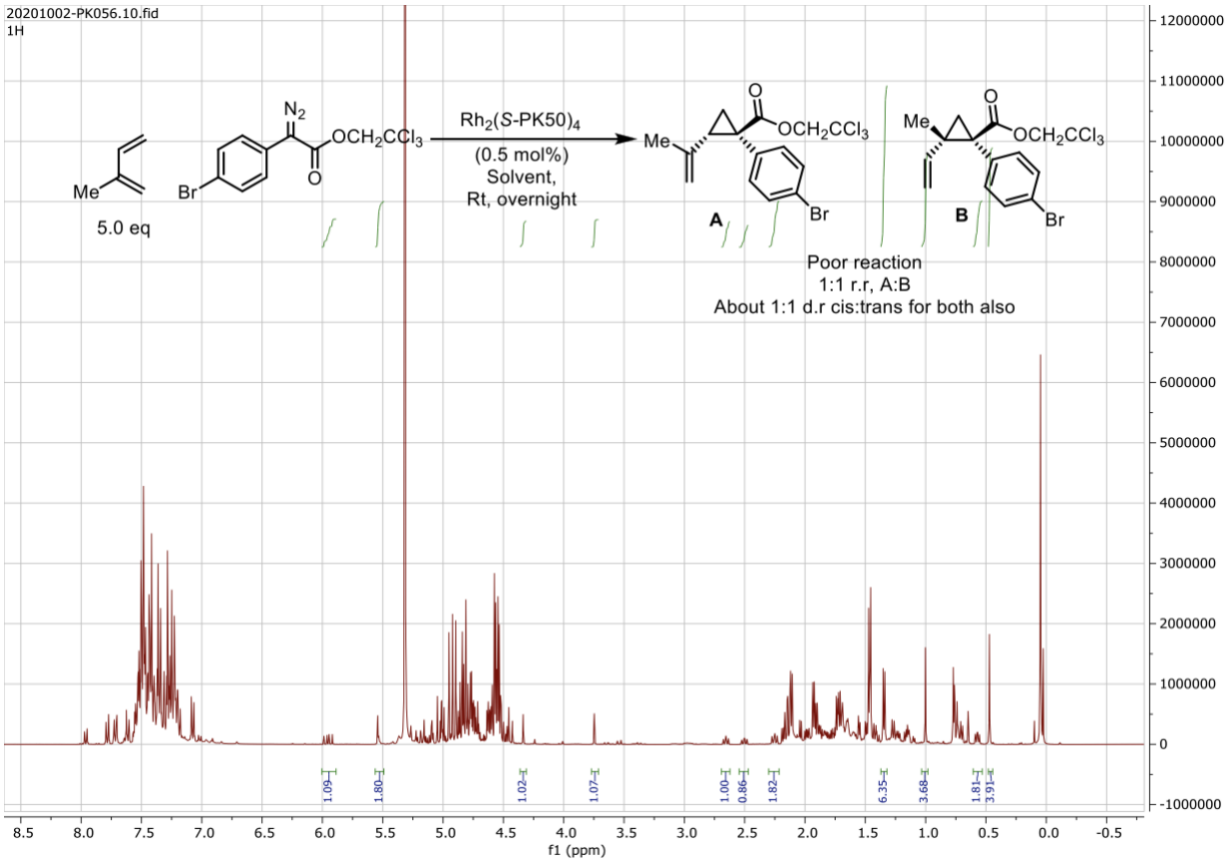

Rh_2(*S-3,5-m*-Br-TPPTTL)$_4$ C-H Functionalization of ^{t}butyl-cyclohexane **Reaction 12**

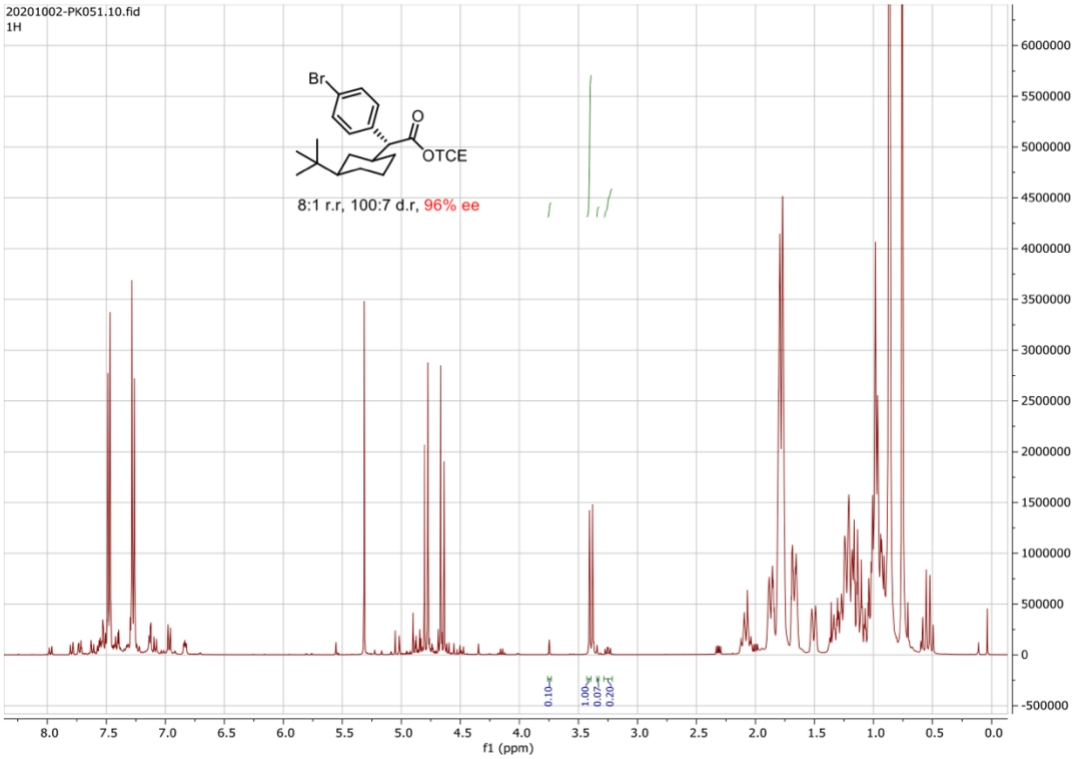

Rh_2(*S-3,5-m*-Br-TPPTTL)$_4$ C-H Functionalization of methylcyclohexane **Reaction 14**

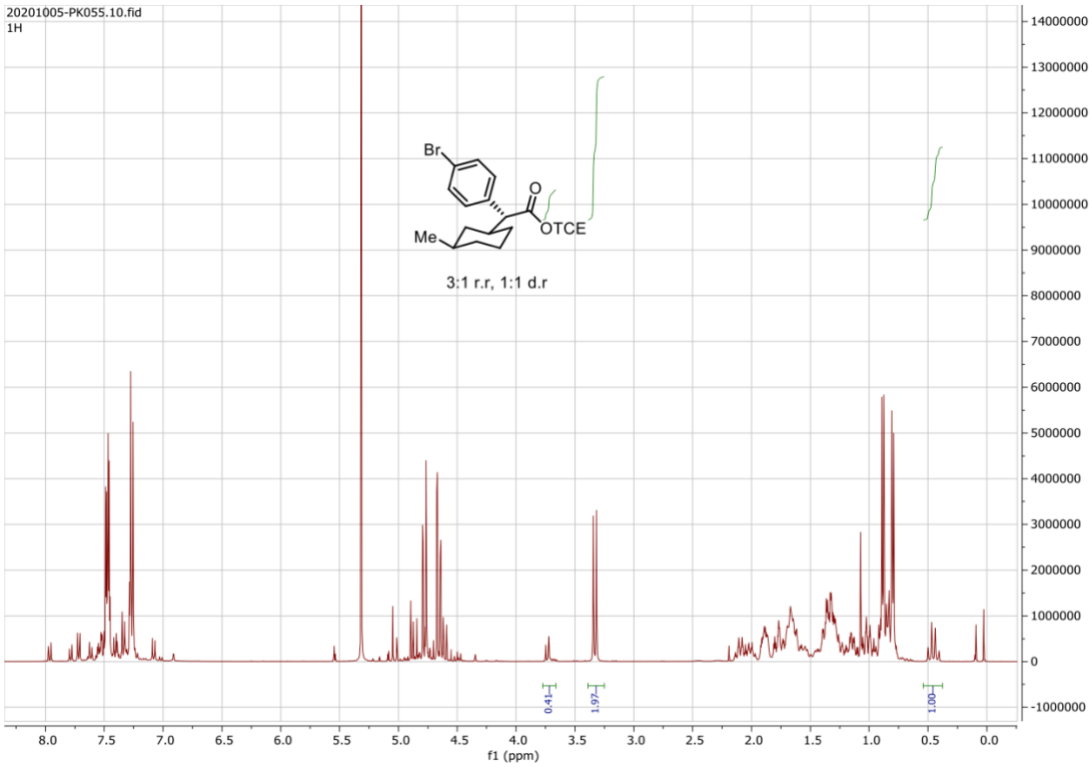

Rh_2(*S*-*p*-^{t}butyl-TPPTTL)$_4$ Catalyst Data

Mass Spectrometry confirmation of product

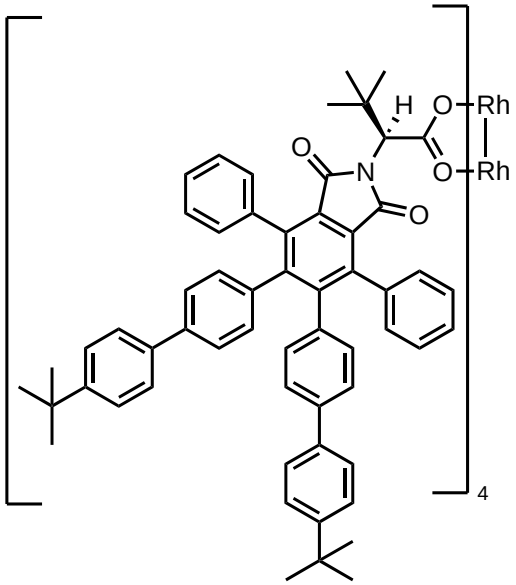

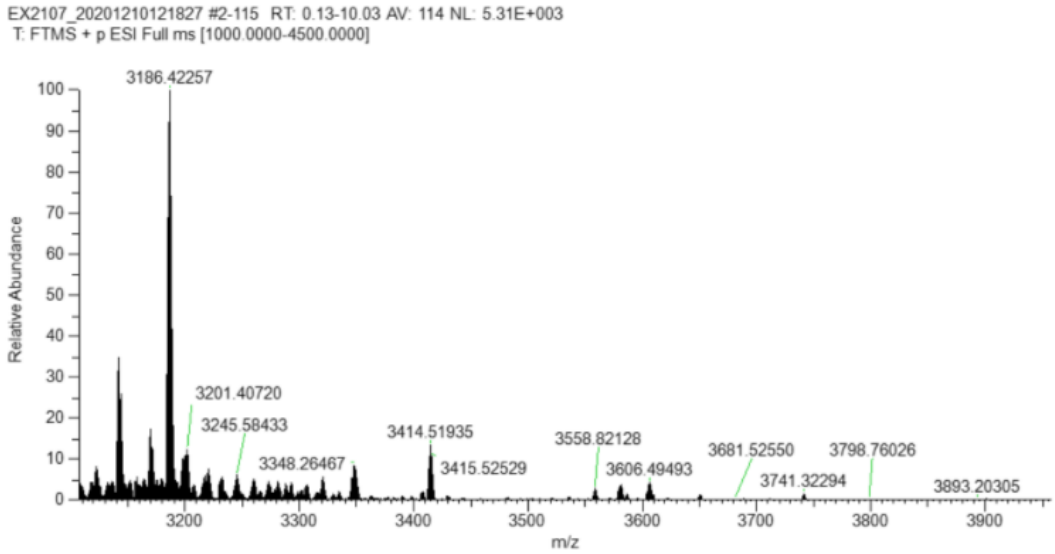

PK1-TBU

Peak Mass	Display Formula	RDB	Delta [ppm]	Delta [mmu]	Theo. mass	Combined Score	MS Cov. [%]
3184.41494	$C_{215}H_{86}O_{16}N_4{}^{103}Rh_2$	177	0.19	0.6	3184.41434	94.6	97.67
3184.41494	$C_{203}H_{215}O_{16}N_5{}^{103}Rh_2$	101	-3.74	-11.9	3184.42684	87.34	91.02
3184.41494	$C_{214}H_{84}O_{16}N_5{}^{103}Rh_2$	177.5	4.14	13.17	3184.40177	82.63	85.83

Rh_2(*S*-*p*-^{t}butyl-TPPTTL)$_4$ cyclopropanation of styrene and 2,2,2-trichloroethyl 2-(4-bromophenyl)-2-diazoacetate **Reaction 9**

Chromatogram :
PK102(OJH_1ML_1%_30MIN)6_channel2

System : Prostar LC System
Method : ADH_30min_1mL_1%-230nm
User : User1

Acquired : 12/16/2020 8:29:03 PM
Processed : 12/17/2020 6:02:47 PM
Printed : 12/17/2020 6:03:13 PM

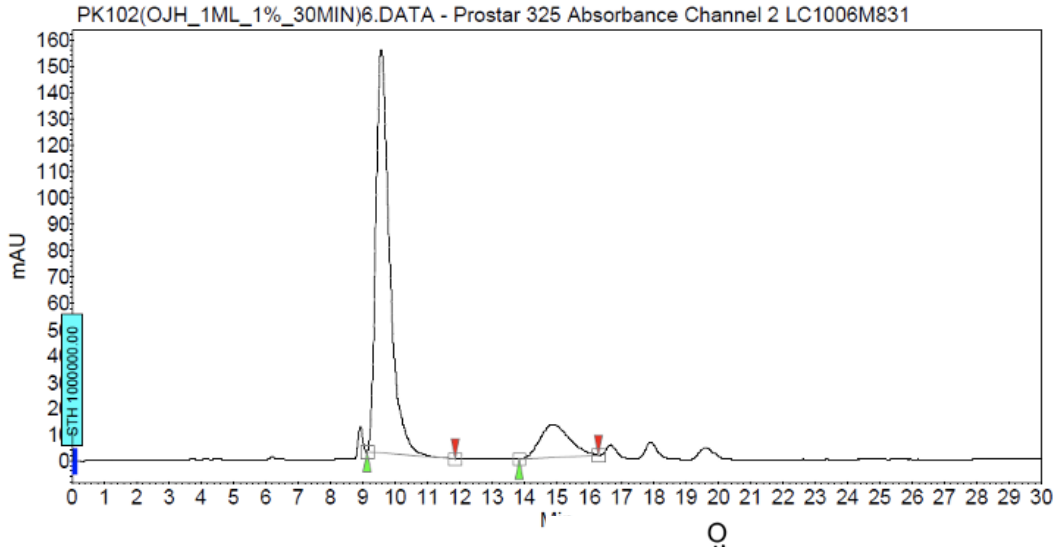

Peak results :

Index	Name	Time [Min]	Quantity [% Area]	Height [mAU]	Area [mAU.Min]	Area % [%]
1	UNKNOWN	9.57	85.29	153.0	76.3	85.288
2	UNKNOWN	14.87	14.71	12.4	13.2	14.712
Total			100.00	165.4	89.5	100.000

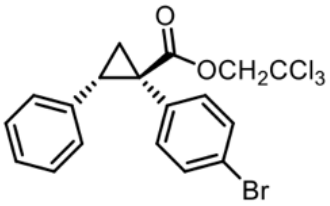

70% ee with CH_2Cl_2

Rh_2(*S*-*p*-^{t}butyl-TPPTTL)$_4$ cyclopropanation of styrene and methyl 2-diazo-2-(2-methoxy-5-methylphenyl) acetate with 0-1.0 equiv. 2-chloropyridine. **Reaction 10.**

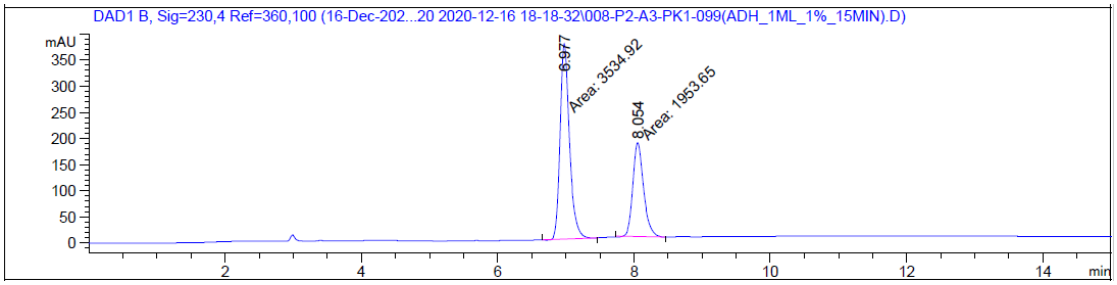

Signal 2: DAD1 B, Sig=230,4 Ref=360,100

Peak #	RetTime [min]	Type	Width [min]	Area [mAU*s]	Height [mAU]	Area %
1	6.977	MM	0.1575	3534.91968	374.00235	64.4051
2	8.054	MM	0.1812	1953.64990	179.66176	35.5949
Totals :				5488.56958	553.66411	

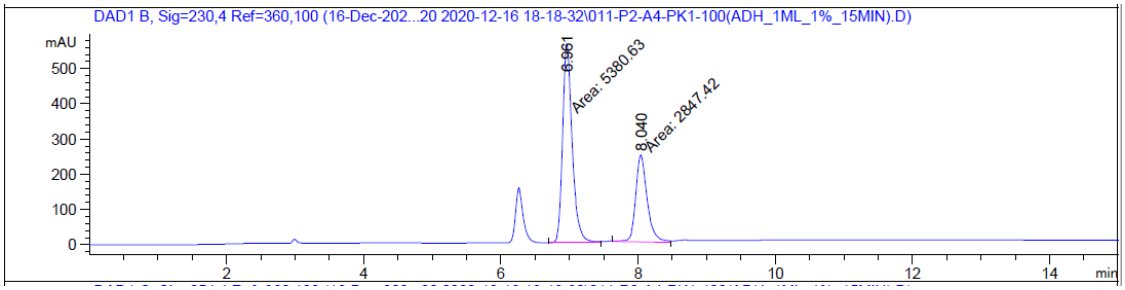

Signal 2: DAD1 B, Sig=230,4 Ref=360,100

Peak #	RetTime [min]	Type	Width [min]	Area [mAU*s]	Height [mAU]	Area %
1	6.961	MM	0.1591	5380.62695	563.63892	65.3937
2	8.040	MM	0.1926	2847.42383	246.35867	34.6063
Totals :				8228.05078	809.99759	

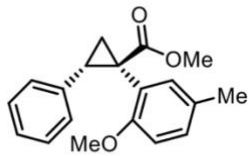

29% ee without additive
31% ee with 1.0 equiv 2-Clpyridine

Rh_2(*S*-*p*-^{t}butyl-TPPTTL)$_4$ Selective cyclopropanation of isoprene **Reaction 11**

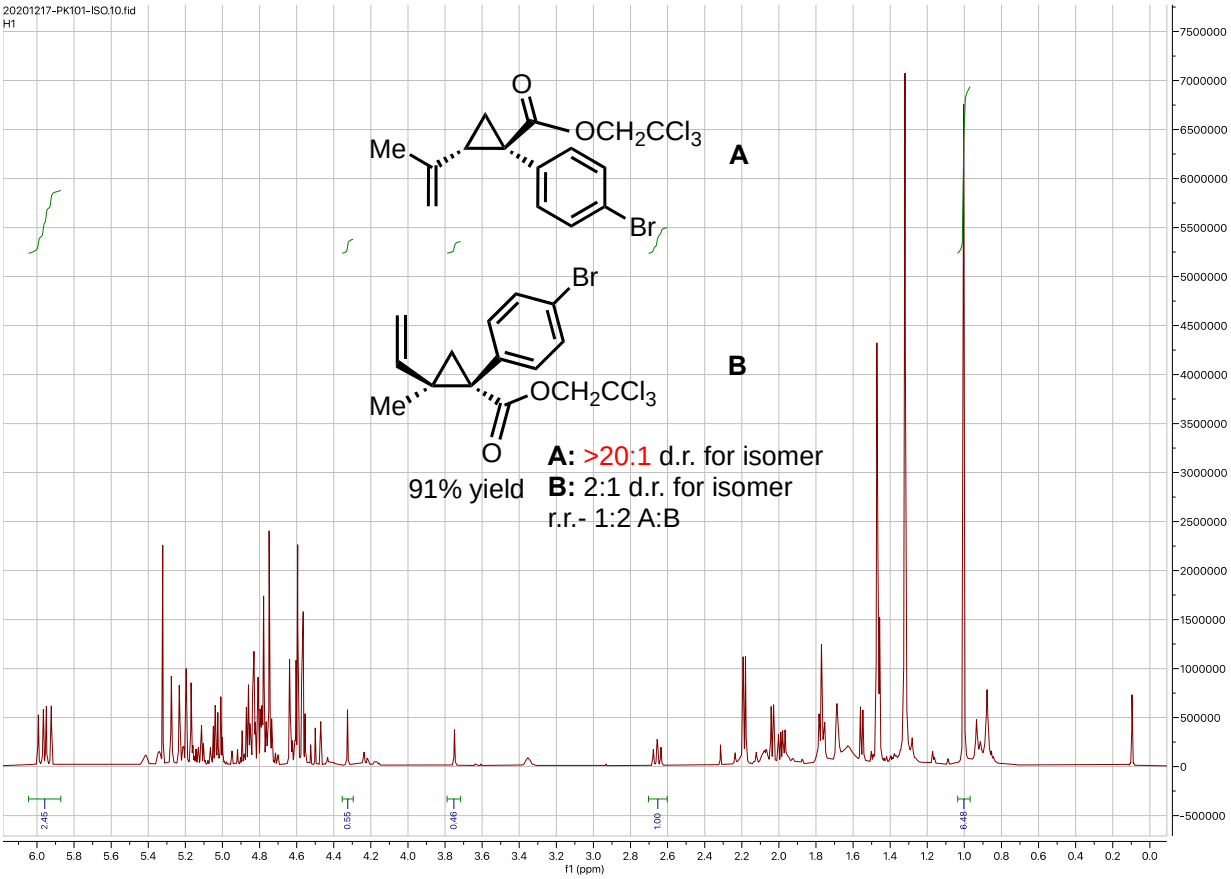

Rh_2(*S*-*p*-^{t}butyl-TPPTTL)$_4$ C-H Functionalization of ^{t}butyl-cyclohexane **Reaction 13**

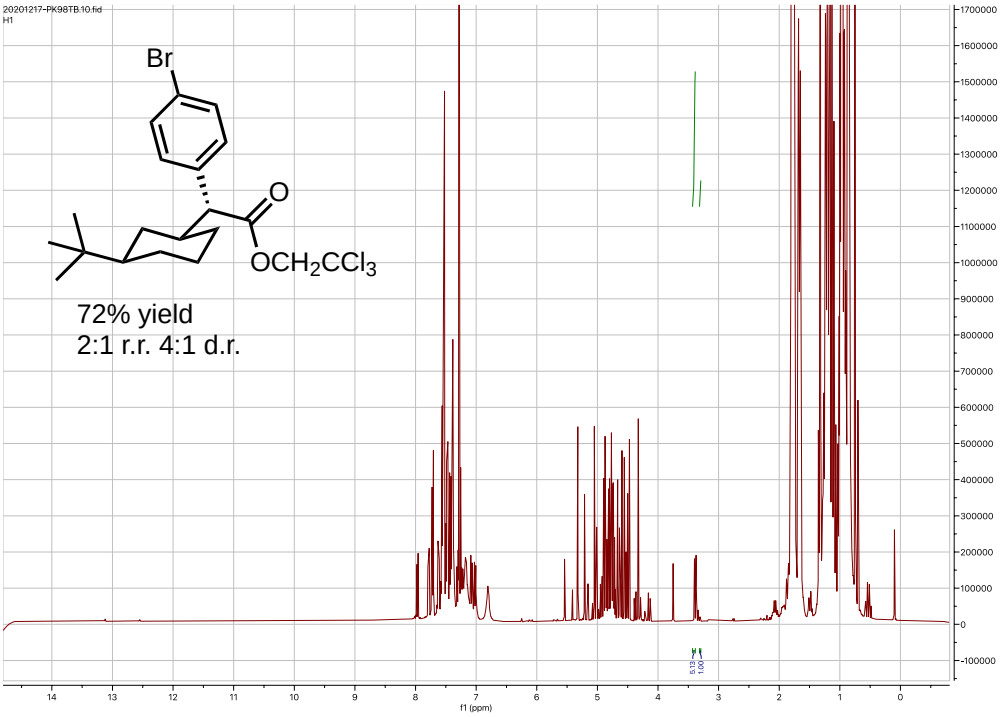

Rh_2(*S*-*p*-^{t}butyl-TPPTTL)$_4$ C-H functionalization of methylcyclohexane **Reaction 14**

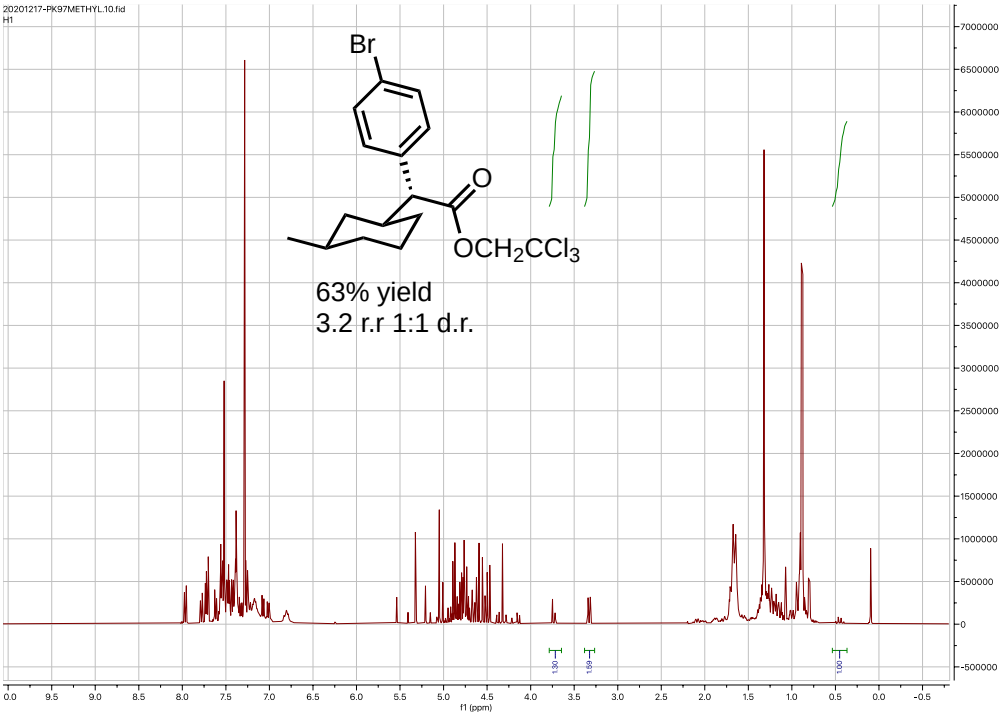

Rh_2(*S*-*p*-bisCF_3-TPPTTL)$_4$ Catalyst Data

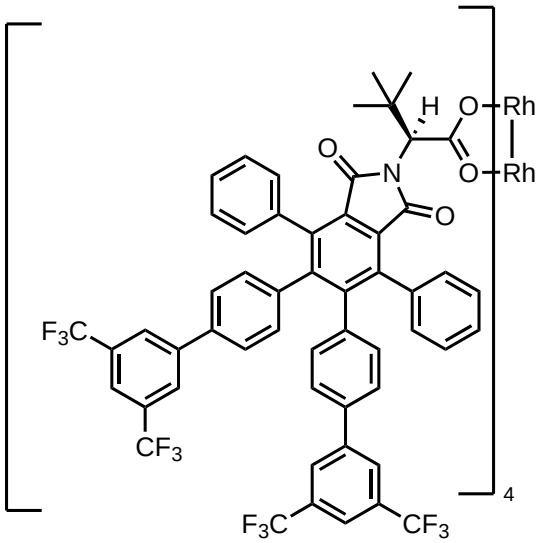

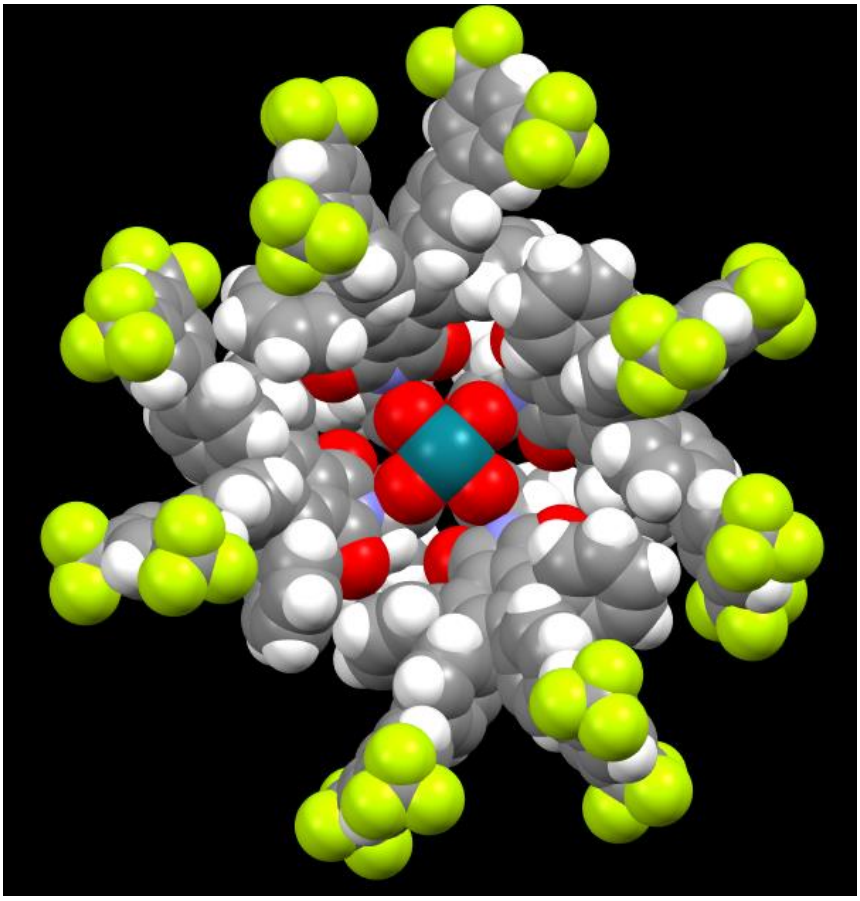

Rh_2(*S*-*p*-bisCF$_3$-TPPTTL)$_4$ Cyclopropanation of styrene and 2,2,2-trichloroethyl 2-(4-bromophenyl)-2-diazoacetate **Reaction 9.**

Chromatogram :
PK96(OJH_1ML_1%_30MIN)3_channel2

System : Prostar LC System
Method : ADH_30min_1mL_1%-230nm
User : User1

Acquired : 12/16/2020 7:11:31 PM
Processed : 12/16/2020 8:25:29 PM
Printed : 12/17/2020 6:03:08 PM

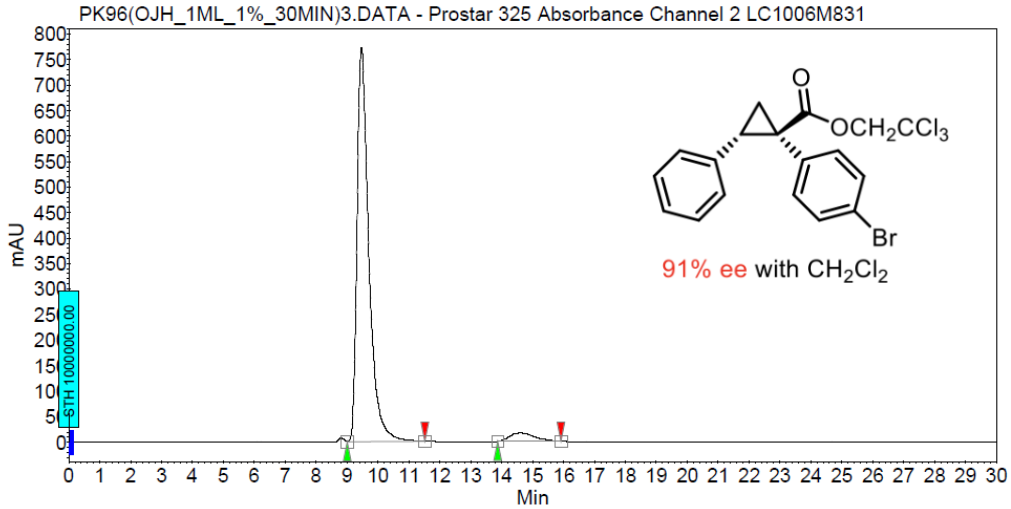

Peak results :

Index	Name	Time [Min]	Quantity [% Area]	Height [mAU]	Area [mAU.Min]	Area % [%]
1	UNKNOWN	9.46	95.63	771.3	341.4	95.634
2	UNKNOWN	14.59	4.37	17.1	15.6	4.366
Total			100.00	788.4	357.0	100.000

Rh_2(*S*-*p*-bisCF$_3$-TPPTTL)$_4$ cyclopropanation of styrene and methyl 2-diazo-2-(2-methoxy-5-methylphenyl) acetate with 0-1.0 equiv. 2-chloropyridine. **Reaction 10.**

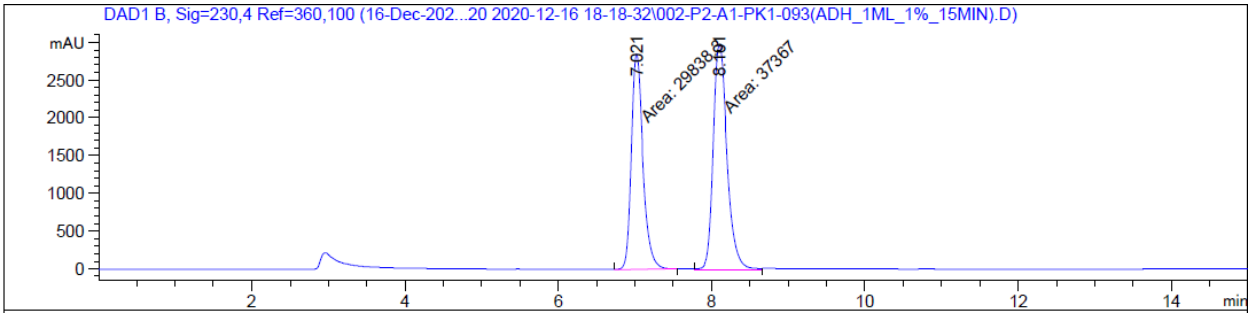

Signal 2: DAD1 B, Sig=230,4 Ref=360,100

Peak #	RetTime [min]	Type	Width [min]	Area [mAU*s]	Height [mAU]	Area %
1	7.021	MM	0.1747	2.98383e4	2846.98120	44.3988
2	8.101	MM	0.2094	3.73670e4	2973.50415	55.6012
Totals :				6.72053e4	5820.48535	

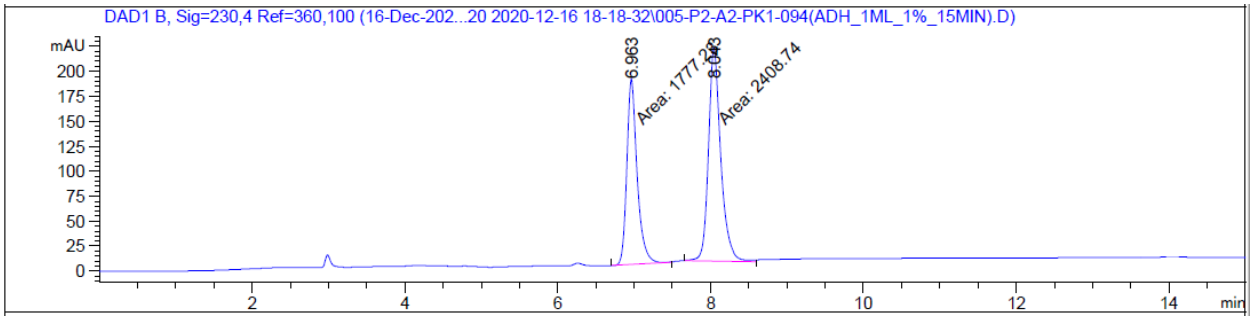

Signal 2: DAD1 B, Sig=230,4 Ref=360,100

Peak #	RetTime [min]	Type	Width [min]	Area [mAU*s]	Height [mAU]	Area %
1	6.963	MM	0.1585	1777.22998	186.82945	42.4569
2	8.043	MM	0.1877	2408.73657	213.92535	57.5431
Totals :				4185.96655	400.75481	

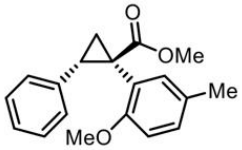

11% ee without additive
15% ee with 1.0 equiv 2-Clpyridine

Rh_2(*S*-*p*-bisCF$_3$-TPPTTL)$_4$ Selective cyclopropanation of isoprene **Reaction 11**

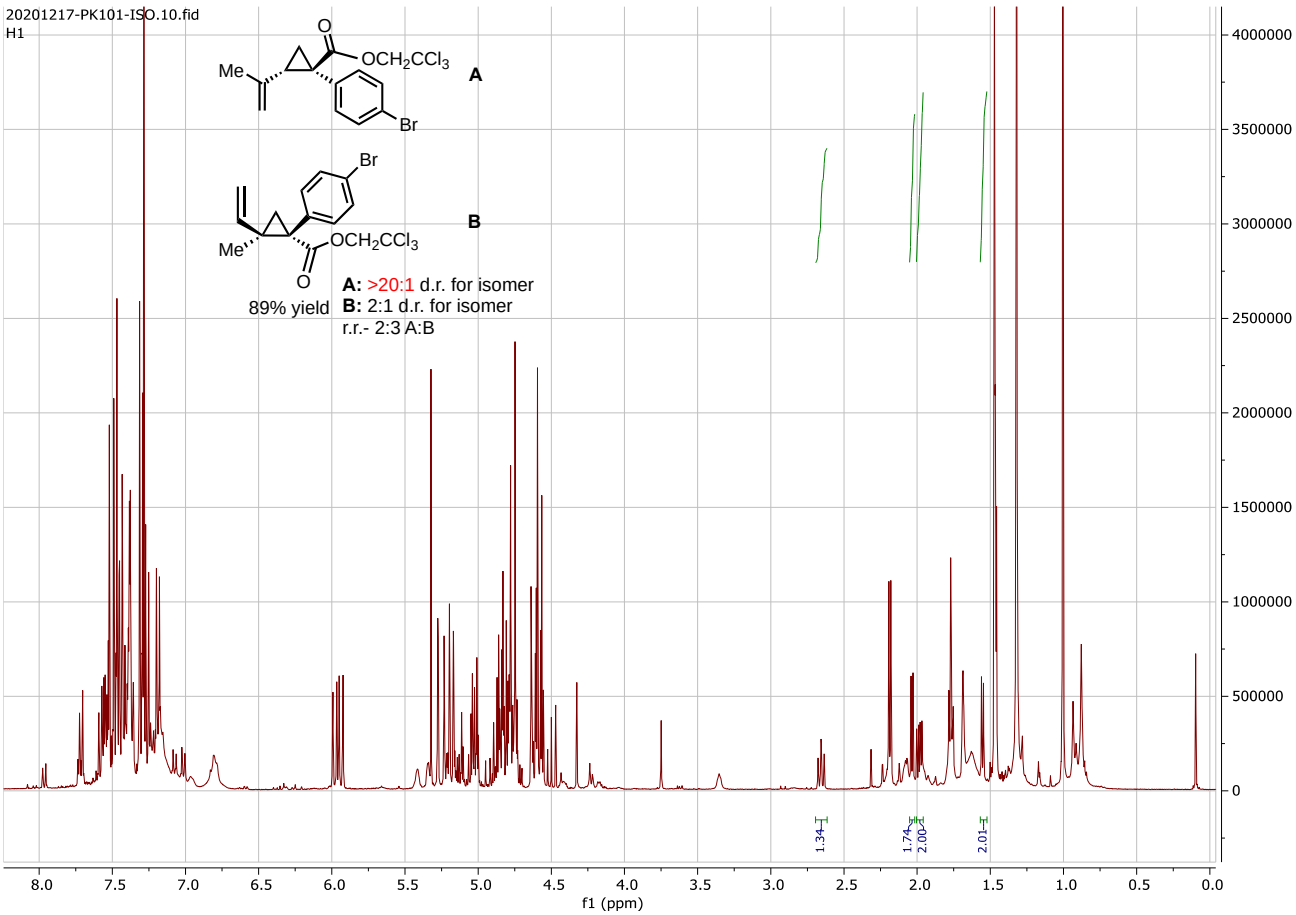

Rh_2(*S*-*p*-bisCF$_3$-TPPTTL)$_4$ C-H functionalization of ^{t}butyl-cyclohexane **Reaction 12.**

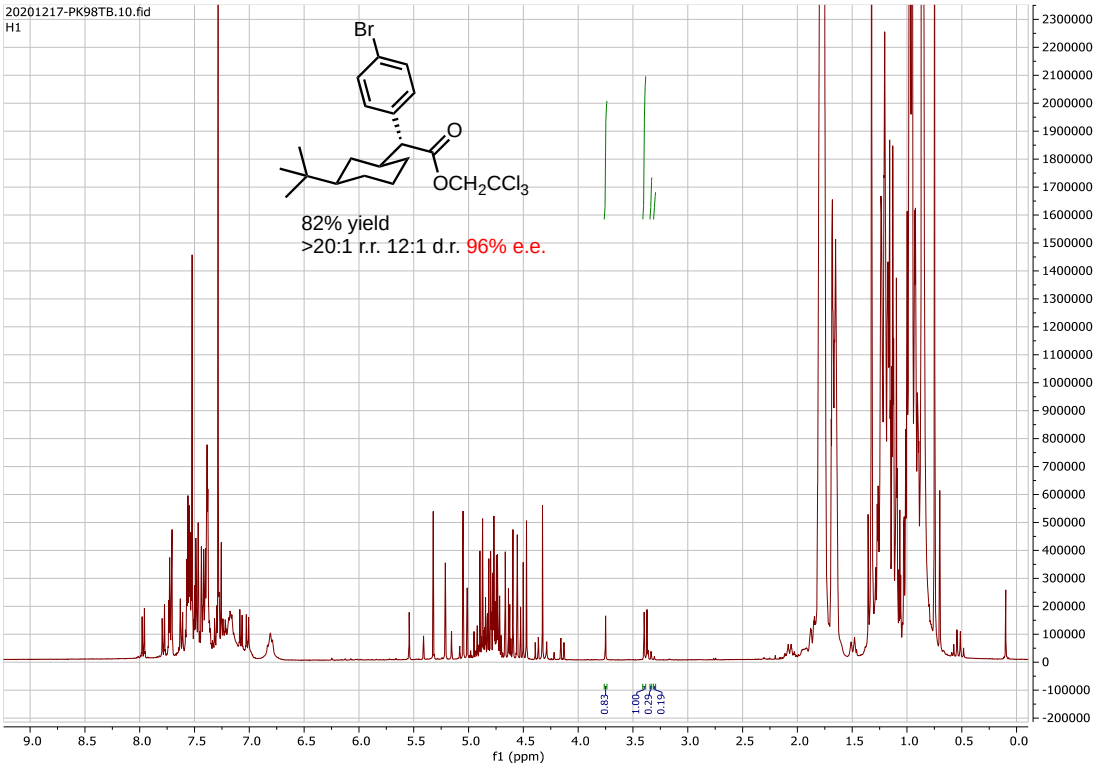

Rh_2(*S*-*p*-bisCF$_3$-TPPTTL)$_4$ C-H functionalization of methylcyclohexane **Reaction 14.**

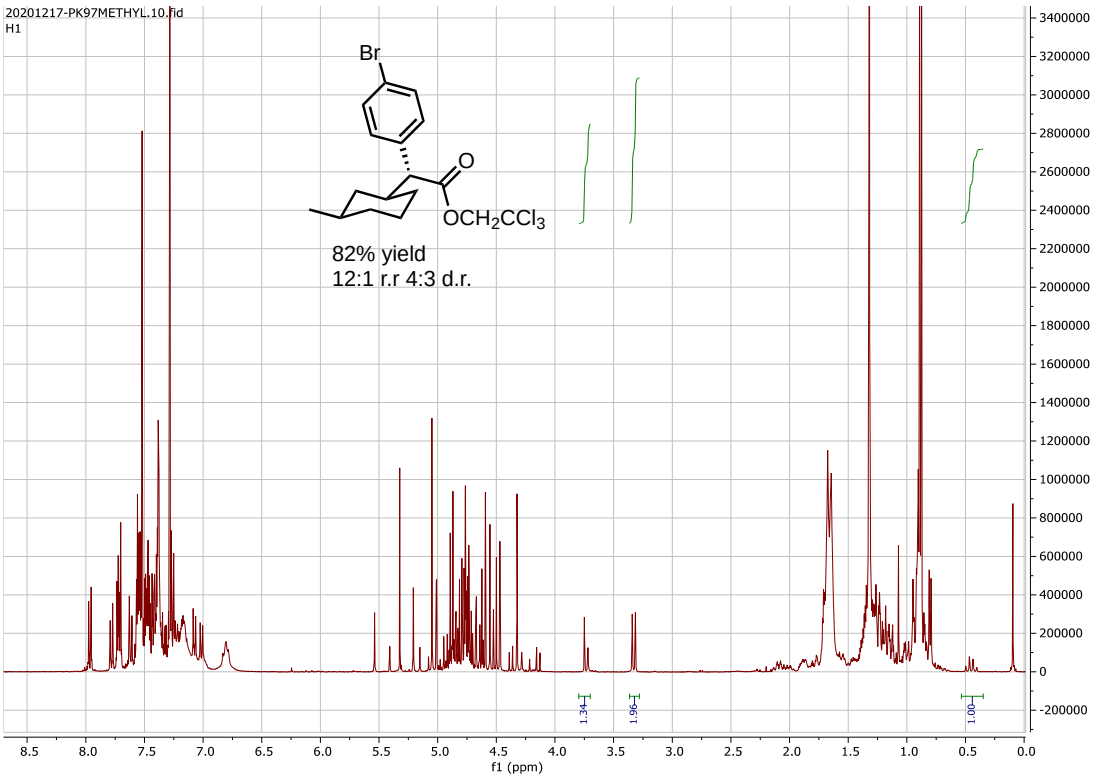

Rh_2(*S*-*p*-mesityl-TPPTTL)$_4$ Catalyst

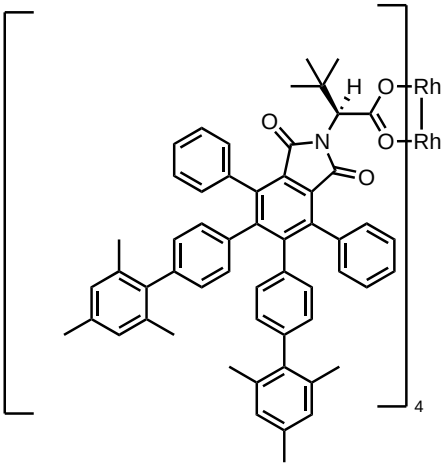

Peak Mass	Display Formula	RDB	Delta [ppm]	Delta [mmu]	Theo. mass	Combined Score	MS Cov. [%]
3408.34293	$C_{224}H_{201}O_{16}N_4{}^{103}Rh_2$	128.5	8.42	28.71	3408.31422	96.09	99.67

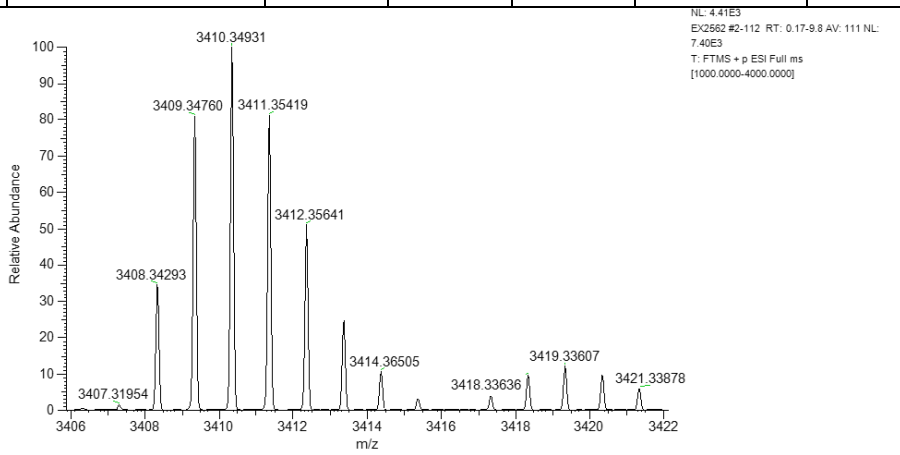

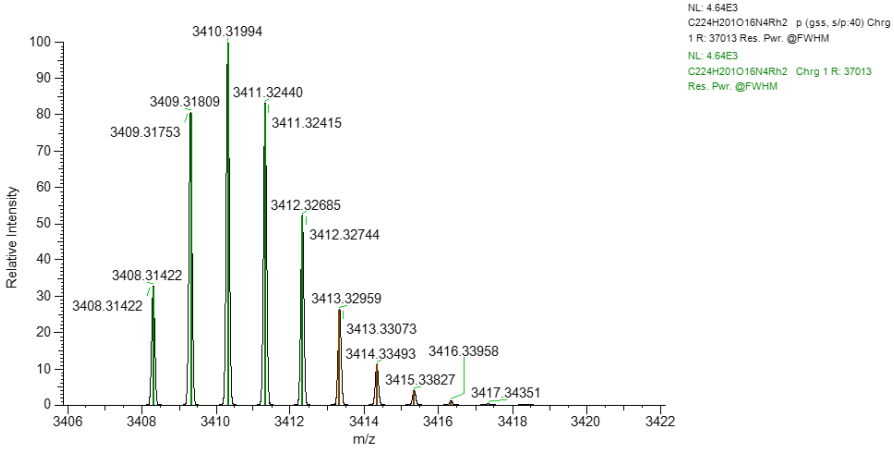

Rh2(S-p-mesityl-TPPTTL)4 Cyclopropanation of styrene and 2,2,2-trichloroethyl 2-(4-bromophenyl)-2-diazoacetate **Reaction 9.**

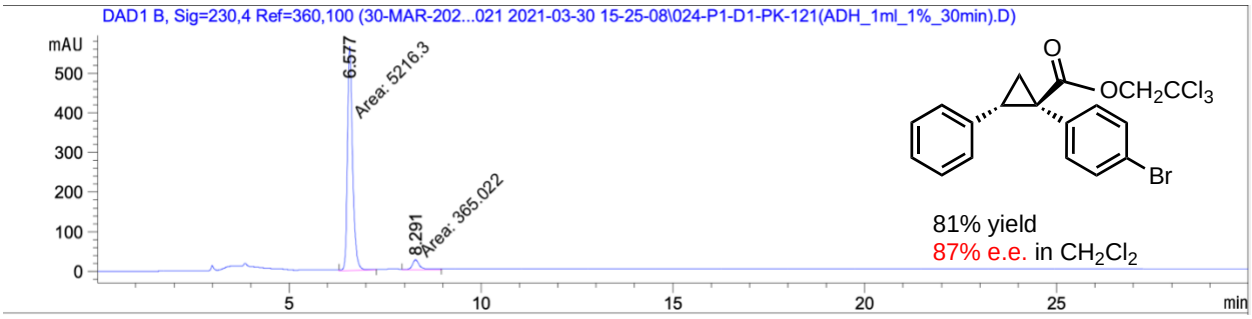

Peak #	RetTime [min]	Type	Width [min]	Area [mAU*s]	Height [mAU]	Area %
1	6.577	MM	0.1537	5216.30078	565.62653	93.4599
2	8.291	MM	0.2475	365.02197	24.58404	6.5401

Rh_2(*S*-*p*-mesityl-TPPTTL)$_4$ cyclopropanation of styrene and methyl 2-diazo-2-(2-methoxy-5-methylphenyl) acetate with 0-1.0 equiv. 2-chloropyridine. **Reaction 10.**

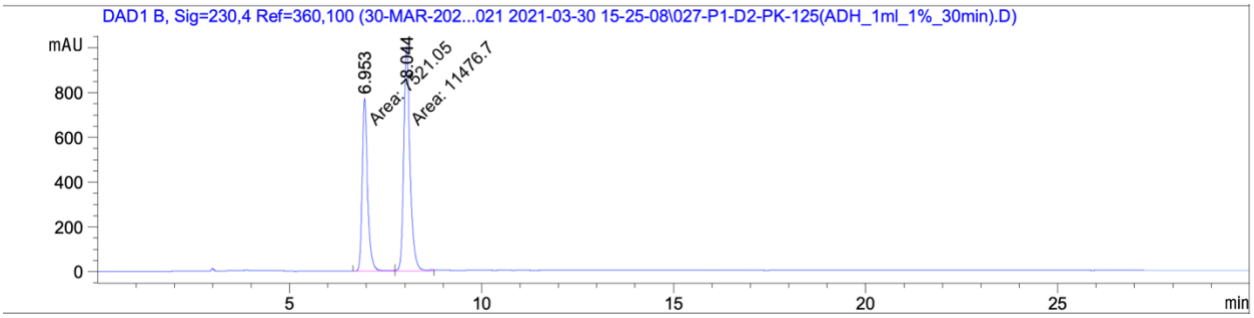

Peak #	RetTime [min]	Type	Width [min]	Area [mAU*s]	Height [mAU]	Area %
1	6.953	MM	0.1628	7521.05322	770.00885	39.5892
2	8.044	MM	0.1907	1.14767e4	1003.17859	60.4108

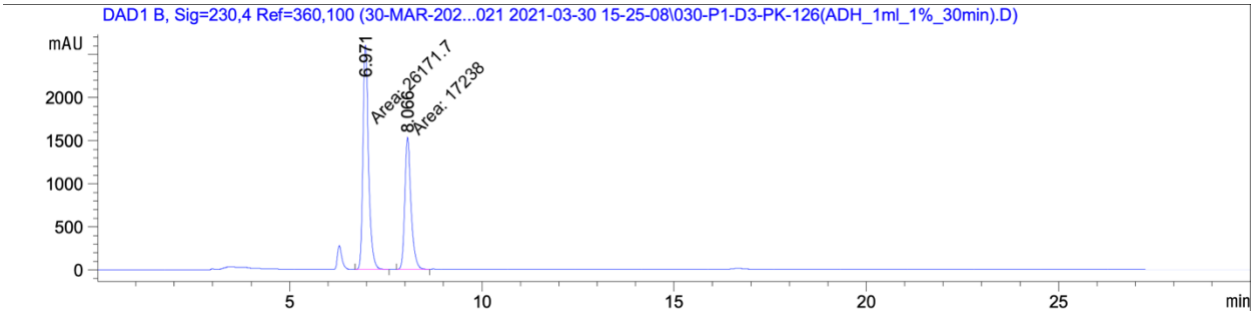

Peak #	RetTime [min]	Type	Width [min]	Area [mAU*s]	Height [mAU]	Area %
1	6.971	MM	0.1677	2.61717e4	2600.43042	60.2901
2	8.066	MM	0.1882	1.72380e4	1526.75342	39.7099

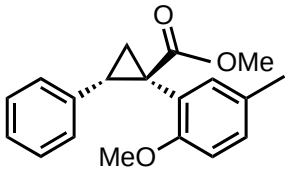

62% yield, 21% e.e. 0.0 equiv 2-chloropyridine
74% yield, 21% inverted e.e. 1.0 equiv 2-chloropyridine

Rh_2(*S*-*p*-mesityl-TPPTTL)$_4$ Selective cyclopropanation of isoprene **Reaction 11**

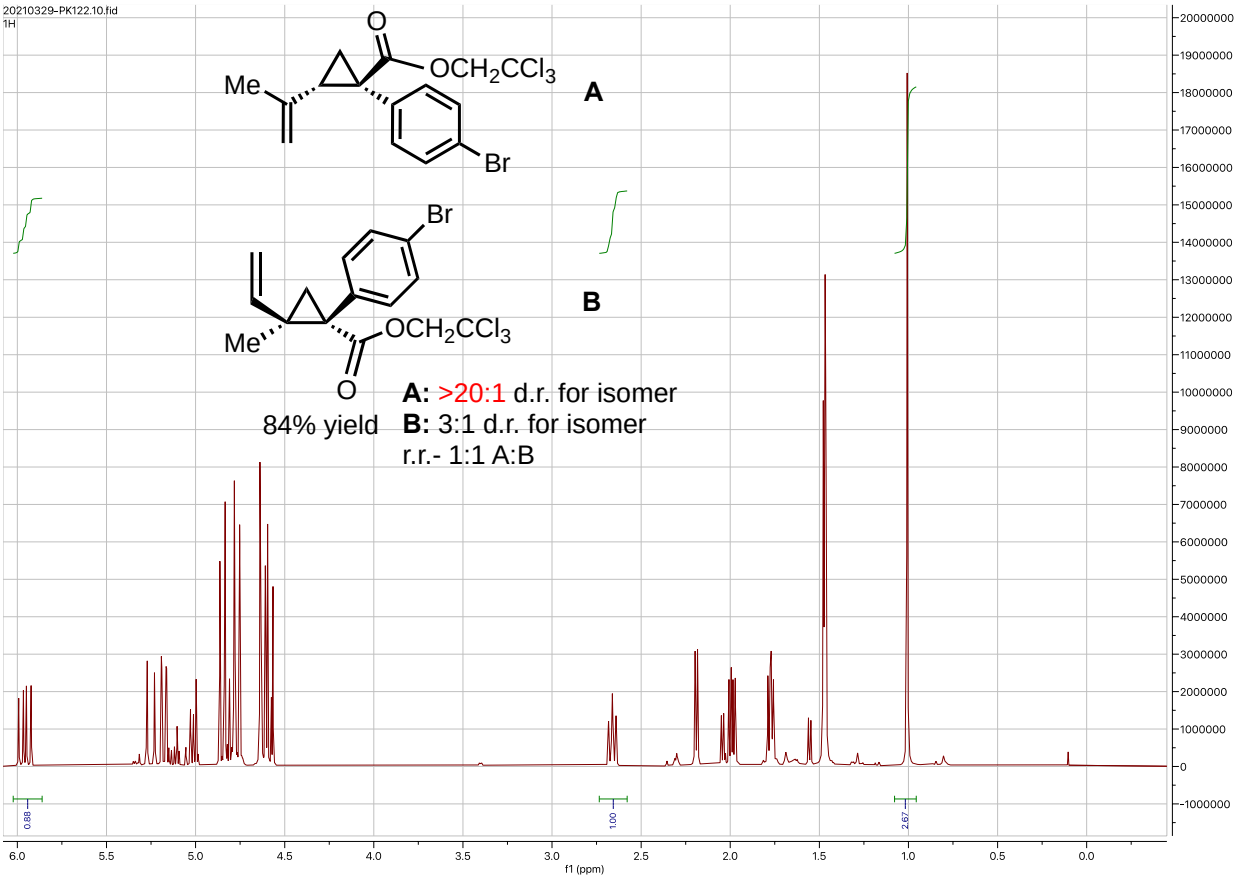

Rh_2(*S*-*p*-mesityl-TPPTTL)$_4$ C-H functionalization of ^{t}butyl-cyclohexane **Reaction 12.**

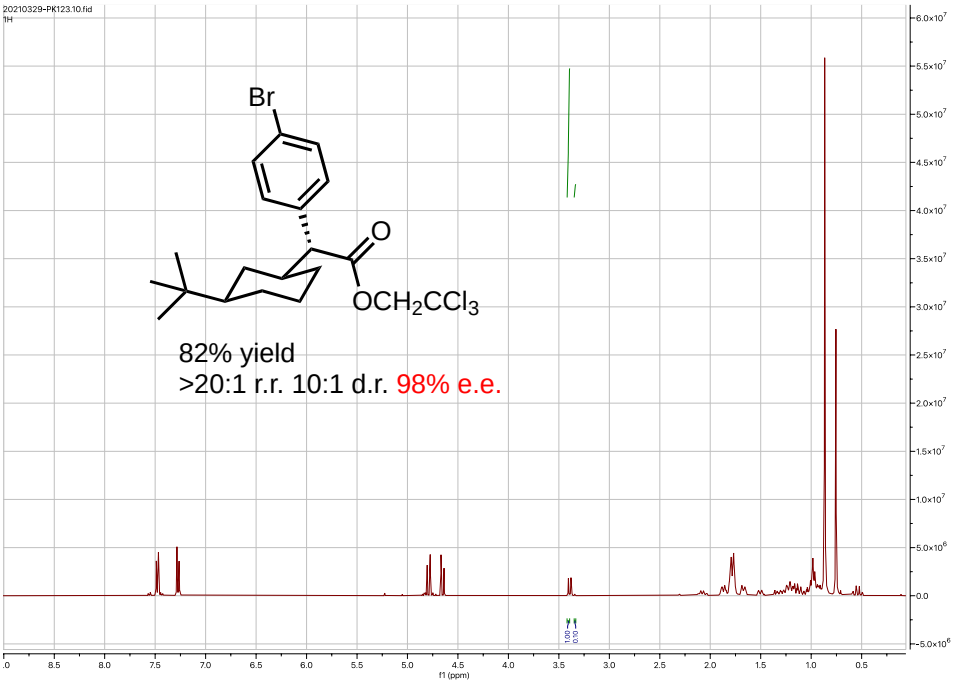

Rh_2(*S*-*p*-mesityl-TPPTTL)$_4$ C-H functionalization of methylcyclohexane **Reaction 14.**

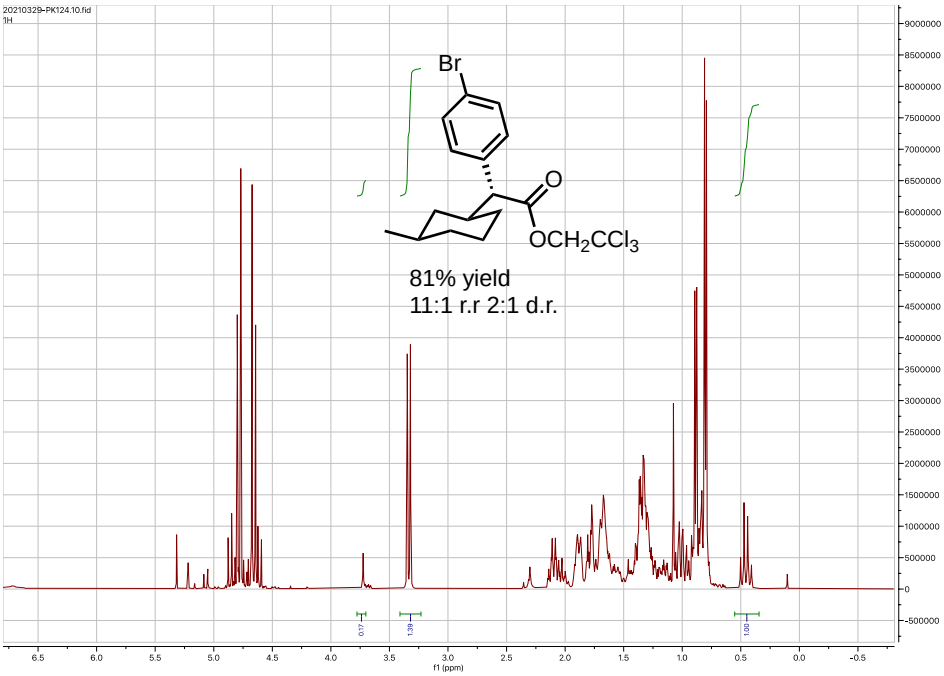

Rh_2(*S-3,5-m*-ph-TPPTTL)$_4$ Catalyst

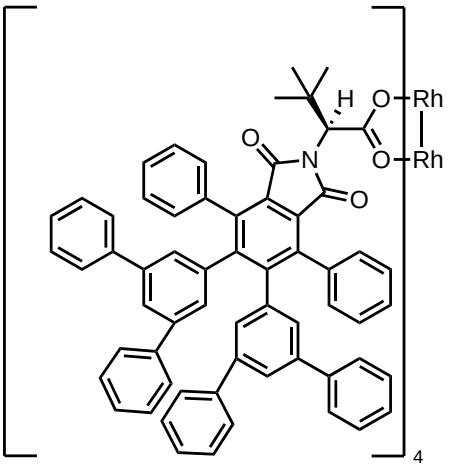

Peak Mass	Display Formula	RDB	Delta [ppm]	Delta [mmu]	Theo. mass	Combined Score	MS Cov. [%]
3679.18511	$C_{248}H_{186}O_{15}N_5{}^{103}Rh_2$	160.5	-5.41	-19.89	3679.205	35.65	37.04
3679.18511	$C_{248}H_{184}O_{16}N_4{}^{103}Rh_2$	161	1.06	3.92	3679.18119	20.06	20.95

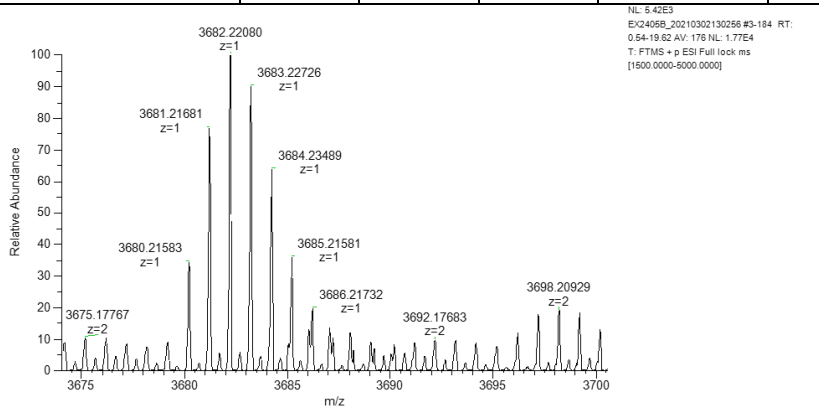

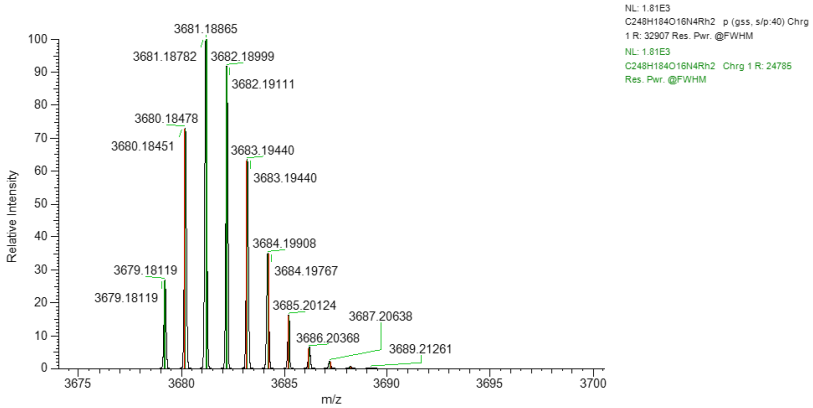

Rh_2(*S-3,5-m*-ph-TPPTTL)$_4$ Cyclopropanation of styrene and 2,2,2-trichloroethyl 2-(4-bromophenyl)-2-diazoacetate **Reaction 9.**

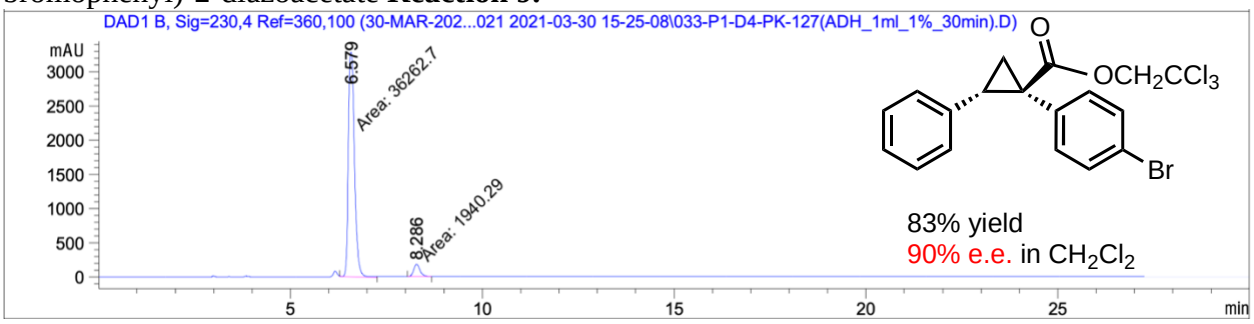

Peak #	RetTime [min]	Type	Width [min]	Area [mAU*s]	Height [mAU]	Area %
1	6.579	MM	0.1844	3.62627e4	3277.44287	94.9211
2	8.286	MM	0.1821	1940.28967	177.62146	5.0789

Rh_2(*S-3,5-m*-ph-TPPTTL)$_4$ cyclopropanation of styrene and methyl 2-diazo-2-(2-methoxy-5-methylphenyl) acetate with 0-1.0 equiv. 2-chloropyridine. **Reaction 10.**

Peak #	RetTime [min]	Type	Width [min]	Area [mAU*s]	Height [mAU]	Area %
1	6.963	MM	0.1599	3768.57764	392.92804	43.4025
2	8.052	MM	0.1873	4914.27930	437.18900	56.5975

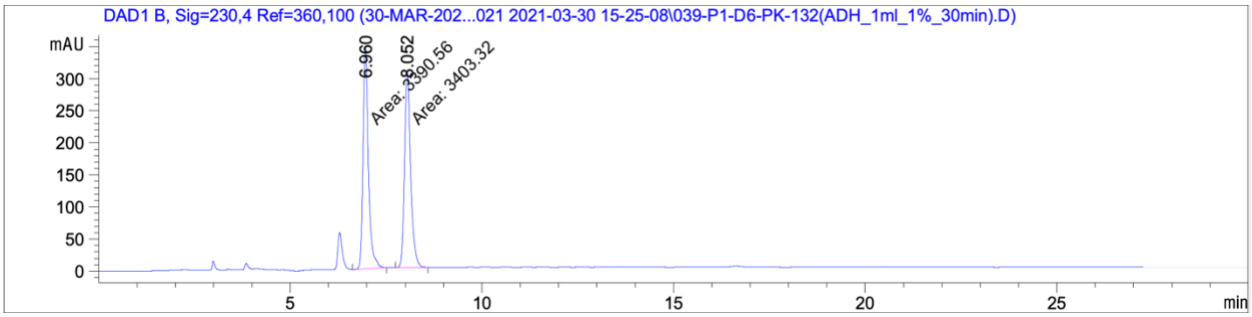

Peak #	RetTime [min]	Type	Width [min]	Area [mAU*s]	Height [mAU]	Area %
1	6.960	MM	0.1628	3390.55884	347.03052	49.9061
2	8.052	MM	0.1856	3403.31934	305.58505	50.0939

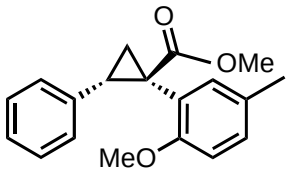

57% yield, 13% e.e. 0.0 equiv 2-chloropyridine
46% yield, 0% e.e. 1.0 equiv 2-chloropyridine

Rh_2(*S-3,5-m*-ph-TPPTTL)$_4$ Selective cyclopropanation of isoprene **Reaction 11**

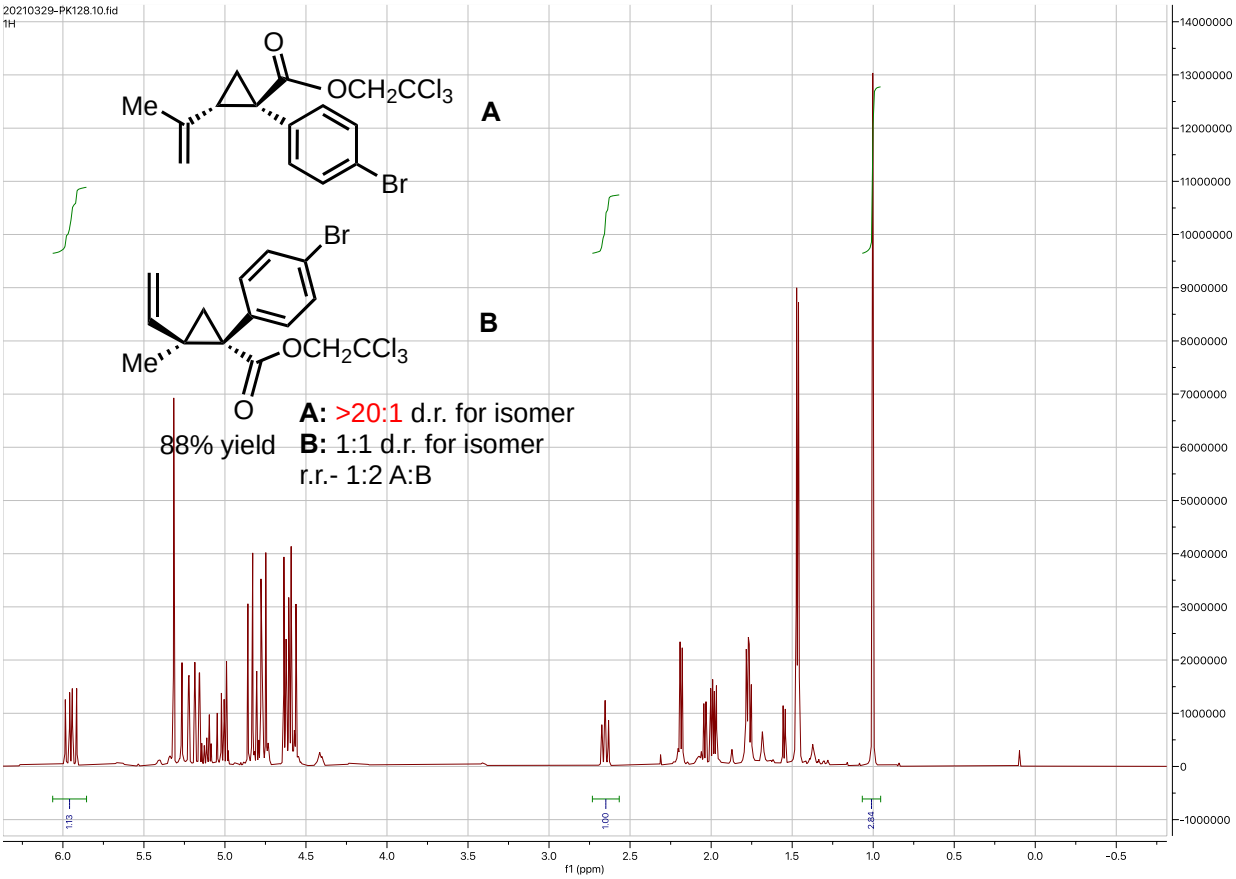

Rh_2(*S-3,5-m*-ph-TPPTTL)$_4$ C-H functionalization of ^{t}butyl-cyclohexane **Reaction 12.**

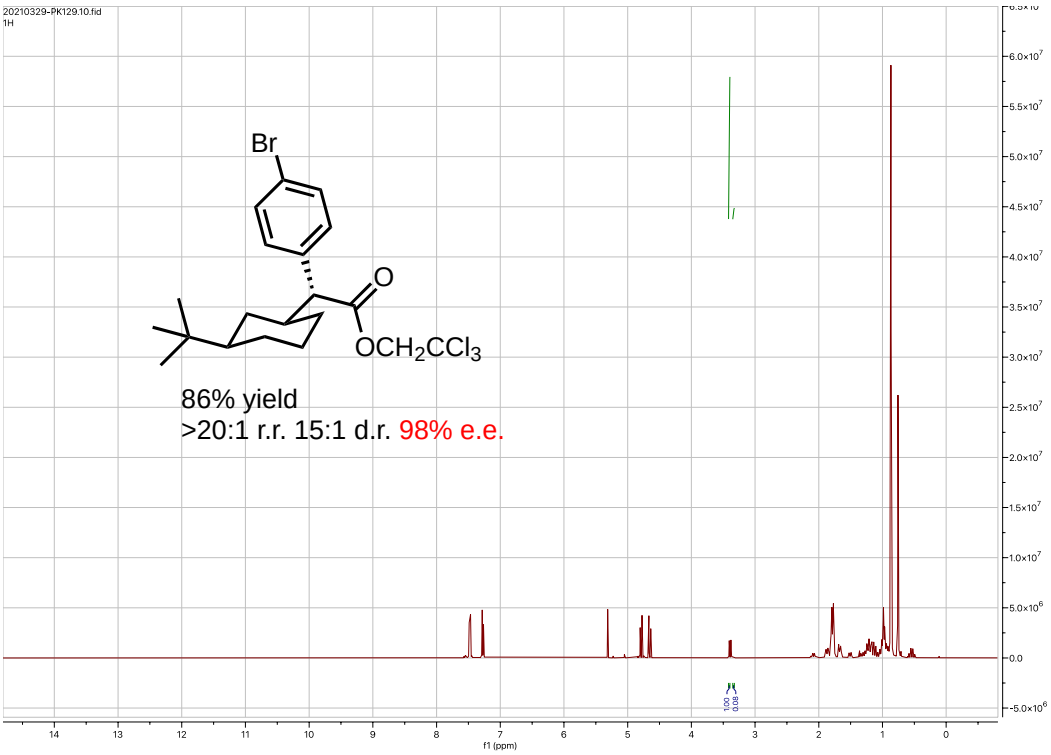

Rh_2(*S-3,5-m*-ph-TPPTTL)$_4$ C-H functionalization of methylcyclohexane **Reaction 14.**

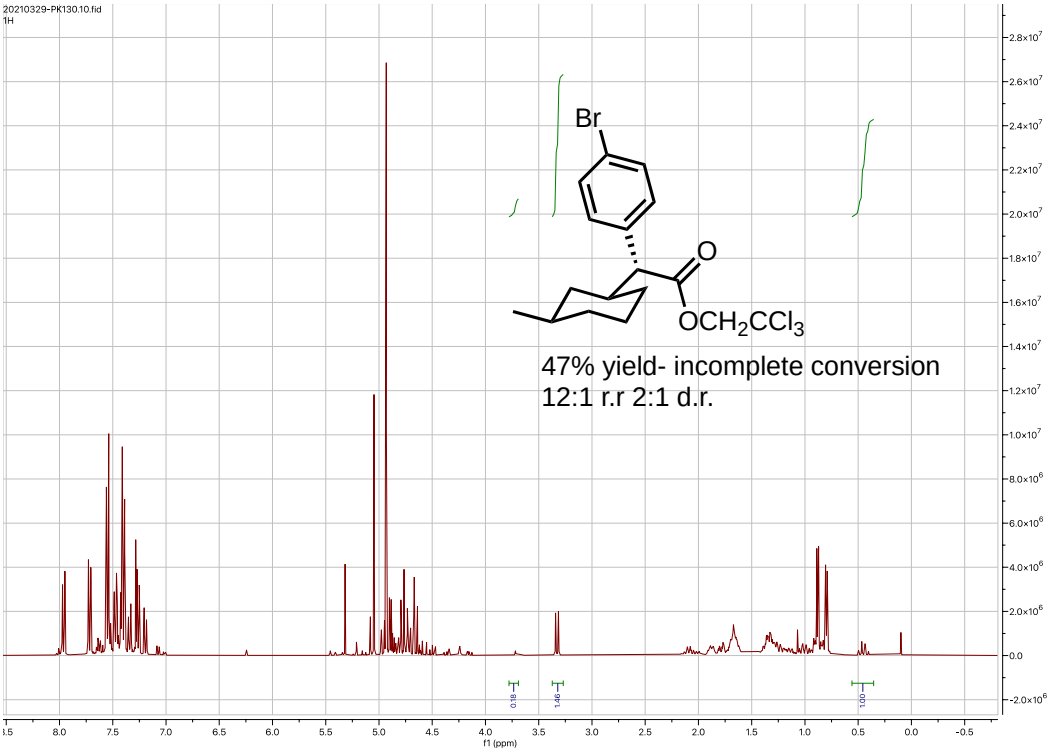

Rh_2(*S-3,5-m*-bisCF_3-TPPTTL)$_4$ Catalyst

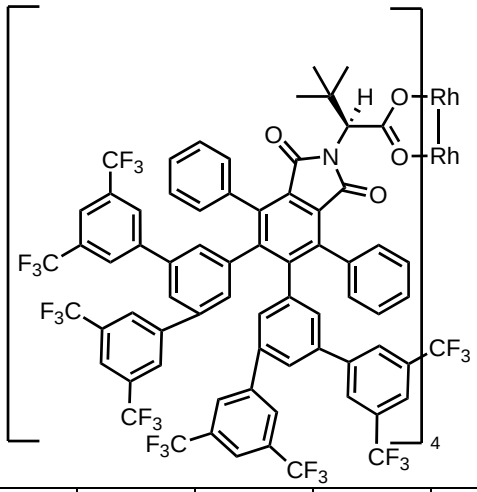

Peak Mass	Display Formula	RDB	Delta [ppm]	Delta [mmu]	Theo. mass	Combined Score	MS Cov. [%]
5854.80014	$C_{269}H_{283}O_{16}N_4F_{96}{}^{103}Rh_2$	84.5	-0.42	-2.44	5854.80258	70.51	72.81
5854.80014	$C_{280}H_{152}O_{16}N_4F_{96}{}^{103}Rh_2$	161	3.87	22.64	5854.7775	55.82	57.67

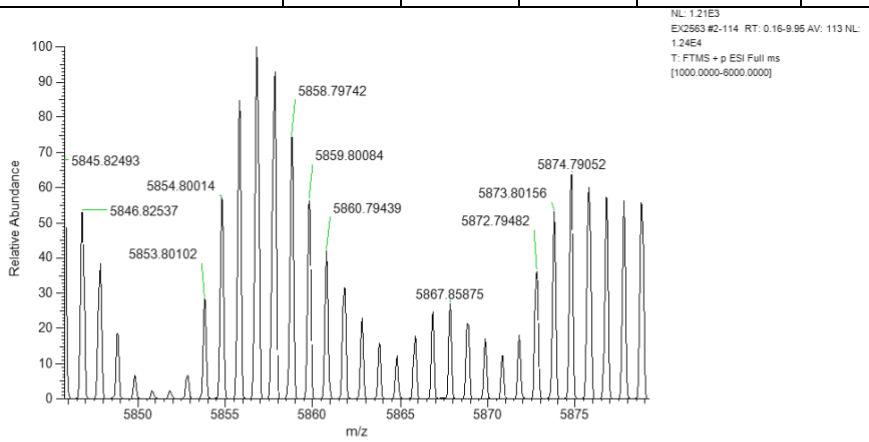

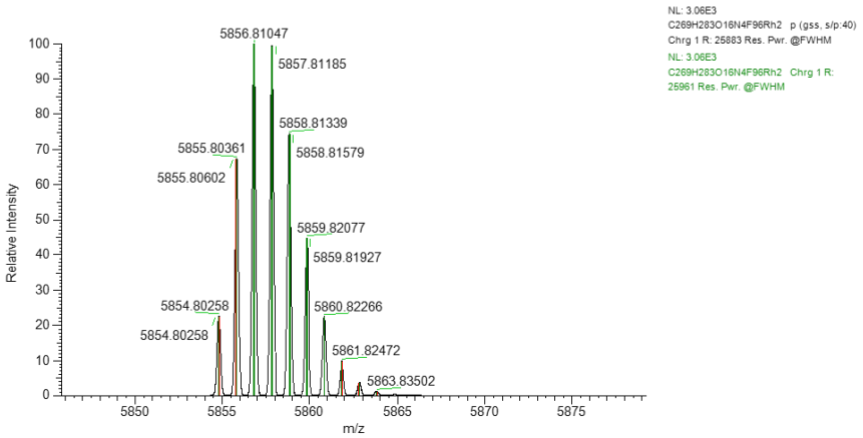

Rh_2(*S-3,5-m*-bisCF_3-TPPTTL)$_4$ Cyclopropanation of styrene and 2,2,2-trichloroethyl 2-(4-bromophenyl)-2-diazoacetate **Reaction 9.**

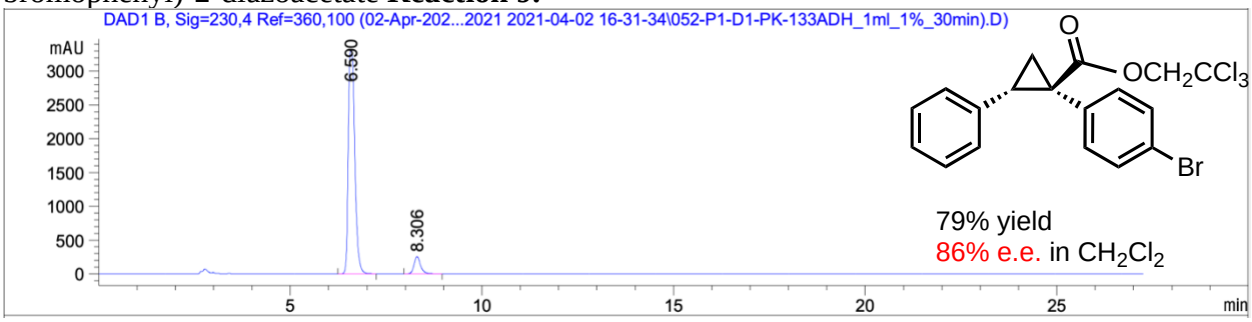

Peak #	RetTime [min]	Type	Width [min]	Area [mAU*s]	Height [mAU]	Area %
1	6.590	BB	0.1801	3.86539e4	3313.10376	92.8331
2	8.306	BB	0.1766	2984.15039	254.83298	7.1669

Rh_2(*S-3,5-m*-bisCF$_3$-TPPTTL)$_4$ Cyclopropanation of styrene and methyl 2-diazo-2-(2-methoxy-5-methylphenyl) acetate with 0-1.0 equiv. 2-chloropyridine. **Reaction 10.**

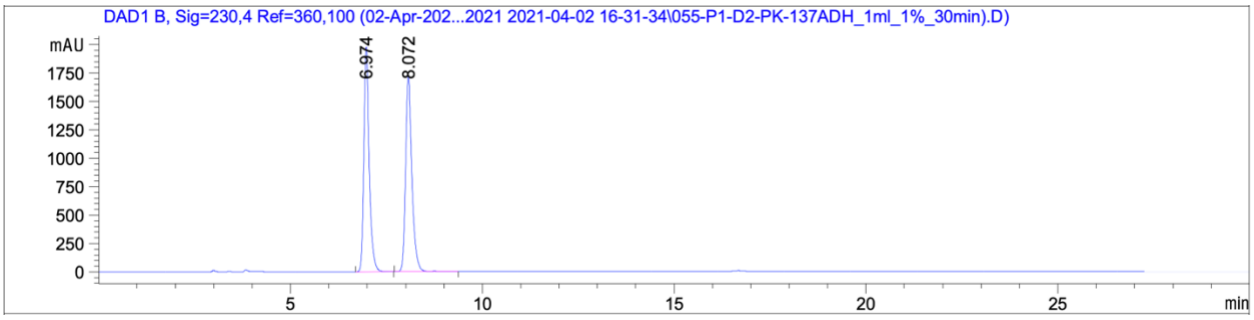

Peak #	RetTime [min]	Type	Width [min]	Area [mAU*s]	Height [mAU]	Area %
1	6.974	BB	0.1457	1.92832e4	1977.82983	49.4483
2	8.072	BV R	0.1708	1.97135e4	1726.84363	50.5517

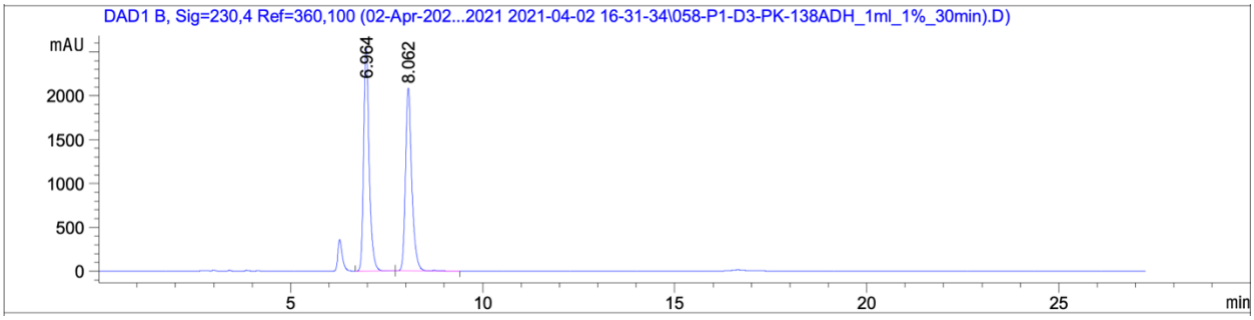

Peak #	RetTime [min]	Type	Width [min]	Area [mAU*s]	Height [mAU]	Area %
1	6.964	BB	0.1530	2.56578e4	2558.96021	51.5575
2	8.062	BV R	0.1744	2.41076e4	2084.24292	48.4425

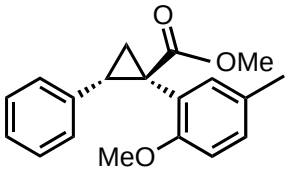

74% yield, 0% e.e. 0.0 equiv 2-chloropyridine
70% yield, 0% e.e. 1.0 equiv 2-chloropyridine

Rh_2(*S-3,5-m*-bisCF_3-TPPTTL)$_4$ Selective cyclopropanation of isoprene **Reaction 11.**

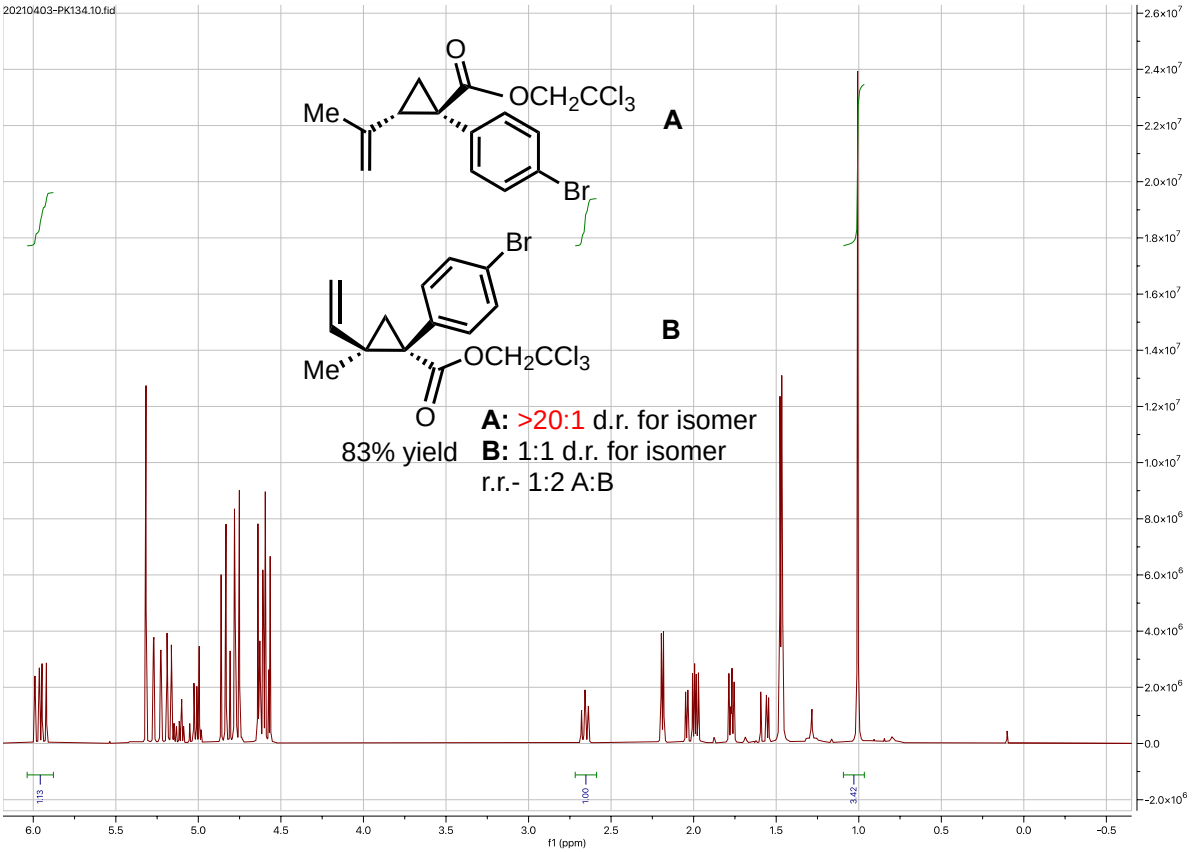

Rh_2(*S-3,5-m*-bisCF_3-TPPTTL)$_4$ C-H functionalization of ^{t}butyl-cyclohexane **Reaction 12.**

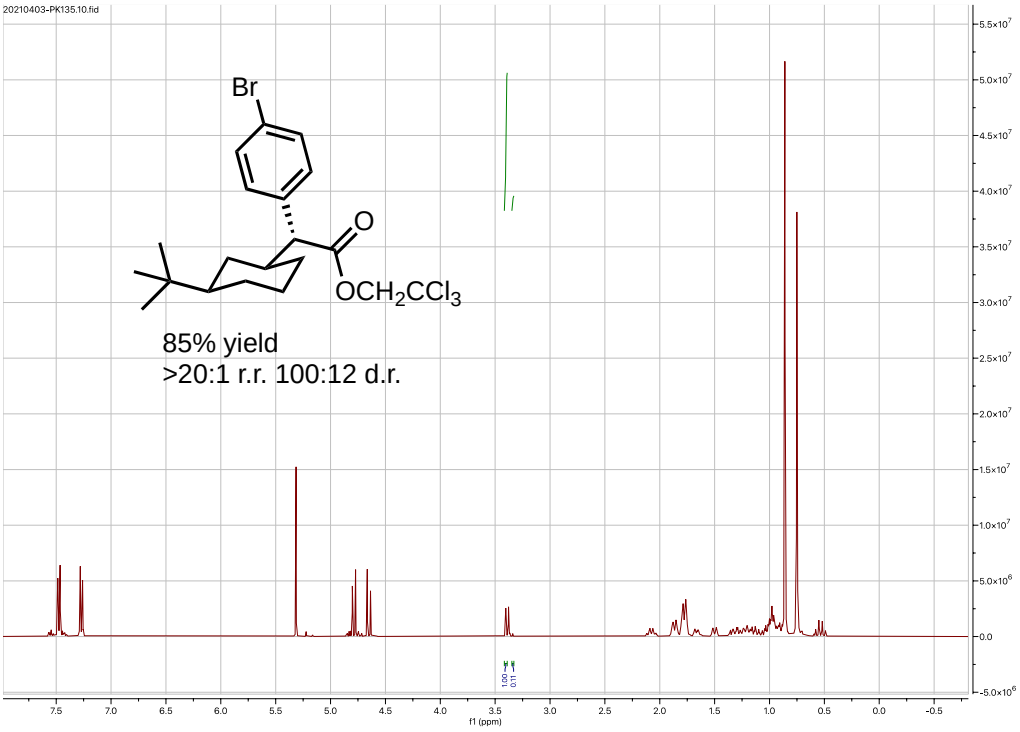

Rh_2(*S-3,5-m*-bisCF_3-TPPTTL)$_4$ C-H functionalization of methylcyclohexane **Reaction 14.**

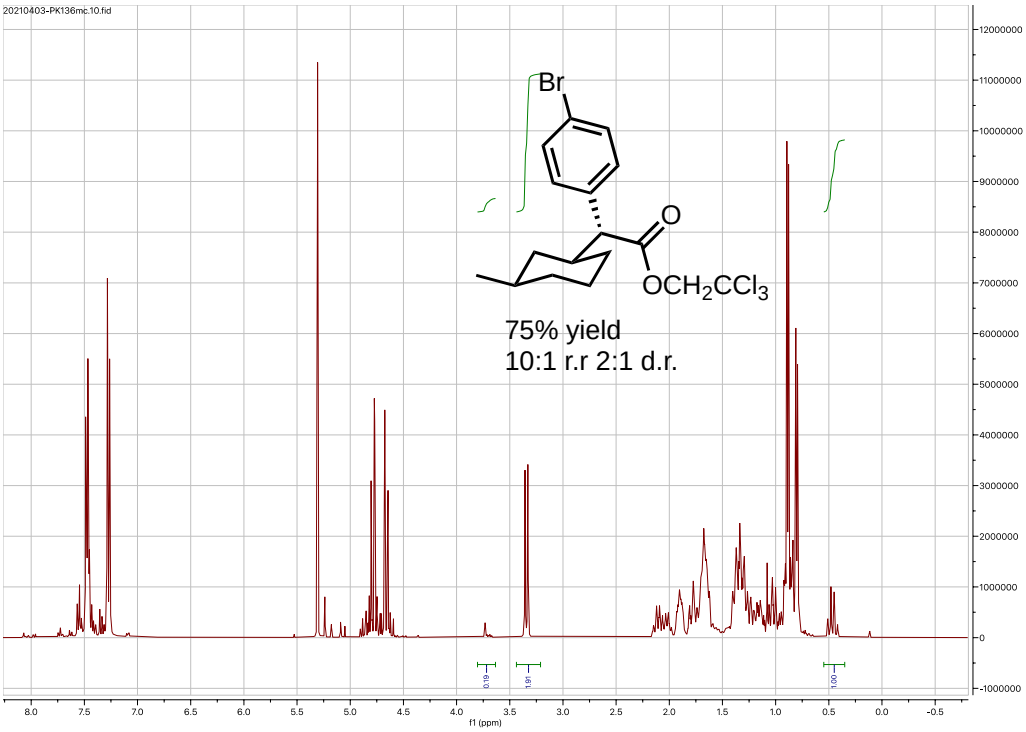

8) References

(1)

Barker, C. A.; Zeng, X.; Bettington, S.; Batsanov, A. S.; Bryce, M. R.; Beeby, A. Porphyrin, Phthalocyanine and Porphyrazine Derivatives with Multifluorenyl Substituents as Efficient Deep-Red Emitters. *Chemistry – A European Journal* **2007**, *13* (23), 6710–6717. https://doi.org/10.1002/chem.200700054.

(2)

Basu, P.; Nigam, A.; Mogesa, B.; Denti, S.; Nemykin, V. Synthesis, Characterization, Spectroscopy, Electronic and Redox Properties of a New Nickel Dithiolene System. *Inorganica Chim Acta* **2010**, *363* (12), 2857–2864. https://doi.org/10.1016/j.ica.2010.04.004.

(3)

Chen, K.; Lei, X. Recent Applications of CH Functionalization in Complex Molecule Synthesis. *Current Opinion in Green and Sustainable Chemistry* **2018**, *11*, 9–14. https://doi.org/10.1016/j.cogsc.2018.01.001.

(4)

Davies, H. M. L. Finding Opportunities from Surprises and Failures. Development of Rhodium-Stabilized Donor/Acceptor Carbenes and Their Application to Catalyst-Controlled C–H Functionalization. *J. Org. Chem.* **2019**, *84* (20), 12722–12745. https://doi.org/10.1021/acs.joc.9b02428.

(5)

Davies, H. M. L.; Liao, K. Dirhodium Tetracarboxylates as Catalysts for Selective Intermolecular C–H Functionalization. *Nature Reviews Chemistry* **2019**, *3* (6), 347–360. https://doi.org/10.1038/s41570-019-0099-x.

(6)

Fu, J.; Ren, Z.; Bacsa, J.; Musaev, D. G.; Davies, H. M. L. Desymmetrization of Cyclohexanes by Site- and Stereoselective C–H Functionalization. *Nature* **2018**, *564* (7736), 395–399. https://doi.org/10.1038/s41586-018-0799-2.

(7)

Gal, J.; Cintas, P. Early History of the Recognition of Molecular Biochirality. *Top Curr Chem* **2013**, *333*, 1–40. https://doi.org/10.1007/128_2012_406.

(8)

Lary, J. M.; Daniel, K. L.; Erickson, J. D.; Roberts, H. E.; Moore, C. A. The Return of Thalidomide: Can Birth Defects Be Prevented? *Drug Saf* **1999**, *21* (3), 161–169. https://doi.org/10.2165/00002018-199921030-00002.

(9)

Liao, K.; Liu, W.; Niemeyer, Z. L.; Ren, Z.; Bacsa, J.; Musaev, D. G.; Sigman, M. S.; Davies, H. M. L. Site-Selective Carbene-Induced C–H Functionalization Catalyzed by Dirhodium Tetrakis(Triarylcyclopropanecarboxylate) Complexes. *ACS Catal.* **2018**, *8* (1), 678–682. https://doi.org/10.1021/acscatal.7b03421.

(10)

Liao, K.; Liu, W.; Niemeyer, Z. L.; Ren, Z.; Bacsa, J.; Musaev, D. G.; Sigman, M. S.; Davies, H. M. L. Site-Selective Carbene-Induced C–H Functionalization Catalyzed by Dirhodium Tetrakis(Triarylcyclopropanecarboxylate) Complexes. *ACS Catal.* **2018**, *8* (1), 678–682. https://doi.org/10.1021/acscatal.7b03421.

(11)

Matsuura, T.; Koshima, H. Introduction to Chiral Crystallization of Achiral Organic Compounds: Spontaneous Generation of Chirality. *Journal of Photochemistry and Photobiology C: Photochemistry Reviews* **2005**, *6* (1), 7–24. https://doi.org/10.1016/j.jphotochemrev.2005.02.002.

(12)
Ren, H.; Tao, Q.; Gao, Z.; Liu, D. Synthesis and Properties of Novel Spirobifluorene-Cored Dendrimers. *Dyes and Pigments* **2012**, *94* (1), 136–142. https://doi.org/10.1016/j.dyepig.2011.12.005.

(13)
Tamura, K. Perspectives on the Origin of Biological Homochirality on Earth. *J Mol Evol* **2019**, *87* (4–6), 143–146. https://doi.org/10.1007/s00239-019-09897-1.

(14)
Mechanism of Rhodium-Catalyzed Carbene Formation from Diazo Compounds | Organic Letters https://pubs.acs.org/doi/abs/10.1021/ol070345n (accessed Mar 31, 2021).

(15)
The First Kilogram Synthesis of Beclabuvir, an HCV NS5B Polymerase Inhibitor | Organic Process Research & Development https://pubs.acs.org/doi/full/10.1021/acs.oprd.8b00214?ref=14390 (accessed Mar 31, 2021).

(16)
Liao, K.; Yang, Y.-F.; Li, Y.; Sanders, J. N.; Houk, K. N.; Musaev, D. G.; Davies, H. M. L. Design of Catalysts for Site-Selective and Enantioselective Functionalization of Non-Activated Primary C–H Bonds. *Nature Chemistry* **2018**, *10* (10), 1048–1055. https://doi.org/10.1038/s41557-018-0087-7.

(17)
Wei, B.; Sharland, J. C.; Lin, P.; Wilkerson-Hill, S. M.; Fullilove, F. A.; McKinnon, S.; Blackmond, D. G.; Davies, H. M. L. In Situ Kinetic Studies of Rh(II)-Catalyzed Asymmetric Cyclopropanation with Low Catalyst Loadings. *ACS Catal.* **2020**, *10* (2), 1161–1170. https://doi.org/10.1021/acscatal.9b04595.